

NOAA Technical Report ERL 408-GLERL 14



# Spectral Growth and Nonlinear Characteristics of Wind Waves in Lake Ontario

Paul Chi Liu  
Great Lakes Experimental Research Laboratory  
Ann Arbor, Michigan

November 1979

**U. S. DEPARTMENT OF COMMERCE**  
Philip M. Klutznik

National Oceanic and Atmospheric Administration  
Richard A. Frank, Administrator

Environmental Research Laboratories  
Boulder, Colorado  
Wilmot Hess, Director

## NOTICE

Mention of a commercial company or product does not constitute an endorsement by NOAA Environmental Research Laboratories. Use for publicity or advertising purposes of information from this publication concerning proprietary products or the tests of such products is not authorized.

This report is based on a dissertation submitted in partial fulfillment of the requirements for the degree of Doctor of Philosophy (Oceanic Science) at the University of Michigan, 1977.

## CONTENTS

	Page
Symbols Used .....	iv
Abstract .....	1
1. Introduction .....	1
2. Theoretical Considerations .....	2
3. Observational Considerations .....	3
4. Data Acquisition and Processing .....	5
5. Spectral Computations .....	6
6. Results and Discussion .....	7
6.1 The Episodes .....	7
6.2 The Unispectra .....	8
6.3 Temporal Growth of Unispectral Components .....	9
6.4 The Source Function—Empirical and Theoretical .....	11
6.5 The Bispectra .....	16
6.6 Temporal Growth of Bispectral Components .....	16
6.7 The Trispectra .....	17
6.8 Temporal Growth of Trispectral Components .....	18
6.9 Further Remarks on Bispectra and Trispectra .....	19
7. Summary and Concluding Remarks .....	23
8. References .....	36
Appendix A. Relationships Between Higher-Order Covariances and Higher-Order Spectra .....	39
Appendix B. Testing for Stationarity .....	43
Appendix C. Application of Barnett's Parameterization of Nonlinear Source Function .....	45
Appendix D. Trispectra During the Episodes on 30 September 1972 and 7 October 1972 .....	47

## SYMBOLS USED

$A(\mathbf{k}, X; \omega, T)$	Fourier coefficient of $\zeta(\mathbf{x}, X; t, T)$ used in appendix A	$p$	index counter
$A(t, \omega)$	a deterministic modulating function, which is unity for a stationary process	$P$	pressure on the free surface resulting from air motion; also used as a counter for data points
$D$	a parameter used in Barnett's parameterization of nonlinear energy transfer that represents the part receiving energy from other components	$r$	position vector
$E$	total energy	$R_n$	$n$ th order covariance function
$f$	linear frequency = $\omega/2\pi$	$S_n$	$n$ th order spectrum; $S$ without subscript $n$ represents a second-order spectrum
$f_0$	mean frequency	$T$	total time; also representing a coupling function in the Boltzmann integral in appendix C
$g$	acceleration due to gravity	$x$	space vector in Cartesian coordinates
$G$	source function; also used in Barnett's parameterization to represent the part that transfers energy to other components	$X$	a space parameter used in appendix A; also used as a Fourier transform, $X(\omega)$ , for data $\zeta_r(t)$
$h_{ij}$	a counting symbol used in stationarity tests	$y$	Cartesian coordinate
$i$	$(-1)^{1/2}$ in complex representation, also used as an index counter	$Y$	complex random function for surface $\zeta$ used in the Fourier-Stieltjes representation
$j$	index counter	$z$	Cartesian coordinate, directed vertically upward
$\mathbf{k}$	wave number vector with magnitude $k =  \mathbf{k} $ ; $k$ also is used as an index counter	$\zeta$	free surface displacement
$K$	counter for data points	$\theta$	wave direction
	index counter	$\pi$	3.14159 . . . .
$L$	counter for data points	$\rho$	density of water
$M$	counter for data points	$\tau$	time
$N$	counter for data points	$\phi$	velocity potential
$N_i$	$N(\mathbf{k}_i)$ action density at wave number $\mathbf{k}_i$ , used in the Boltzmann integral in appendix C	$\Phi$	complex random function for $\phi$ used in the Fourier-Stieltjes representation
		$\omega$	radian wave frequency

# SPECTRAL GROWTH AND NONLINEAR CHARACTERISTICS OF WIND WAVES IN LAKE ONTARIO

Paul Chi Liu

**ABSTRACT.** Recent studies have shown that the growth processes of wind waves are primarily associated with the nonlinear energy flux due to wave-wave interactions. A detailed empirical examination of these interactions uses calculated unispectra, bispectra, and trispectra of continuously recorded wave data during three episodes of growing waves. While the unispectrum provides information on the energy content of the frequency components, the bispectrum and trispectrum generally provide information on the interactive relations between two- and three-frequency components respectively. These higher-order interactive relations can be considered characterizations of nonlinear interactions. The results indicate that the peak-energy frequency transfers more energy to the lower frequency components than to the higher ones, which is confirmation that unispectral peaks shift progressively toward lower frequencies during wave growth.

## 1. INTRODUCTION

The study of wind-generated waves has experienced significant and extensive development during the last 20 years or so. Ursell's (1956) review, in which he found the state of our knowledge of wind-wave generation profoundly unsatisfactory with respect to both theory and observation, has often been credited with providing the major stimulation for modern studies. After two decades and vast theoretical and experimental efforts, a recent review by Barnett and Kenyon (1975) observed that

At the time Ursell reviewed the field, the body of theoretical work exceeded that of the experimental work, but both were in an unsatisfactory state. Today the same ratio holds in that the theoretical ideas are still ahead of the experimental testing. In particular, field observations relevant to wave generation and dissipation in the oceans in 1955 were nearly nonexistent. Today they are simply very scarce.

Theory often leads experiment in science. In the study of wind waves, however, the difference is so large that experiment cannot interact with theory very efficiently. Theoretical analyses result in mathematical complexity, which prevents exact and practicable solutions; at the same time a lack of basic knowledge of the actual wave processes limits the ability to develop new models. This report presents a detailed empirical examination of the temporal evolution processes of the energy spectrum of wind-generated surface waves. Our measurements and analyses, presented here, help satisfy the need for basic information about wave processes.

Because several recent studies (Hasselmann et al., 1973; Longuet-Higgins, 1976; Fox, 1976) stress

the importance of nonlinear energy transfer in the wave-growth processes, we have examined these implications empirically. Since the nonlinearity comes from the higher-order terms in the equations of motion, the first step in evaluating the nonlinearity of a set of wave data recorded from a single station is to analyze the higher-order moments of the process. In practice, this is equivalent to performing bispectral and trispectral analyses of the data.

A bispectrum is the two-dimensional Fourier transform of the third-order covariance function of the data. A trispectrum is the three-dimensional Fourier transform of the fourth-order covariance function of the data. As two- and three-dimensional Fourier transforms of the corresponding covariance functions are very cumbersome, we have found a way to calculate bispectra and trispectra by using a fast Fourier transform algorithm directly on the wave data. (The details will be discussed in section 5.) Physically, just as the unispectra provide information on the energy content of the frequency components, the bispectra and trispectra provide information on the interactive relations between two-frequency components and between three-frequency components, respectively. We consider these higher-order relations to be estimates or characterizations of nonlinear interactions.

Hasselmann, Munk, and McDonald (1962) and Garrett (1970) have demonstrated that calculations of observed bispectra of ocean waves correlate reasonably well with theoretically derived bispectra. These studies, however, are not extensive enough to provide much insight into the detailed behavior of the physical processes.

Using continuous wave data recorded in Lake Ontario, this report examines, identifies, and resolves the temporal characteristics of linear and nonlinear interactions during wave growth. Our demonstration that the mean energy of the waves is closely

related to the unispectra, bispectra, and trispectra of the data provides some analytical background to our basically intuitive approach.

## 2. THEORETICAL CONSIDERATIONS

All theoretical studies of surface waves start from basic equations of fluid dynamics with varied idealizations or assumptions for obtaining the solutions. We assume irrotational motion of a horizontally unbounded incompressible fluid with infinite depth and a free surface at  $z = \zeta(x, t)$ , where  $x = (x, y)$  and  $z$  are Cartesian coordinates and the  $z$ -axis is directed vertically upward; then a velocity potential  $\phi(x, z, t)$  exists and the motion is governed by the Laplace equation

$$\nabla^2 \phi = 0, \text{ for } z < \zeta. \quad (1)$$

Further neglecting the surface tension, the kinetic and dynamic boundary conditions at the free surface  $z = \zeta$  are given, respectively, by

$$\frac{\partial \zeta}{\partial t} - \frac{\partial \phi}{\partial z} + \nabla \zeta \cdot \nabla \phi = 0 \quad (2)$$

and

$$\frac{\partial \phi}{\partial t} + g\zeta + \frac{1}{2}(\nabla \phi)^2 = -\frac{p}{\rho}, \quad (3)$$

where  $p$  represents the pressure on the free surface resulting from the air motion,  $\rho$  the water density, and  $g$  the acceleration due to gravity. Now if we assume that the random surface displacement is statistically stationary with respect to both space and time, we can use the Fourier-Stieltjes representation (Phillips, 1966) as

$$\zeta(x, t) = \int_{\mathbf{k}} \int_{\omega} dY(\mathbf{k}, \omega) e^{-i(\mathbf{k} \cdot \mathbf{x} - \omega t)}. \quad (4)$$

Under the same assumptions and the further assumption that  $\phi \rightarrow 0$  as  $z \rightarrow -\infty$ , the solution to (1) can be represented by

$$\phi(x, z, t) = \int_{\mathbf{k}} \int_{\omega} d\Phi(\mathbf{k}, \omega) e^{kz - i(\mathbf{k} \cdot \mathbf{x} - \omega t)}. \quad (5)$$

Here  $d\Phi(\mathbf{k}, \omega)$  and  $dY(\mathbf{k}, \omega)$  are complex random functions of the horizontal wave number vector  $\mathbf{k}$  and frequency  $\omega$  with  $k = |\mathbf{k}|$ . Analogously, the pressure on the surface resulting from air motion can be represented by

$$p(x, t) = \int_{\mathbf{k}} \int_{\omega} dP(\mathbf{k}, \omega) e^{-i(\mathbf{k} \cdot \mathbf{x} - \omega t)}. \quad (6)$$

The representations (4), (5), and (6) are quite general and appropriate for studying stationary random wave processes. Most of the studies in the literature consider processes that are stationary only with respect to space and thus reduce the equations of motion into differential equations with time derivatives only. Examples are Phillips (1960), Hasselmann

(1962), and Benney (1962). Assuming the process is stationary with respect to both space and time, however, further reduces the equations of motion into algebraic operations. Substituting (4), (5), and (6) into (2) and (3); expanding the factor  $e^{k\zeta}$  in (5) as a power series; and using (4) again in the series, we obtain

$$\begin{aligned} & -i\omega dY(\mathbf{k}, \omega) - kd\Phi(\mathbf{k}, \omega) \\ & - \int_{\mathbf{k}'} \int_{\omega'} k'^2 d\Phi(\mathbf{k}', \omega') dY(\mathbf{k} - \mathbf{k}', \omega - \omega') \\ & - \int_{\mathbf{k}'} \int_{\omega'} \int_{\mathbf{k}''} \int_{\omega''} \frac{k'^3}{2} d\Phi(\mathbf{k}', \omega') dY(\mathbf{k}'', \omega'') \\ & \times dY(\mathbf{k}' - \mathbf{k}' - \mathbf{k}'', \omega - \omega' - \omega'') \\ & + \int_{\mathbf{k}'} \int_{\omega'} -\mathbf{k}' \cdot (\mathbf{k} - \mathbf{k}') d\Phi(\mathbf{k}', \omega') \\ & \times dY(\mathbf{k} - \mathbf{k}', \omega - \omega') \\ & + \int_{\mathbf{k}'} \int_{\omega'} \int_{\mathbf{k}''} \int_{\omega''} -\mathbf{k}' \cdot \mathbf{k}'' k' d\Phi(\mathbf{k}', \omega') \\ & \times dY(\mathbf{k}'', \omega'') dY(\mathbf{k} - \mathbf{k}' - \mathbf{k}'', \omega - \omega' - \omega'') \\ & = 0, \end{aligned} \quad (7)$$

and

$$\begin{aligned} & -i\omega d\Phi(\mathbf{k}, \omega) + gdY(\mathbf{k}, \omega) \\ & + \int_{\mathbf{k}'} \int_{\omega'} \{-i\omega' k' d\Phi(\mathbf{k}', \omega') dY(\mathbf{k} - \mathbf{k}', \omega - \omega') \\ & + \frac{1}{2}[k' |\mathbf{k} - \mathbf{k}'| - \mathbf{k}' \cdot (\mathbf{k} - \mathbf{k}')] d\Phi(\mathbf{k}, \omega) \\ & \times d\Phi(\mathbf{k} - \mathbf{k}', \omega - \omega')\} \\ & + \int_{\mathbf{k}'} \int_{\omega'} \int_{\mathbf{k}''} \int_{\omega''} \left[ -i\omega' \frac{k'^2}{2} d\Phi(\mathbf{k}', \omega') dY(\mathbf{k}'', \omega'') \right. \\ & \times dY(\mathbf{k} - \mathbf{k}' - \mathbf{k}'', \omega - \omega' - \omega'') \\ & \left. + \frac{1}{2}(k' + k'')(k' k'' - \mathbf{k}' \cdot \mathbf{k}'') d\Phi(\mathbf{k}', \omega') \right. \\ & \left. \times d\Phi(\mathbf{k}'', \omega'') dY(\mathbf{k} - \mathbf{k}' - \mathbf{k}'', \omega - \omega' - \omega'') \right] \\ & = -\frac{1}{\rho} dP(\mathbf{k}, \omega) \end{aligned} \quad (8)$$

Equations (7) and (8), retaining terms to the third order, can be solved for  $dY(\mathbf{k}, \omega)$  and  $d\Phi(\mathbf{k}, \omega)$  if the representation  $dP(\mathbf{k}, \omega)$  is given. From the point of view of the empirical study, the higher order terms in (7) and (8) clearly point to the need for study of higher order spectra. Most of the nonlinear studies in the literature assume the processes are undisturbed by air motion; hence  $dP(\mathbf{k}, \omega) = 0$  in (8). Linearized analyses by Phillips (1957) and Miles (1957) considered  $dP(\mathbf{k}, \omega)$  to be primarily associated with the turbulent wind field and to consist of two parts: the part produced by the turbulent eddies in the wind and in random phase with the wave field, and the part directly induced by and phase-locked with the wave field. A combination of the two mechanisms (Phillips, 1966) shows that the growth of wave

energy is initially linear with time under the turbulent pressure alone and subsequently becomes exponential because of the induced pressure acting on the growing waves. A more realistic representation for  $dP(\mathbf{k}, \omega)$  is not available.

The Fourier-Stieltjes transforms  $dY(\mathbf{k}, \omega)$  and  $d\Phi(\mathbf{k}, \omega)$ , solvable from (7) and (8), are closely related to the distribution of energy per unit among the components of the wave field. The mean energy of the waves per unit projected surface area is

$$E = E_{\text{potential}} + E_{\text{kinetic}} \\ = \frac{1}{2} \overline{\rho g \zeta^2} + \frac{1}{2} \int_{-\infty}^{\zeta} \overline{\rho (\nabla \phi)^2} dz, \quad (9)$$

where the bars denote ensemble averages. It can be shown (e.g., Phillips, 1961) that

$$E = \frac{1}{2} \overline{\rho \left[ g \zeta^2 + \left( \phi \frac{\partial \zeta}{\partial t} \right)_{z=\zeta} \right]}; \quad (10)$$

hence, substituting (4) and (5) into (10), we obtain

$$E = \frac{1}{2} \overline{\rho \int_{\mathbf{k}} \int_{\omega} \int_{\mathbf{k}'} \int_{\omega'} \left[ g dY(\mathbf{k}', \omega') dY(\mathbf{k} - \mathbf{k}', \omega - \omega') \right.} \\ \left. + i \omega' \overline{dY(\mathbf{k}', \omega') d\Phi(\mathbf{k} - \mathbf{k}', \omega - \omega')} \right.} \\ \left. + \int_{\mathbf{k}''} \int_{\omega''} i \omega' k'' \overline{dY(\mathbf{k}', \omega') d\Phi(\mathbf{k}'', \omega'')} \right.} \\ \left. \times \overline{dY(\mathbf{k} - \mathbf{k}' - \mathbf{k}'', \omega - \omega' - \omega'')} \right.} \\ \left. + \dots \right] e^{-i(\mathbf{k} \cdot \mathbf{x} - \omega t)}. \quad (11)$$

The relation between  $d\Phi(\mathbf{k}, \omega)$  and  $dY(\mathbf{k}, \omega)$ , correct to the first order, is given by

$$d\Phi(\mathbf{k}, \omega) = \frac{-i\omega}{k} dY(\mathbf{k}, \omega). \quad (12)$$

Furthermore, since we assume stationarity with respect to both time and space, we expect non-zero contributions to the integral in (11) to occur only when both  $\mathbf{k} = 0$  and  $\omega = 0$ ; thus (11) becomes

$$E = \frac{1}{2} \overline{\rho \int_{\mathbf{k}} \int_{\omega} \left[ (2g) \overline{dY(\mathbf{k}, \omega) dY^*(\mathbf{k}, \omega)} \right.} \\ \left. + \int_{\mathbf{k}_1} \int_{\omega_1} \omega \omega_1 \overline{dY(\mathbf{k}, \omega) dY(\mathbf{k}_1, \omega_1) dY^*(\mathbf{k} + \mathbf{k}_1, \omega + \omega_1)} \right.} \\ \left. + \int_{\mathbf{k}_1} \int_{\omega_1} \int_{\mathbf{k}_2} \int_{\omega_2} \frac{\omega \omega_1^3}{2g} \overline{dY(\mathbf{k}, \omega) dY(\mathbf{k}_1, \omega_1)} \right.} \\ \left. \times \overline{dY(\mathbf{k}_2, \omega_2) dY^*(\mathbf{k} + \mathbf{k}_1 + \mathbf{k}_2, \omega + \omega_1 + \omega_2)} \right.} \\ \left. + \dots \right], \quad (13)$$

where  $dY^*(\mathbf{k}, \omega)$  is the complex conjugate of  $dY(\mathbf{k}, \omega)$ . From appendix A, we see that the averages  $\overline{dY(\mathbf{k}, \omega) dY(\mathbf{k}_1, \omega_1) \dots dY(\mathbf{k}_n, \omega_n)}$  relate to the  $n$ th order spectrum. Thus, to study the complete energy distribution, it is necessary to examine the higher order spectra.

### 3. OBSERVATIONAL CONSIDERATIONS

The results presented in section 2 and appendix A are derived for the characterization of the whole lake surface. To correlate the results with actual wave observations, usually made from a wave gage installed at a single selected location, the equations are integrated and normalized over all directions and wave numbers; this explicitly depends on time and wave frequency only. We can rewrite equations A.8 and A.9 as

$$\frac{\overline{dY(\omega_1) dY(\omega_2) \dots dY(\omega_{n-1}) dY^*(\omega_n)}}{d\omega_1 d\omega_2 \dots d\omega_{n-1}} \\ = \frac{1}{(2\pi)^{n-1}} \int \dots \int R_n(\tau_1, \dots, \tau_{n-1}) e^{-i \sum_{j=1}^{n-1} \omega_j \tau_j} \\ \times d\tau_1 \dots d\tau_{n-1} \\ = S_n(\omega_1, \omega_2, \dots, \omega_{n-1}), \\ \text{if } \omega_n = \omega_1 + \omega_2 + \dots + \omega_{n-1}; \quad (14)$$

and

$$\frac{\overline{dY(\omega_1) dY(\omega_2) \dots dY(\omega_{n-1}) dY^*(\omega_n)}}{d\omega_1 d\omega_2 \dots d\omega_{n-1}} \\ = 0, \text{ if } \omega_n \neq \omega_1 + \omega_2 + \dots + \omega_{n-1}. \quad (15)$$

Equation (13) now becomes

$$E = \frac{1}{2} \overline{\rho \int_{\omega} \left[ 2g \overline{dY(\omega) dY^*(\omega)} \right.} \\ \left. + \int_{\omega_1} \omega \omega_1 \overline{dY(\omega) dY(\omega_1) dY^*(\omega + \omega_1)} \right.} \\ \left. + \int_{\omega_1} \int_{\omega_2} \frac{\omega \omega_1^3}{2g} \overline{dY(\omega) dY(\omega_1) dY(\omega_2)} \right.} \\ \left. \times \overline{dY^*(\omega_1 + \omega_2 + \omega)} + \dots \right] \\ = \frac{1}{2} \overline{\rho \int_{\omega} \left[ 2g S_2(\omega) d\omega + \int_{\omega_1} \omega \omega_1 S_3(\omega, \omega_1) d\omega d\omega_1 \right.} \\ \left. + \int_{\omega_1} \int_{\omega_2} \frac{\omega \omega_1^3}{2g} S_4(\omega, \omega_1, \omega_2) d\omega d\omega_1 d\omega_2 \right.} \\ \left. + \dots \right], \quad (16)$$

where  $S_2(\omega)$ ,  $S_3(\omega, \omega_1)$ , and  $S_4(\omega, \omega_1, \omega_2)$  are the uni-spectrum, bispectrum, and trispectrum, respectively.

For a completely stationary process with respect to both time and space,  $E$  is constant in (16). However, our intent is to examine the time rate of change of the mean energy during a growing wave process that is in general nonstationary. Because in the non-stationary case  $E$  changes with time, its application seems to be somewhat contradictory. To pursue our interest within the framework of (16), we use a basic

assumption of local stationarity in which the process is assumed to be stationary and  $E$  constant only within a given segment of data, a segment long enough to provide sufficient degrees of freedom to lead to reasonable spectral estimates. Although  $E$  and hence the spectra are constant within the given segment, they invariably change from segment to segment. Therefore if we calculate  $S_2$ ,  $S_3$ , and  $S_4$  over consecutive overlapping segments during wave growth, we can indirectly examine the temporal growth behavior of the energy spectra.

The above scheme is demonstrated graphically by figure 1. The discrete time series  $\eta(t_n)$ ,  $t_n = n\Delta t$ ,  $n = 1, 2, \dots, N$  represents an episode of growing wave data  $N\Delta t$  in total time length with a sampling rate of  $1/\Delta t$ . We subdivide  $\eta(t_n)$  into  $M$  overlapping segments  $\zeta_m(t_\ell)$ ,  $t_\ell = \ell\Delta t$ ,  $\ell = 1, 2, \dots, L$ ,  $m = 1, 2, \dots, M$ . Each  $\zeta_m(t_\ell)$  is  $L\Delta t$  in time length. The data  $\ell = K$  to  $\ell = L$  of  $\zeta_m(t_\ell)$  overlap the data  $\ell = 1$  to  $\ell = L - K + 1$  of  $\zeta_{m+1}(t_\ell)$ . Thus we have  $N = (M - 1)K + L$ . While the process  $\eta(t_n)$  is not stationary, we assume each  $\zeta_m(t_\ell)$  is locally stationary and hence all considerations we have presented pertaining to  $\zeta(t)$  can be applied to  $\zeta_{\Delta t}(\ell\Delta t)$ ,  $\ell = 1, 2, \dots, L$ .

Since we represented  $\zeta(t)$  as a continuous process,

$$\zeta(t) = \int_{\omega} e^{i\omega t} dY(\omega). \quad (17)$$

To use the discrete time series, we write

$$\zeta_{\Delta t}(\ell\Delta t) = \int_{2\pi/\Delta t} e^{i\omega\ell\Delta t} dY_{\Delta t}(\omega), \quad (18)$$

where

$$dY_{\Delta t}(\omega) = \sum_{\ell} dY(\omega + 2\pi\ell/\Delta t) \quad (19)$$

can be considered as complex amplitudes at frequencies  $\omega + 2\pi\ell/\Delta t$ , in view of the fact that  $e^{i\omega\ell\Delta t}$  is periodic at frequency  $\omega + 2\pi/\Delta t$ . The relationship between the continuous  $n$ th order spectrum  $S_n(\omega_1, \dots, \omega_n)$  and the discrete  $n$ th order spectrum  $S_{n,\Delta t}(\omega_1, \dots, \omega_n)$  has been given by Brillinger and Rosenblatt (1967) as

$$S_{n,\Delta t}(\omega_1, \dots, \omega_n) = \sum_{j_1} \dots \sum_{j_n} S_n\left(\omega_1 + \frac{2\pi j_1}{\Delta t}, \dots, \omega_n + \frac{2\pi j_n}{\Delta t}\right), \quad (20)$$

with

$$\omega_n = \omega_1 + \dots + \omega_{n-1},$$

and

$$\omega_n + \frac{2\pi j_n}{\Delta t} = \sum_{\ell=1}^{n-1} \left(\omega_{\ell} + \frac{2\pi j_{\ell}}{\Delta t}\right).$$

Thus using the Nyquist frequency of  $\pi/\Delta t$  radians per second or  $1/(2\Delta t)$  Hz in sampling to avoid aliasing problems, we can effectively represent the continuous process with a discrete time series in our subsequent analysis.

Some further remarks concerning our stationarity assumption can be stated here:

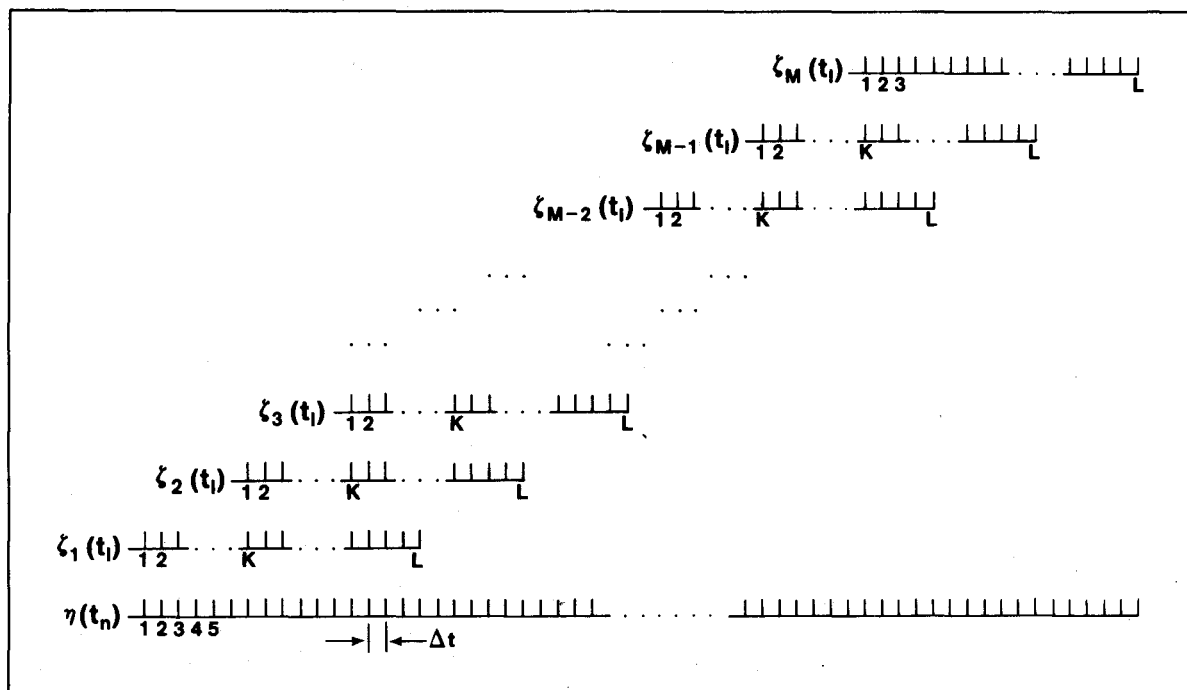


Figure 1.—Graphical demonstration of data segments.

(1) The use of the local stationarity assumption is not new; Kolmogoroff (1941) used local homogeneity in his turbulence studies. Most wave growth studies in the literature use this assumption implicitly. To evaluate the approximate validity of this assumption, appendix B gives some nonparametric stationarity tests on the data used in this study. The results show that the assumption is generally within the acceptable range of the tests and can be considered valid for our purpose.

(2) We are not attempting explicitly to calculate  $E$  in (16). Rather we use (16) to show the significance of the spectral terms in connection with mean energy and thus concentrate our interests on the temporal growths of the frequency components of  $S_2(\omega)$ ,  $S_3(\omega, \omega_1)$ , and  $S_4(\omega, \omega_1, \omega_2)$  and their physical implications.

(3) A different approach to analyzing a non-stationary process, perhaps more rigorous statistically, was developed by Priestly (1965). He introduced a representation of

$$\zeta(t) = \int_{\omega} A(t, \omega) dY(\omega) e^{-i\omega t}, \quad (21)$$

where  $A(t, \omega)$  is a deterministic modulating function that approaches unity when the process approaches stationarity. This representation could have been used in our analyses. However, since  $A(t, \omega)$  is not a known function and its application inevitably requires further assumptions and complications, we did not use it. It is of interest to note that Priestly's model leads to the conclusion that "the evolutionary spectrum at each instant of time may be estimated from a single realization of a process." This is exactly what the local stationarity assumption implies.

(4) We define local stationarity here in its literal sense. Silverman (1957) introduced the concept of a locally stationary random process with a locally stationary covariance that can be written as the product of a stationary covariance and a nonnegative function. Since we allow our local covariance to vary from segment to segment and the variation is generally smooth and gradual, it seems analogously possible that a nonnegative function could depend on time segments and that a stationary covariance can be deduced from our consecutive local covariances. As we expect the property to apply to third- and fourth-order covariances also, our assumption carries a different sense than Silverman's rigorous process.

#### 4. DATA ACQUISITION AND PROCESSING

The data used in this study were recorded in Lake Ontario from 1 April 1972 to 31 March 1973, the International Field Year for the Great Lakes (IFYGL). Seven Waverider Buoys and a large number of Physical Data Collection System (PDCS) buoys

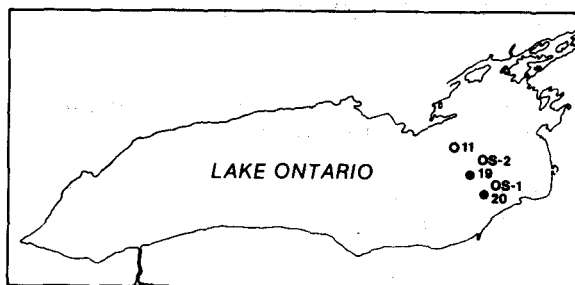


Figure 2.—Location of wind and wave gages in Lake Ontario.

were deployed for the IFYGL programs. The wave data in this study were recorded from the two Waveriders designated as OS-1 and OS-2 (figure 2); the corresponding wind data used here were recorded from PDCS buoy 11.

The Waveriders were deployed in 150 m of water and freely moored to a chain sinker with a mooring line approximately twice the depth of the water. The Waverider Buoy, manufactured by Datawell, Holland, is of spherical shape 1 m in diameter and weighs about 100 kg. It contains two main components: an accelerometer and a transmitter. The accelerometer, mounted on a pendulous system, measures the vertical component of acceleration as the buoy moves with the waves. Two electronic integrators in cascade then transform the output into a voltage that represents the vertical displacement of the buoy. This voltage controls the frequency of an audio oscillator, which in turn modulates a crystal-controlled transmitter that transmits the signal by telemetry to a shore receiver. The telemetered wave data were recorded continuously on analog magnetic tapes. The analog wave data tapes were subsequently processed through a computer digitization and editing system (Liu and Robbins, 1974) to obtain final data tapes, which were digitized at a sampling rate of approximately three per second. This sampling rate is more than sufficient to avoid an aliasing problem, since the buoy response is such as to adequately damp waves having a frequency of  $> 1.0$  Hz. On the other hand the Waverider's frequency range is given as between 0.065 Hz and 0.50 Hz; hence, in the actual computations we use a sampling period of  $\Delta t = 2/3$  s to yield a Nyquist frequency of 0.75 Hz for the computed spectra. Referring to the scheme discussed in the last section, we use the following numbers in the analysis:

$$\begin{aligned} N &= 15975, \\ M &= 64, \\ L &= 1800, \\ K &= 225. \end{aligned}$$

Consequently each selected episode is 177.5 minutes long. The episodes are subdivided into 64 equal segments of 20 minutes each, with an overlap of 17.5 minutes from one segment to the next.

## 5. SPECTRAL COMPUTATIONS

In the previous discussion we have been using general  $n$ th order spectra. For the actual applications, however, we shall concentrate only on  $n = 2, 3$ , and 4 for the unispectrum, bispectrum, and trispectrum, respectively, defined as

$$S_2(\omega) = \frac{dY(\omega)dY^*(\omega)}{d\omega} = \int_{\omega} R_2(\tau) e^{-i\omega\tau} d\tau, \quad (22)$$

$$S_3(\omega_1, \omega_2) = \frac{dY(\omega_1)dY(\omega_2)dY^*(\omega_1 + \omega_2)}{d\omega_1 d\omega_2} = \int_{\omega_1} \int_{\omega_2} R_3(\tau_1, \tau_2) e^{-i(\omega_1\tau_1 + \omega_2\tau_2)} d\tau_1 d\tau_2, \quad (23)$$

and

$$S_4(\omega_1, \omega_2, \omega_3) = \frac{dY(\omega_1)dY(\omega_2)dY(\omega_3)dY^*(\omega_1 + \omega_2 + \omega_3)}{d\omega_1 d\omega_2 d\omega_3} = \int_{\omega_1} \int_{\omega_2} \int_{\omega_3} R_4(\tau_1, \tau_2, \tau_3) e^{-i(\omega_1\tau_1 + \omega_2\tau_2 + \omega_3\tau_3)} \times d\tau_1 d\tau_2 d\tau_3, \quad (24)$$

where

$$R_2(\tau) = \overline{\xi(t)\xi(t + \tau)}, \quad (25)$$

$$R_3(\tau_1, \tau_2) = \overline{\xi(t)\xi(t + \tau_1)\xi(t + \tau_2)}, \quad (26)$$

and

$$R_4(\tau_1, \tau_2, \tau_3) = \overline{\xi(t)\xi(t + \tau_1)\xi(t + \tau_2)\xi(t + \tau_3)}. \quad (27)$$

The above definitions lead to the following symmetry relations:

$$R_2(\tau) = R_2(-\tau), \quad (28)$$

$$R_3(\tau_1, \tau_2) = R_3(\tau_2, \tau_1) = R_3(-\tau_2, \tau_1 - \tau_2) = R_3(\tau_1 - \tau_2, -\tau_2) = R_3(-\tau_1, \tau_2 - \tau_1) = R_3(\tau_2 - \tau_1, -\tau_1), \quad (29)$$

and

$$\begin{aligned} R_4(\tau_1, \tau_2, \tau_3) &= R_4(\tau_1, \tau_3, \tau_2) = R_4(\tau_2, \tau_1, \tau_3) \\ &= R_4(\tau_2, \tau_3, \tau_1) \\ &= R_4(\tau_3, \tau_1, \tau_2) = R_4(\tau_3, \tau_2, \tau_1) \\ &= R_4(-\tau_1, \tau_2 - \tau_1, \tau_3 - \tau_1) \\ &= R_4(-\tau_1, \tau_3 - \tau_1, \tau_2 - \tau_1) \\ &= R_4(\tau_2 - \tau_1, -\tau_1, \tau_3 - \tau_1) \\ &= R_4(\tau_2 - \tau_1, \tau_3 - \tau_1, -\tau_1) \\ &= R_4(\tau_3 - \tau_1, -\tau_1, \tau_2 - \tau_1) \\ &= R_4(\tau_3 - \tau_1, \tau_2 - \tau_1, -\tau_1) \\ &= R_4(-\tau_2, \tau_1 - \tau_2, \tau_3 - \tau_2) \end{aligned}$$

$$\begin{aligned} &= R_4(-\tau_2, \tau_3 - \tau_2, \tau_1 - \tau_2) \\ &= R_4(\tau_1 - \tau_2, -\tau_2, \tau_3 - \tau_2) \\ &= R_4(\tau_1 - \tau_2, \tau_3 - \tau_2, -\tau_2) \\ &= R_4(\tau_3 - \tau_2, -\tau_2, \tau_1 - \tau_2) \\ &= R_4(\tau_3 - \tau_2, \tau_1 - \tau_2, -\tau_2) \\ &= R_4(-\tau_3, \tau_1 - \tau_3, \tau_2 - \tau_3) \\ &= R_4(-\tau_3, \tau_2 - \tau_3, \tau_1 - \tau_3) \\ &= R_4(\tau_2 - \tau_3, -\tau_3, \tau_1 - \tau_3) \\ &= R_4(\tau_2 - \tau_3, \tau_1 - \tau_3, -\tau_3) \\ &= R_4(\tau_1 - \tau_3, -\tau_3, \tau_2 - \tau_3) \\ &= R_4(\tau_1 - \tau_3, \tau_2 - \tau_3, -\tau_3). \end{aligned} \quad (30)$$

The corresponding transforms of the symmetry relations are

$$S_2(\omega) = S_2(-\omega), \quad (31)$$

$$\begin{aligned} S_3(\omega_1, \omega_2) &= S_3(\omega_2, \omega_1) = S_3(\omega_2, -\omega_1 - \omega_2) \\ &= S_3(-\omega_1 - \omega_2, \omega_2) \\ &= S_3(\omega_1, -\omega_1 - \omega_2) = S_3(-\omega_1 - \omega_2, \omega_1), \end{aligned} \quad (32)$$

and

$$\begin{aligned} S_4(\omega_1, \omega_2, \omega_3) &= S_4(\omega_1, \omega_3, \omega_2) = S_4(\omega_2, \omega_1, \omega_3) \\ &= S_4(\omega_2, \omega_3, \omega_1) \\ &= S_4(\omega_3, \omega_1, \omega_2) = S_4(\omega_3, \omega_2, \omega_1) \\ &= S_4(-\omega_1 - \omega_2 - \omega_3, \omega_2, \omega_3) \\ &= S_4(-\omega_1 - \omega_2 - \omega_3, \omega_3, \omega_2) \\ &= S_4(\omega_2, -\omega_1 - \omega_2 - \omega_3, \omega_3) \\ &= S_4(\omega_2, \omega_3, -\omega_1 - \omega_2 - \omega_3) \\ &= S_4(\omega_3, -\omega_1 - \omega_2 - \omega_3, \omega_2) \\ &= S_4(\omega_3, \omega_2, -\omega_1 - \omega_2 - \omega_3) \\ &= S_4(-\omega_1 - \omega_2 - \omega_3, \omega_1, \omega_3) \\ &= S_4(-\omega_1 - \omega_2 - \omega_3, \omega_3, \omega_1) \\ &= S_4(\omega_1, -\omega_1 - \omega_2 - \omega_3, \omega_3) \\ &= S_4(\omega_1, \omega_3, -\omega_1 - \omega_2 - \omega_3) \\ &= S_4(\omega_3, -\omega_1 - \omega_2 - \omega_3, \omega_1) \\ &= S_4(\omega_3, \omega_1, -\omega_1 - \omega_2 - \omega_3) \\ &= S_4(-\omega_1 - \omega_2 - \omega_3, \omega_1, \omega_2) \\ &= S_4(-\omega_1 - \omega_2 - \omega_3, \omega_2, \omega_1) \\ &= S_4(\omega_1, -\omega_1 - \omega_2 - \omega_3, \omega_2) \\ &= S_4(\omega_1, \omega_2, -\omega_1 - \omega_2 - \omega_3) \\ &= S_4(\omega_2, -\omega_1 - \omega_2 - \omega_3, \omega_1) \\ &= S_4(\omega_2, \omega_1, -\omega_1 - \omega_2 - \omega_3). \end{aligned} \quad (33)$$

Because of these symmetries, we need only to estimate the  $S_n$ 's,  $n = 2, 3$ , and 4, within a fundamental region. The fundamental region for unispectrum  $S_2(\omega)$  is the line segment  $0 \leq \omega \leq \omega_N$ ; for bispectrum  $S_3(\omega_1, \omega_2)$  is the triangle defined by  $0 \leq \omega_2 \leq \omega_1$ , and  $0 \leq \omega_1 \leq \omega_N$ ; and for trispectrum  $S_4(\omega_1, \omega_2, \omega_3)$  is the tetrahedron defined by  $0 \leq \omega_3 \leq \omega_2$ ,  $0 \leq \omega_2 \leq \omega_1$ , and  $0 \leq \omega_1 \leq \omega_N$ , with  $\omega_N = 2\pi/(2\Delta t)$  representing the Nyquist frequency.

Comparing the definitions (22), (23), and (24) with (A.19) in appendix A, we see that for a finite segment of a time series the coefficients of its Fourier transform  $X(\omega)$  can be used as approximations for the theoretical values  $dY(\omega)$  and hence for the appropriate products of Fourier coefficients for estimating

corresponding spectral densities. We used the following approach generally similar to those discussed by Haubrich (1965) and Hinch and Clay (1968).

Starting with  $\zeta(\ell\Delta t)$ ,  $\ell = 1, 2, \dots, L$ , we subdivide the series into  $P$  non-overlapping groups each of length  $K$ , such that for  $p = 0, 1, \dots, P-1$  and  $k = 1, 2, \dots, K$  we have

$$\zeta_p(k\Delta t) = \zeta[(pK + k)\Delta t],$$

and the  $K$  complex Fourier coefficients for each group are given by

$$X_p(\omega) = \left(\frac{\Delta t}{2\pi K}\right)^{1/2} \sum_{j=1}^K \zeta_p(j\Delta t) e^{i2\pi kj/K},$$

$$k = 1, 2, \dots, K. \quad (34)$$

We can then sum and obtain the average estimates by

$$S_2(\omega) = \frac{1}{P} \sum_{p=1}^P X_p(\omega) X_p^*(\omega), \quad (35)$$

$$S_3(\omega_1, \omega_2) = \frac{1}{P} \sum_{p=1}^P X_p(\omega_1) X_p(\omega_2) X_p^*(\omega_1 + \omega_2), \quad (36)$$

and

$$S_4(\omega_1, \omega_2, \omega_3) = \frac{1}{P} \sum_{p=1}^P X_p(\omega_1) X_p(\omega_2) X_p(\omega_3) \times X_p^*(\omega_1 + \omega_2 + \omega_3). \quad (37)$$

Equations (34)-(37) represent the basic approach in spectral computations used in this report. The approach is quite efficient and feasible, especially with the fast Fourier transform algorithm (Cooley and Tukey, 1965) available as a computing subroutine. In the actual computations, we use  $P = 30$  for each data segment of  $L = 1800$  to obtain smoothed spectral estimates with 60 degrees of freedom and a 95 percent confidence interval between 1.48 and 0.72.

## 6. RESULTS AND DISCUSSION

### 6.1 The Episodes

From the ample supply of wave data recorded in Lake Ontario during IFYGL, we selected three episodes for our study:

9 August 1972 EST 1215-1515,  
30 September 1972 EST 0540-0840,  
7 October 1972 EST 0000-0300.

The August and October episodes were recorded from Waverider OS-2 shown in figure 2; the September episode was recorded from Waverider OS-1. The

wind conditions during these periods, recorded at 10-minute intervals at 4 m above the lake surface on PDCS buoy 11, are shown in figures 3, 4, and 5. The group of short and straight lines plotted on the figures under wind direction and wind speed indicate the locations in time of the 64 overlapping segments of wave data analyzed for each episode. Each segment is 20 minutes long and has a 17.5-minute overlap with the next segment. Although each of the episodes represents a growing, nonstationary wave field, the 20-minute segments are assumed to be locally stationary, and thus we can calculate unispectrum, bispectrum, and trispectrum for each segment using equations (35), (36), and (37), respectively.

The three episodes are representative of growing wave conditions in the Great Lakes. Because we are interested in the early stage of wave growth, none of the episodes is under severe storm conditions. The 9 August episode started at a wind speed of  $8 \text{ m s}^{-1}$  and increased to more than  $11 \text{ m s}^{-1}$  in 3 hours. The

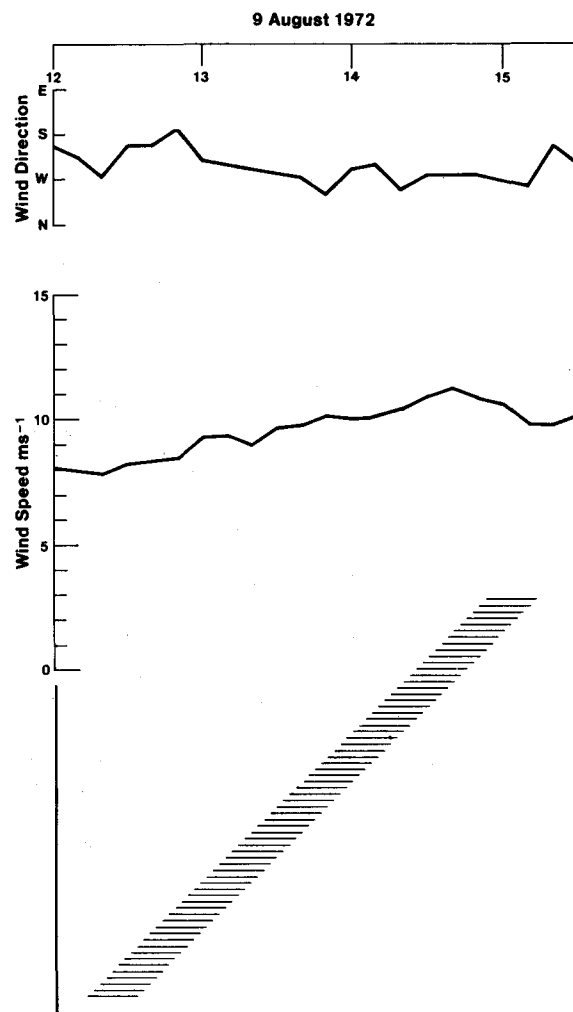


Figure 3.—Wind conditions for the episode of 9 August 1972. The series of short lines in the lower part indicates the locations in time of the 64 overlapping segments of wave data analyzed.

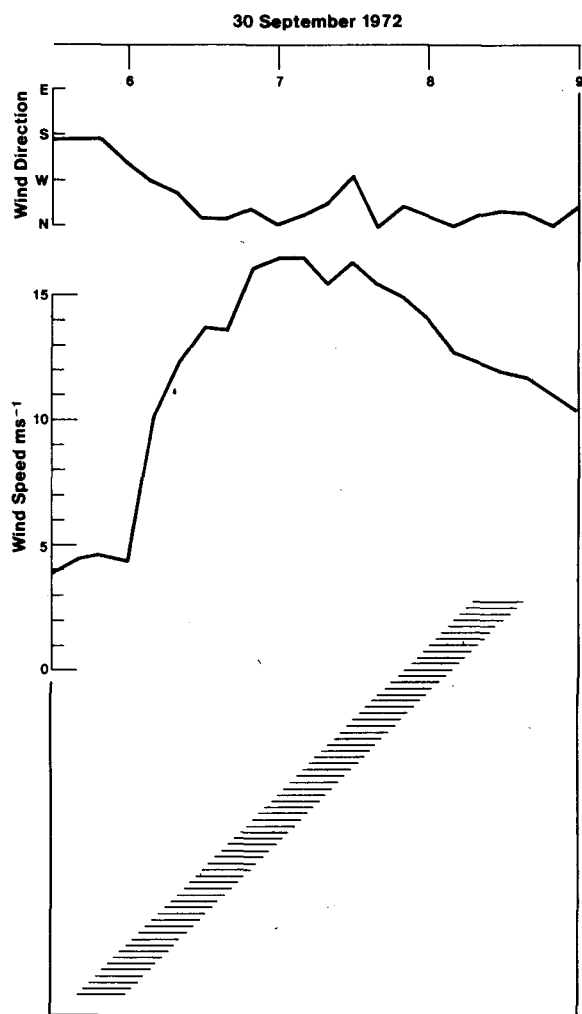


Figure 4.—Wind conditions for the episode of 30 September 1972. The series of short lines in the lower part indicates the locations in time of the 64 overlapping segments of wave data analyzed.

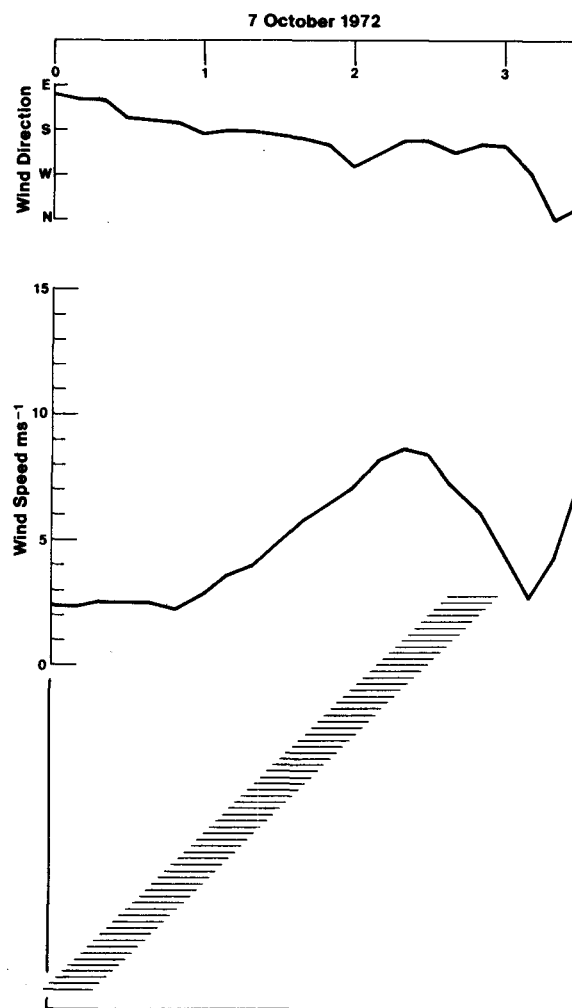


Figure 5.—Wind conditions for the episode of 7 October 1972. The series of short lines in the lower part indicates the locations in time of the 64 overlapping segments of wave data analyzed.

westerly wind direction provided long and approximately constant fetches during the episode. The 30 September episode included the passage of a steep low-pressure center directly over eastern Lake Ontario, and wind speeds increased from  $4 \text{ m s}^{-1}$  to more than  $14 \text{ m s}^{-1}$  within an hour, while wind directions were changing rapidly from south through west to north during the early part of the episode. The 7 October episode was milder with wind speed increased from  $2.5 \text{ m s}^{-1}$  to  $8.5 \text{ m s}^{-1}$  under south-westerly direction. The total wave energy under these three wind fields was growing steadily in each of the three cases.

## 6.2. The Unispectra

We first plot the computed unispectral density versus frequency versus time for three episodes as shown in figures 6, 7, and 8. These three-dimensional perspective figures present a clear overview of the

spectral growth of the episodes. Several basic characteristics can be observed from these figures:

- (1) The growth activity is mainly concentrated over the low-frequency side; the high-frequency side does not change much during the episode.
- (2) During the growth period, the peaks of the spectra tend to shift toward lower frequencies.
- (3) The growth rate varies for different frequency components.
- (4) Once a frequency component grows to be the spectral peak, it reaches a relative equilibrium and its growth rate tends to diminish.
- (5) A comparison of these local spectral growth episodes with their respective wind conditions shown in figures 3, 4, and 5 indicates that dominant growth of the spectra happens during increasing wind speeds.

The above features are generally known; similar results were obtained in laboratory studies, e.g., Jacobson and Colonell (1972) and more recently by Wu et al. (1979).

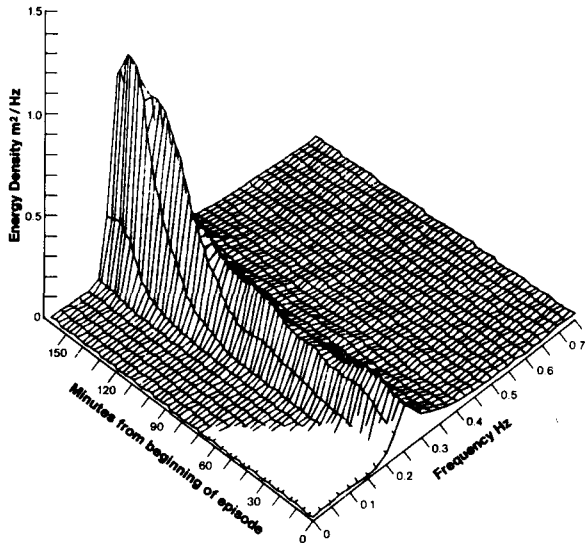


Figure 6.—Perspective view of the unispectrum during the episode of 9 August 1972.

With respect to the well-known shifting of spectral peaks during wave growth, Hasselmann et al. (1973) suggested that nonlinear energy transfer plays a dominant role in the process. They concluded that the spectral form results from the self-stabilizing property of the nonlinear interactions that continually readjust the energy distribution within the spectrum. We shall further explore these implications.

### 6.3 Temporal Growth of Unispectral Components

To examine the time-dependent behavior of the frequency components individually, we first smooth them in time by hanning and then plot them semi-logarithmically. The components have different time dependences, but they can be grouped into three frequency ranges. The results are shown in figure 9 for the 9 August episode, in figure 10 for the 30 September episode, and in figure 11 for the 7 October episode.

(1) Figures 9(a), 10(a), and 11(a) show the low-frequency group that contains components with frequencies less than all the peak-energy frequencies during the episode. The components in this group can be characterized by their sensitivity to the wind field. Their growth seems to follow directly with the increases in wind speed. The approximate linearity during the growth as shown in the logarithmic plot indicates the exponential growth that Miles' theory predicts.

(2) Figures 9(c), 10(c), and 11(c) show the high-frequency group that contains components with frequencies beyond the peak-energy frequencies during the episode. The components in this group represent the portion of the spectrum that is usually considered

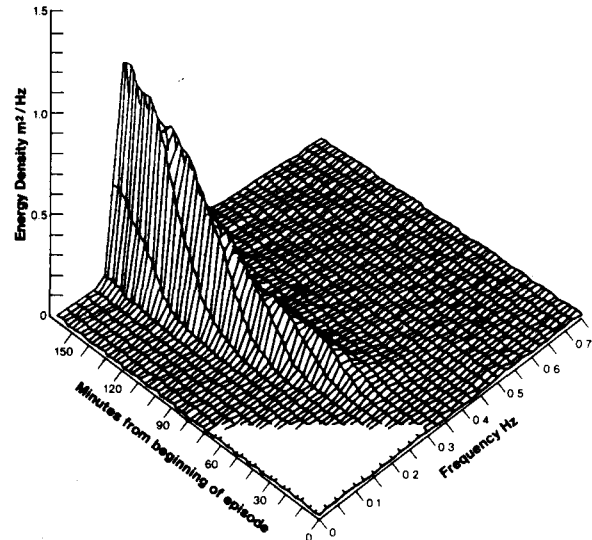


Figure 7.—Perspective view of the unispectrum during the episode of 30 September 1972.

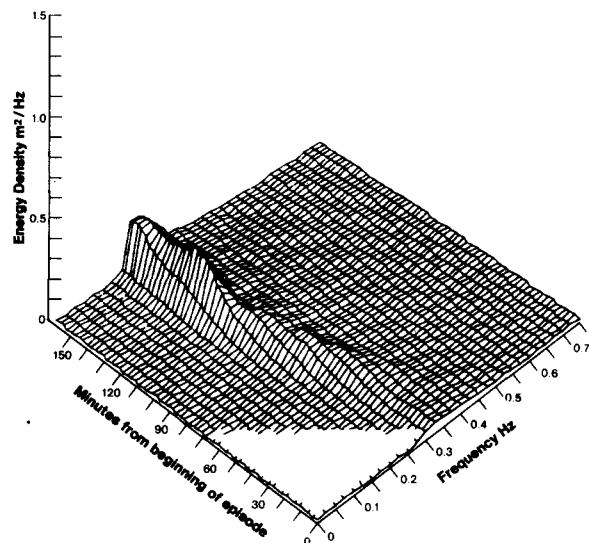


Figure 8.—Perspective view of the unispectrum during the episode of 7 October 1972.

to be the equilibrium range. They tend to parallel each other in time and are insensitive to either increasing wind speed or time duration. Some anomalous behavior shown in figure 10(c) during the early stage may be due to the fact that wind direction during this short time interval was changing continuously and thus further complicated the whole picture.

(3) Figures 9(b), 10(b), and 11(b) show the components, lying between groups 1 and 2, that have been peak frequency during the episode. The behavior of components in this group is complicated since they have mixed properties of both of the first two groups. This group contains a large part of the total spectral energy.

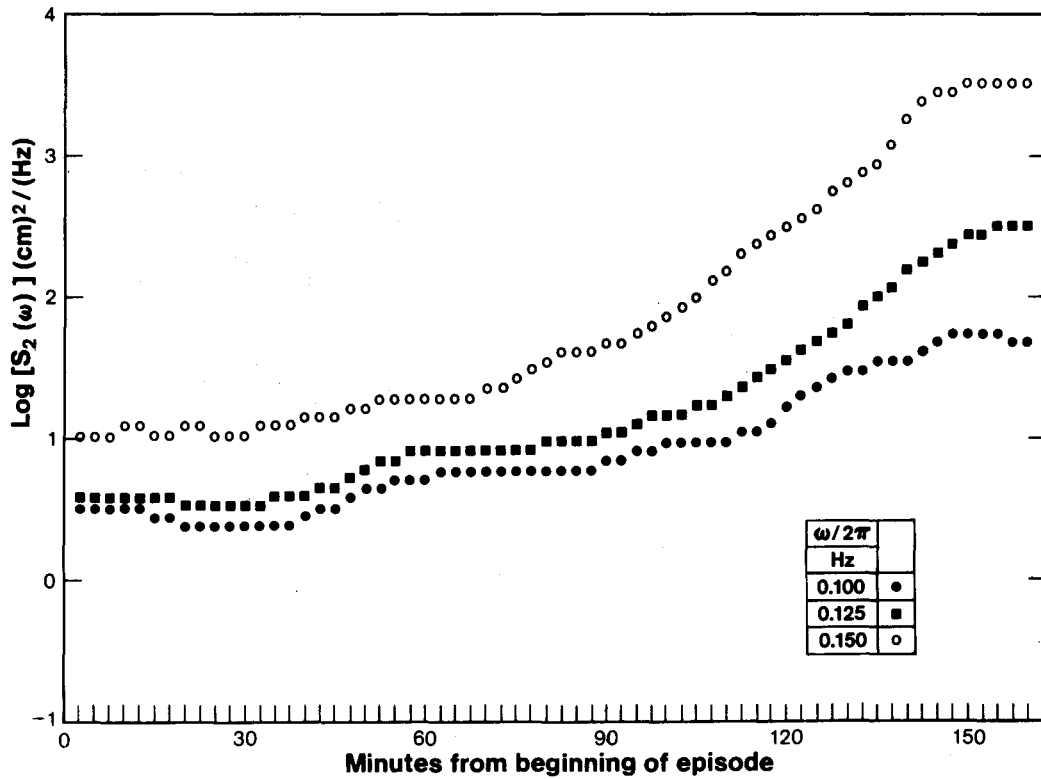


Figure 9a.—Growth of low-frequency unispectral components during the episode of 9 August 1972.

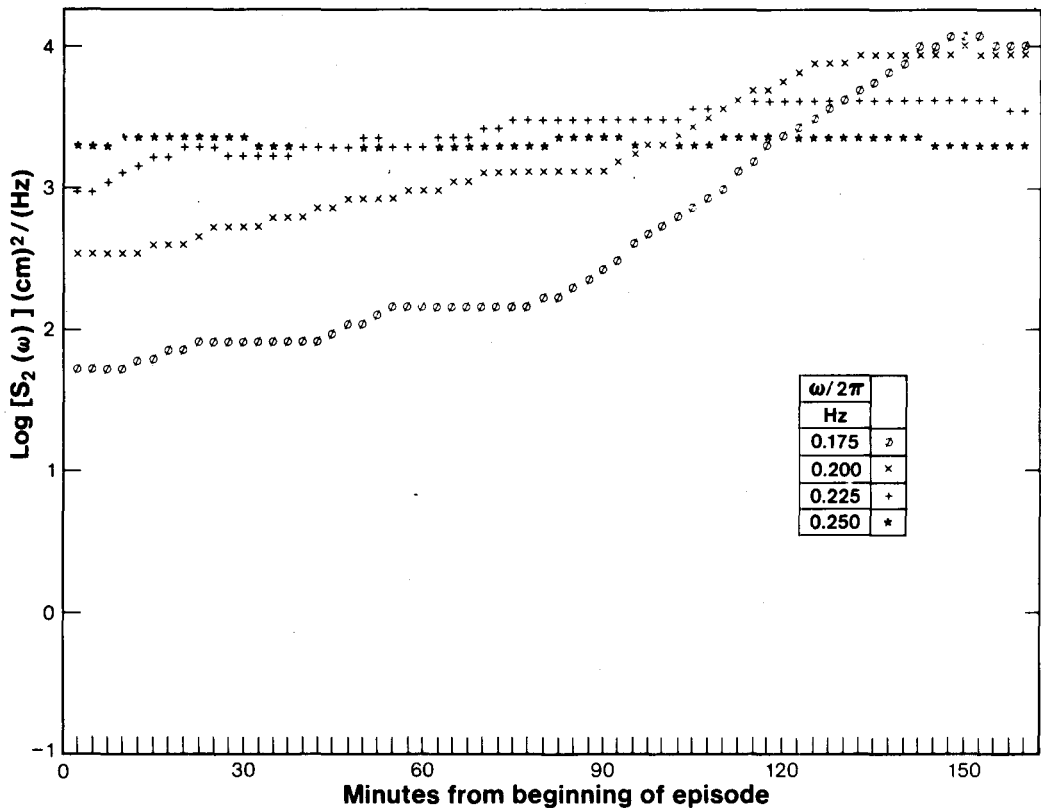


Figure 9b.—Growth of middle-frequency unispectral components during the episode of 9 August 1972.

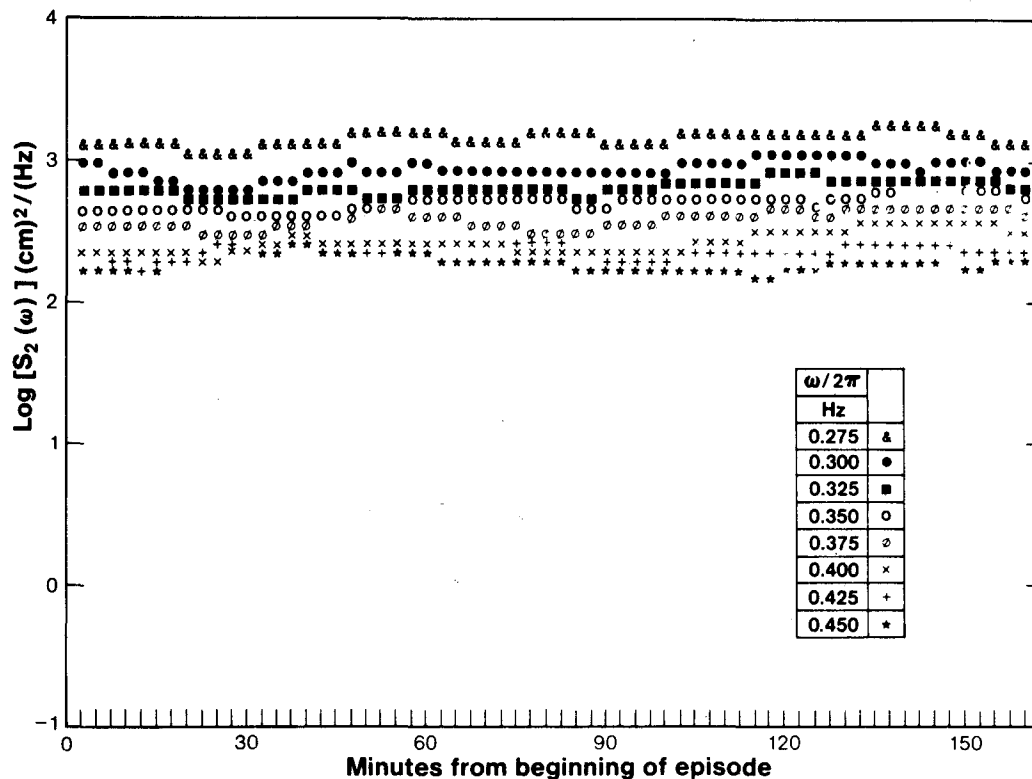


Figure 9c.—Growth of high-frequency unispectral components during the episode of 9 August 1972.

#### 6.4 The Source Function— Empirical and Theoretical

One of the main problems in developing wave growth models is determining the source function  $G$  in the energy balance equation (Gelci et al., 1956; Hasselmann, 1960):

$$\frac{\partial E}{\partial t} + \dot{\mathbf{x}} \cdot \nabla_{\mathbf{x}} E + \dot{\mathbf{K}} \cdot \nabla_{\mathbf{k}} E = G, \quad (38)$$

where  $E$  is the energy density, the second and third terms on the left side represent the advection and refraction of the processes, respectively; the dots denote the time derivatives. The source function  $G$  is the total rate of change of the energy representing all processes of generation, dissipation, and linear and nonlinear interactions. Most wave studies in recent years have aimed at assessing some aspects of the source function. Perhaps the most significant one is the Joint North Sea Wave Project (JONSWAP) in which Hasselmann et al. (1973) found that the nonlinear energy transfer, computed from integrating the theoretical Boltzmann integral (appendix C), is important for explaining the form of the wave spectrum during wave growth.

With the available temporal functions of the frequency components, we estimated  $\partial E / \partial t$  empirically for each spectrum  $S_2(\omega)$  by fitting a smooth cubic spline curve through the components and calculating

their time derivatives. For waves at a single location, if both the advection and refraction terms can be ignored in equation (38), the empirical  $\partial S_2(\omega) / \partial t$  also represents the empirical source function. (Given duration  $t$ , fetch  $L$ , and group velocity  $v$ , advection can be neglected if  $t \ll L/v$ . This condition is generally satisfied in this study since duration is small for increasing wind speed and fetch is large during the episodes.)

Hasselmann et al. (1973) also calculated empirical source functions by parameterization of (38). Their method includes the advection term. However, they give only one average source function for each episode. Our method, on the other hand, provides consecutive source functions throughout the episode and thus more detailed information.

With these empirical source functions available, the next task is to correlate them with the theoretical nonlinear source functions. The numerical integration of the Boltzmann integral by Sell and Hasselmann (1972) requires 30 minutes of computer time for each spectrum and, at this stage, is rather impractical. In appendix C we show that Barnett's (1966) parameterization of Hasselmann's earlier calculations (1963a,b) leads to essentially the same conclusions as those obtained by Sell and Hasselmann. Therefore we choose to use the low-frequency part of the results calculated from Barnett's parameterized scheme to represent the theoretical nonlinear source function in

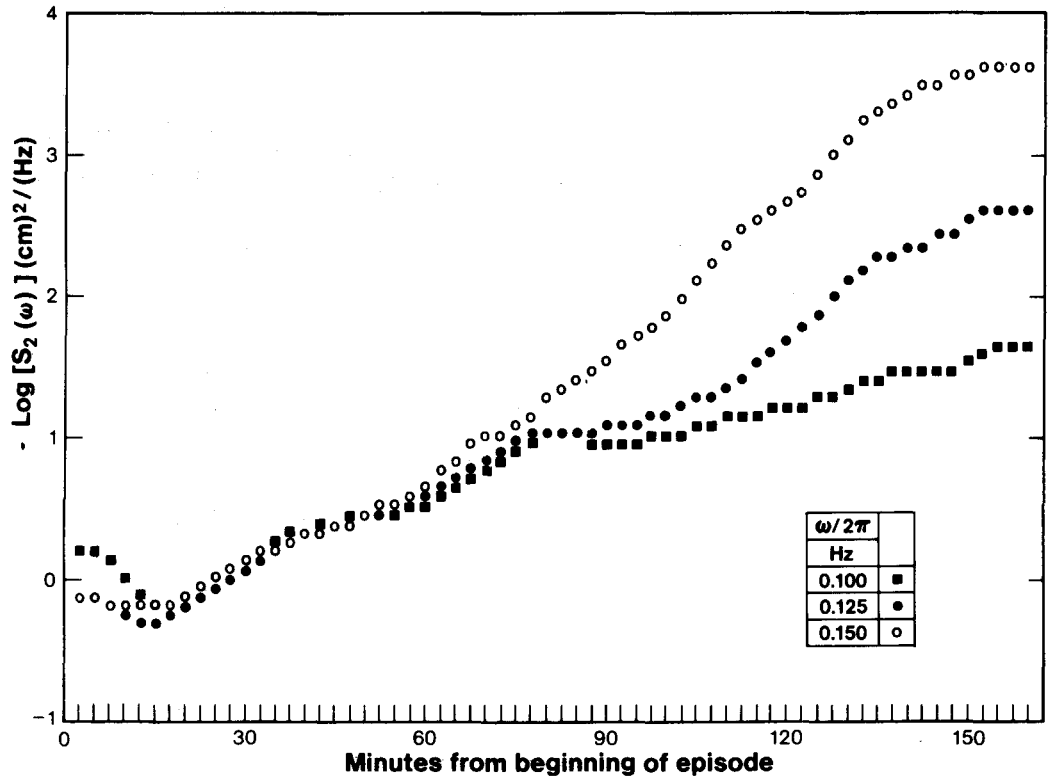


Figure 10a.—Growth of low-frequency unispectral components during the episode of 30 September 1972.

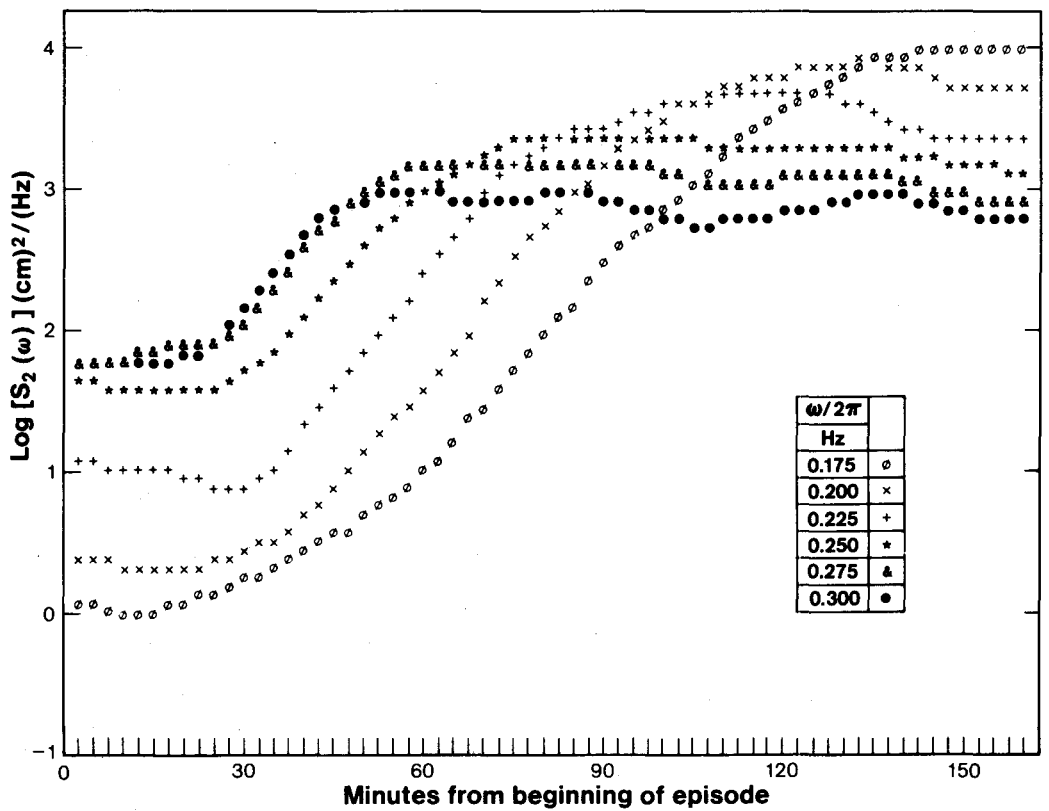


Figure 10b.—Growth of middle-frequency unispectral components during the episode of 30 September 1972.

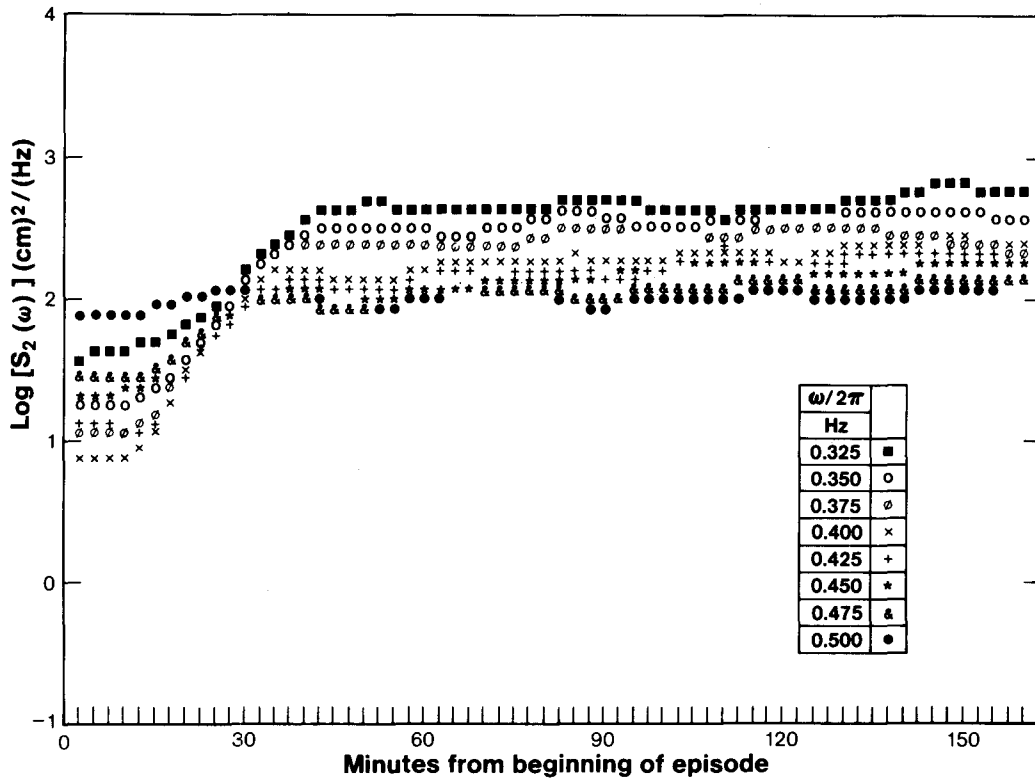


Figure 10c.—Growth of high-frequency unispectral components during the episode of 30 September 1972.

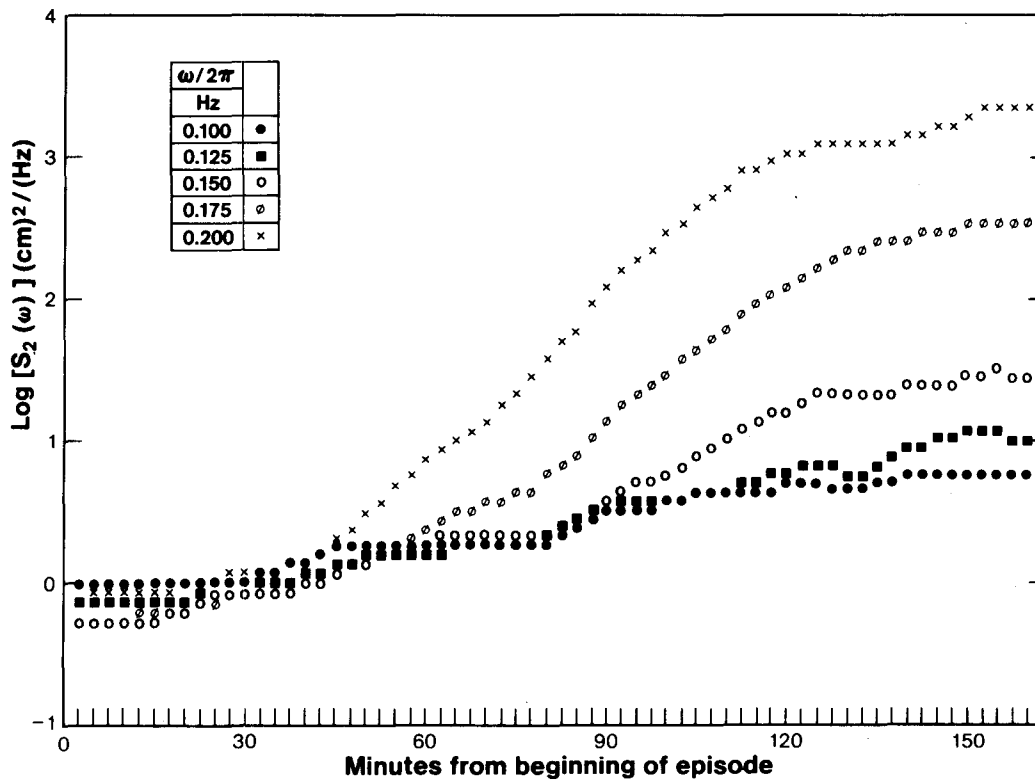


Figure 11a.—Growth of low-frequency unispectral components during the episode of 7 October 1972.

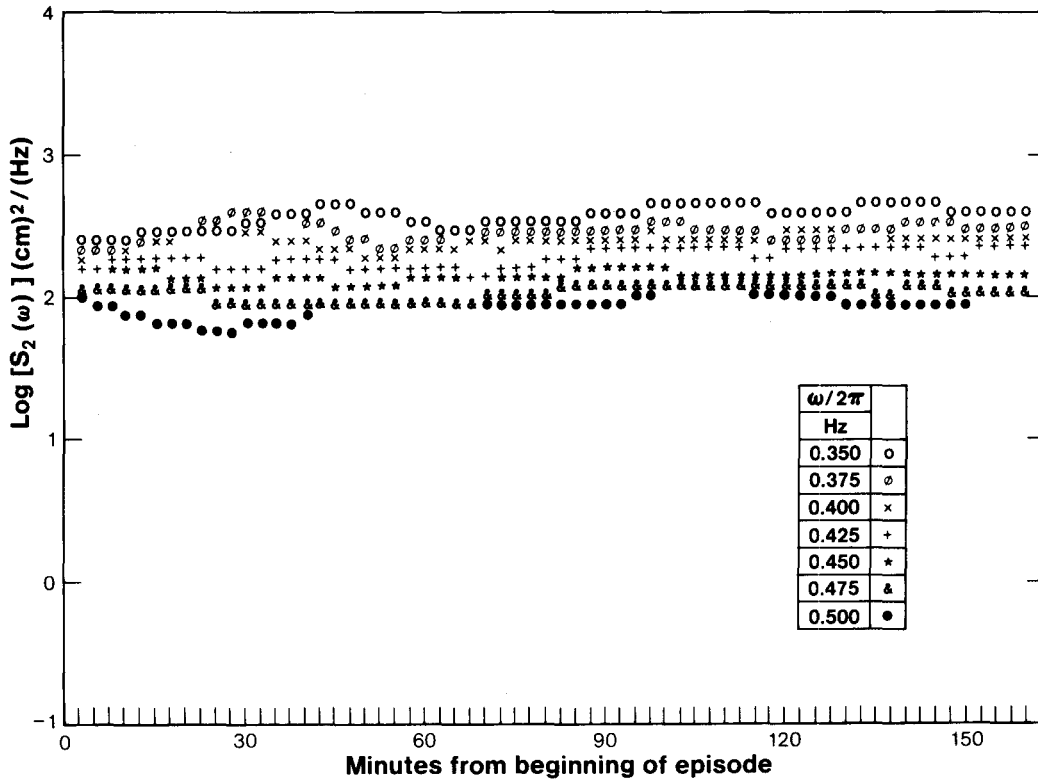


Figure 11b.—Growth of middle-frequency unispectral components during the episode of 7 October 1972.

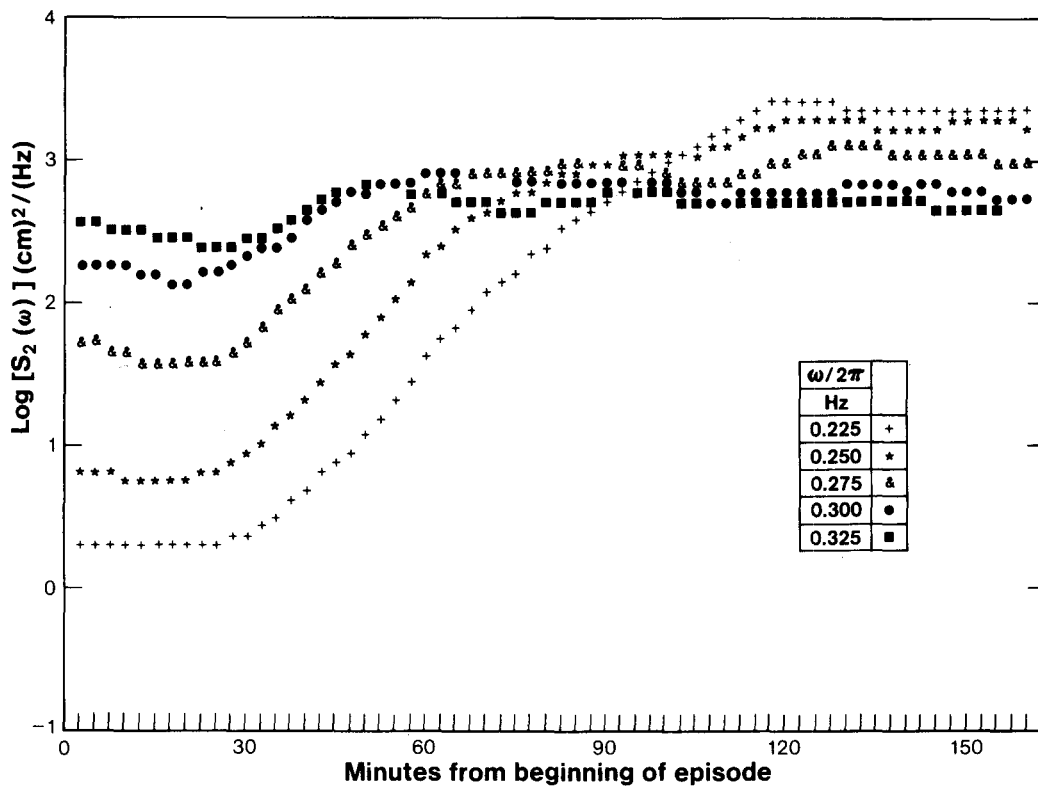


Figure 11c.—Growth of high-frequency unispectral components during the episode of 7 October 1972.

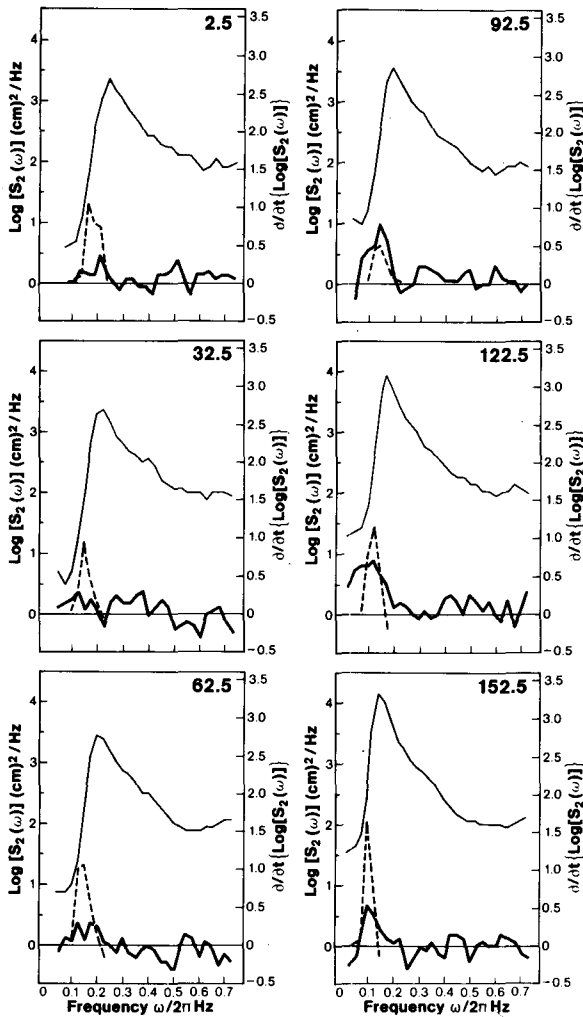


Figure 12.—Unispectra (—) and empirical (—) and Barnett's (····) source functions during the episode of 9 August 1972. The numbers 2.5, 32.5, . . . , and 152.5 are minutes from beginning of episode.

our subsequent comparisons. (More recently, Wu et al. (1979) also used Barnett's parametric equation in calculating nonlinear energy transfer and found good comparisons in the low and intermediate frequency region of a wave spectrum.) We ignore the high frequency part of the parameterized results because it was based on Neumann's (1953) assumption that energy density is proportional to  $\omega^{-6}$  at the high frequency side rather than to  $\omega^{-5}$ , which most recent studies have confirmed as correct. The results for the three episodes are shown in figures 12, 13, and 14. Because of gradual changes in the process, we present only six spectra and source functions for each episode at 30 minutes apart to show the essential features. In the figures we plot the logarithm of unispectra  $\log S_2(\omega)$ , and the empirical and calculated  $\partial[\log S_2(\omega)]/\partial t$  all with respect to the frequency of  $\omega/2\pi$ . The distinction between the empirical and calculated "theoretical" source functions is quite evident. The theoretical source function consistently has large

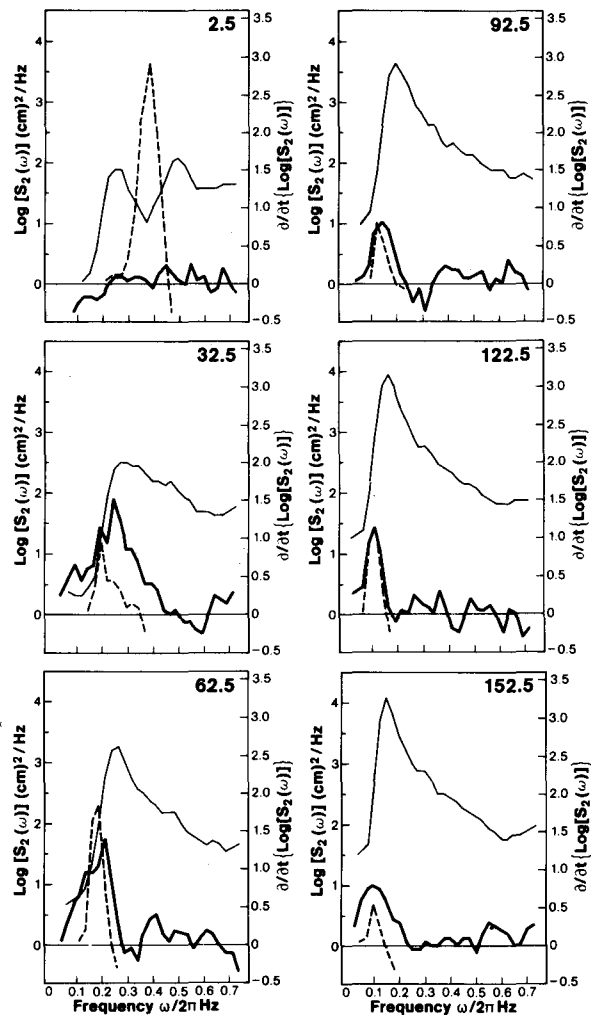


Figure 13.—Unispectra (—) and empirical (—) and Barnett's (····) source functions during the episode of 30 September 1972. The numbers 2.5, 32.5, . . . , and 152.5 are minutes from beginning of episode.

positive lobes at frequencies below the peak-energy frequency. The empirical source function develops similar positive lobes only toward latter stages of the episode when the growth activity is intense. At the beginning of the episode when the growth is generally slow or when the waves are well developed and further growth is slowing down, the empirical source function tends to be much less pronounced in its lobes, positive and negative.

This behavior of the empirical and theoretical source functions is not particularly surprising since the theoretical results are dependent on the shape of the spectrum whereas the empirical results are dependent on temporal changes in the spectrum. This also provides a possible explanation for the dominance of nonlinear interactions during growth. If we assume that the empirical results represent the complete source function and the theoretical results only the nonlinear interactions, their differences then represent the other processes, such as wave breaking and

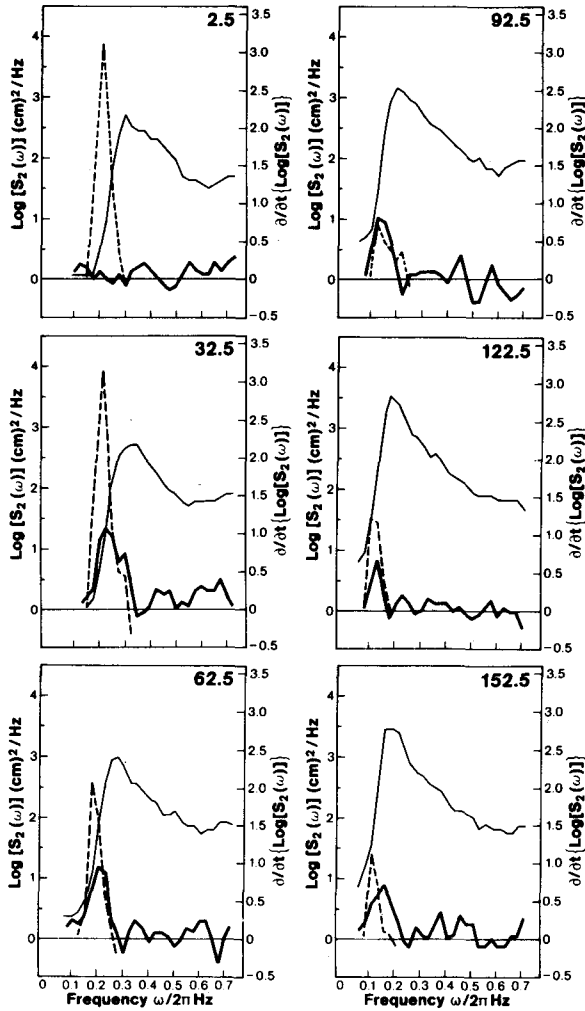


Figure 14.—Unispectra (—) and empirical (—) and Barnett's (---) source functions during the episode of 7 October 1972. The numbers 2.5, 32.5, . . . , and 152.5 are minutes from beginning of episode.

dissipation. At the beginning of the episode, when growth is generally slow or when the waves are well developed and growth is also slowing down, the nonlinear interactions must be balanced by some equally important dissipation process in order to yield the smaller total source function. During rapid growth, on the other hand, both the nonlinear interactions and the total source functions have large positive peaks, which implies that dissipation is less significant and that most of the growth is through nonlinear interaction.

### 6.5 The Bispectra

There are three published bispectral studies on wind-generated waves: Hasselmann, Munk, and McDonald (1962), and Garrett (1970) compared four bispectra computed from actual wave data with those theoretically derived and found satisfactory

agreement, and Houmb (1974) presented three examples of computed wave bispectra. In the present study we are interested in the higher order interactions during wave growth. As a first step we have computed 64 consecutive bispectra for each of the three growth episodes. Because the temporal variations are gradual, we present only six bispectra from each episode at 30 minutes apart as representative of the whole process. Figures 15, 16, and 17 show the sample bispectra for episodes 9 August, 30 September, and 7 October.

Since the bispectrum  $S_3(\omega_1, \omega_2)$ , computed from equation (36), is complex, it is convenient to express it as a bispectral amplitude rather than as co-bispectra and quadrature-bispectra separately. Figures 15, 16, and 17 show the contours of the logarithms of bispectral amplitude plotted in the fundamental region of  $0 \leq \omega_2 \leq \omega_1$  and  $0 \leq \omega_1 \leq \omega_N$ .

Several main features can be seen in these figures:

(1) The bispectrum has a hill at  $(\omega_p, \omega_p)$ , where  $\omega_p$  is the frequency of the spectral peak in the corresponding unispectrum.

(2) Each bispectrum also shows two ridges approximately parallel to the two frequency axes and sloping down from the bispectral hill toward both higher and lower frequencies.

(3) The magnitude of the bispectral amplitude increases and the hills and ridges migrate toward lower frequencies during wave growth.

(4) These observed characteristics are qualitatively similar to those depicted by Hasselmann, Munk, and McDonald's (1962) deep-water wave co-bispectrum.

It is not readily discernible that these features result from a nonlinear process. However, from the qualitative resemblance to Hasselmann, Munk, and McDonald's results and the fact that their results agree with those derived from a theoretical nonlinear process, we may conjecture that these features are characteristic of a weakly nonlinear wave growth process and hence proceed to examine their temporal behavior.

### 6.6 Temporal Growth of Bispectral Components

Since the predominant bispectral interactions occur when the frequency of the spectral peak in the corresponding unispectrum interacts with itself and these interactions migrate toward lower frequencies during wave growth, it is sufficient that we examine the time-dependent behavior of those bispectral components on the  $45^\circ$  line whose frequencies interact with themselves. We proceed in a manner similar to that for unispectral components by temporally smoothing them with hanning and then plotting them semi-logarithmically as a function of time. The results are quite similar to those unispectral components. We again separate them into three groups for the three episodes (figures 18, 19, and 20).

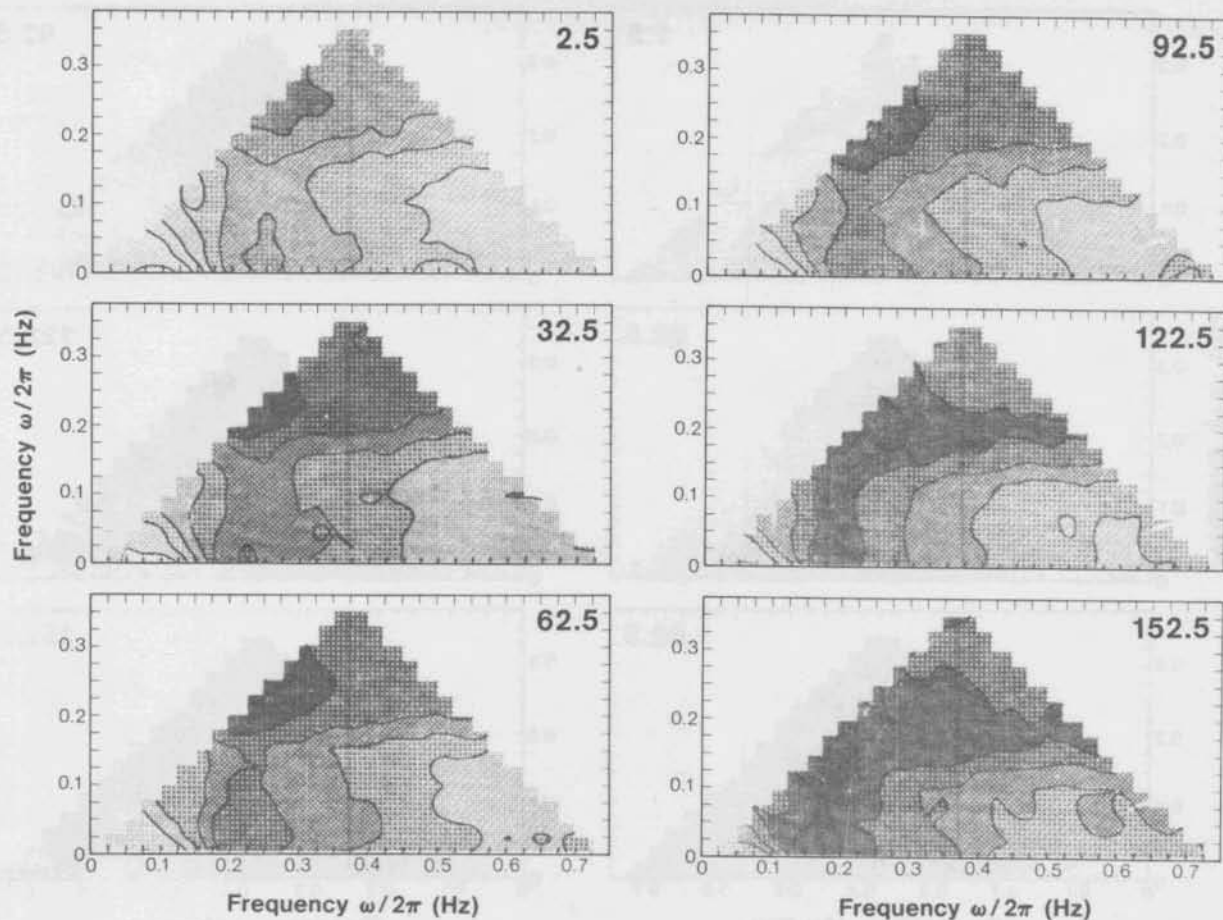


Figure 15.—Bispectra during the episode of 9 August 1972. The numbers 2.5, 32.5, . . . , and 152.5 are minutes from beginning of episode.

Several points should be noted here:

(1) The figures are plotted with  $\log[S_3(\omega, \omega)]$  versus linear time as before but with a smaller range. Consequently the exponential growth rates shown in figures 18, 19, and 20 that appear comparable with those shown in figures 9, 10, and 11 are actually about four times smaller.

(2) We have seen that in unispectral growth the spectral peak moves to a lower frequency during wave growth. The bispectra provide some indication of phenomena that can be attributed to this transfer, namely, that the interactions of the peak frequency with the next lower frequency grow consistently stronger relative to the interactions with the next higher frequency during the latter part of the growth. Examples are shown in figures 21, 22, and 23. As growth continues, the component of the next lower frequency eventually becomes the spectral peak.

(3) If the bispectral amplitudes represent the second-order nonlinear interactions in the wave growth process, as we have conjectured, then our results show that the nonlinear interactions should also have functional relationships with respect to time. This is not unexpected. Since the theoretical nonlinear

source term is a function of the unispectrum, it must vary with time if the unispectrum does.

## 6.7 The Trispectra

Brillinger and Rosenblatt (1967) presented one set of calculated trispectra for daily sunspot numbers. Their work represents the only trispectral calculations available in the literature. They did not, however, provide an interpretation of their results. Trispectral analysis has remained relatively unexplored.

By extending the calculation scheme Haubrich (1965) used in bispectral calculations one step further and using equation (37), we have been able to calculate a trispectrum for each of the 64 data segments for each episode. It is not immediately clear how to visualize and present the trispectra effectively. It is even more cumbersome to try to present them in time. Since the fundamental region for the trispectrum is the tetrahedron defined by  $0 \leq \omega_3 \leq \omega_2$ ,  $0 \leq \omega_2 \leq \omega_1$ , and  $0 \leq \omega_1 \leq \omega_N$ , we have the trispectral density  $S_4(\omega_1, \omega_2, \omega_3)$  in addition to the three frequency axes to form a four-dimensional manifold imbedded in three-dimensional Euclidean geometry. By

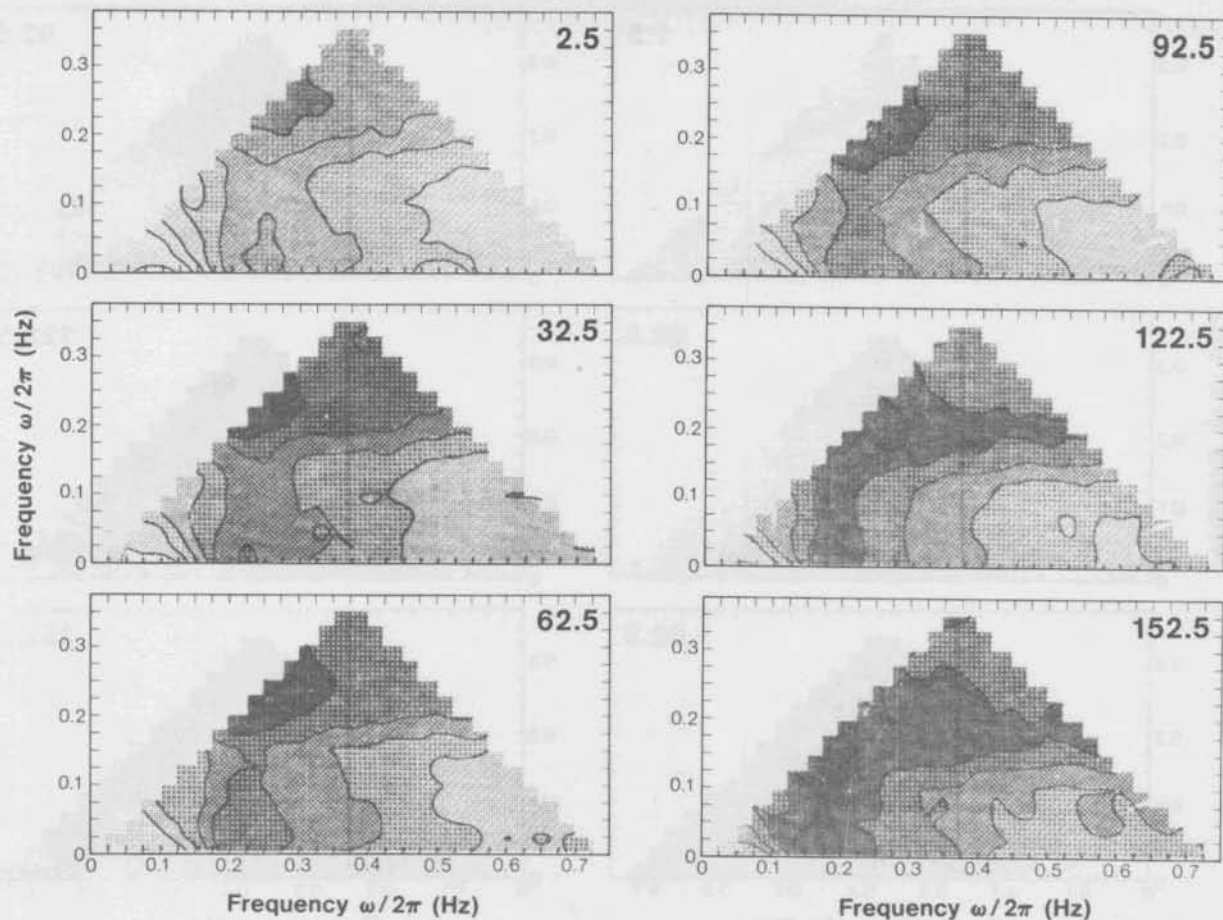


Figure 15.—Bispectra during the episode of 9 August 1972. The numbers 2.5, 32.5, . . . , and 152.5 are minutes from beginning of episode.

Several points should be noted here:

(1) The figures are plotted with  $\log[S_3(\omega, \omega)]$  versus linear time as before but with a smaller range. Consequently the exponential growth rates shown in figures 18, 19, and 20 that appear comparable with those shown in figures 9, 10, and 11 are actually about four times smaller.

(2) We have seen that in unispectral growth the spectral peak moves to a lower frequency during wave growth. The bispectra provide some indication of phenomena that can be attributed to this transfer, namely, that the interactions of the peak frequency with the next lower frequency grow consistently stronger relative to the interactions with the next higher frequency during the latter part of the growth. Examples are shown in figures 21, 22, and 23. As growth continues, the component of the next lower frequency eventually becomes the spectral peak.

(3) If the bispectral amplitudes represent the second-order nonlinear interactions in the wave growth process, as we have conjectured, then our results show that the nonlinear interactions should also have functional relationships with respect to time. This is not unexpected. Since the theoretical nonlinear

source term is a function of the unispectrum, it must vary with time if the unispectrum does.

## 6.7 The Trispectra

Brillinger and Rosenblatt (1967) presented one set of calculated trispectra for daily sunspot numbers. Their work represents the only trispectral calculations available in the literature. They did not, however, provide an interpretation of their results. Trispectral analysis has remained relatively unexplored.

By extending the calculation scheme Haubrich (1965) used in bispectral calculations one step further and using equation (37), we have been able to calculate a trispectrum for each of the 64 data segments for each episode. It is not immediately clear how to visualize and present the trispectra effectively. It is even more cumbersome to try to present them in time. Since the fundamental region for the trispectrum is the tetrahedron defined by  $0 \leq \omega_3 \leq \omega_2$ ,  $0 \leq \omega_2 \leq \omega_1$ , and  $0 \leq \omega_1 \leq \omega_N$ , we have the trispectral density  $S_4(\omega_1, \omega_2, \omega_3)$  in addition to the three frequency axes to form a four-dimensional manifold imbedded in three-dimensional Euclidean geometry. By

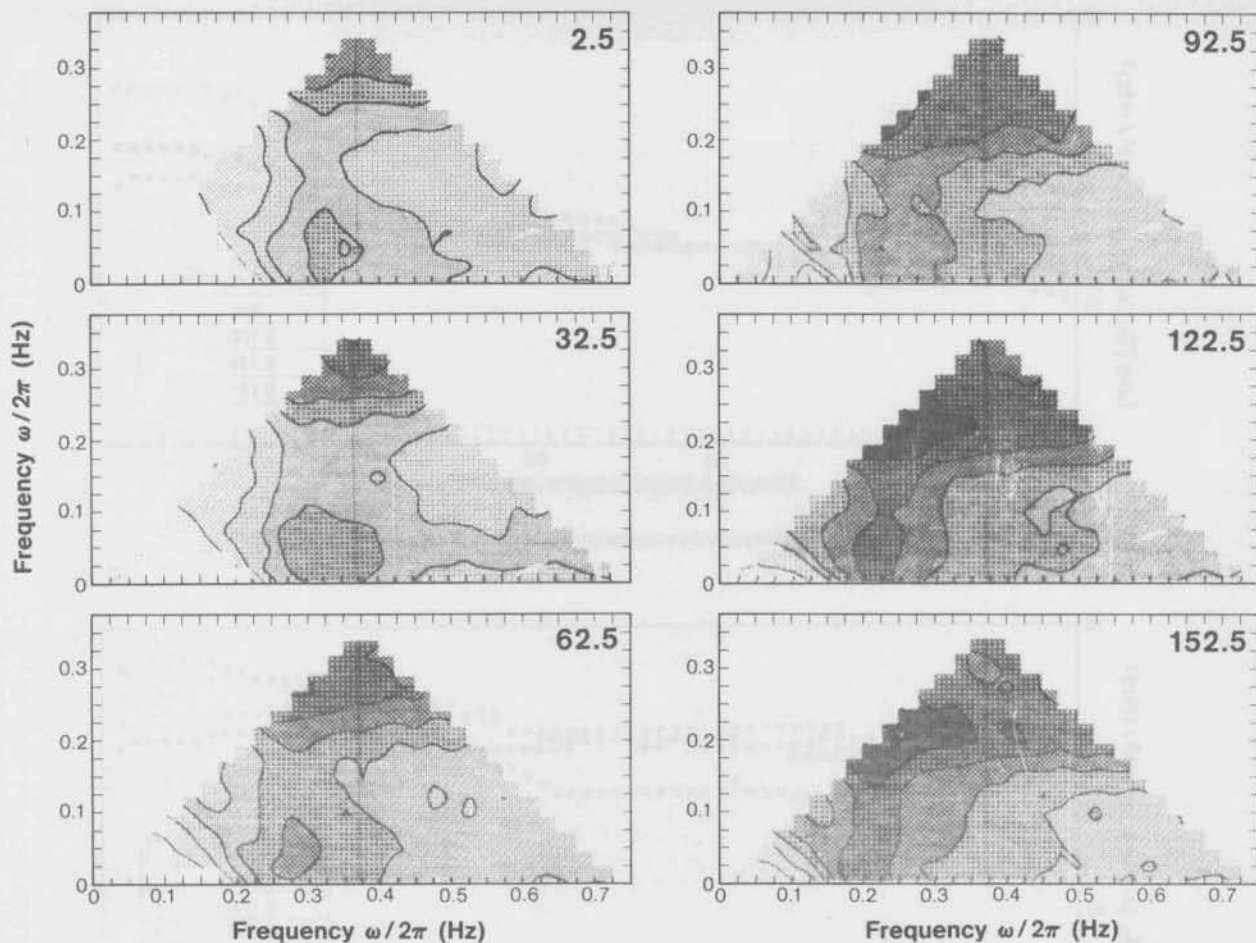


Figure 17.—Bispectra during the episode of 7 October 1972. The numbers 2.5, 32.5, . . . , and 152.5 are minutes from beginning of episode.

time. The results, shown in figures 25, 26, and 27, are again quite similar to the unispectral and bispectral components. Since we have only the lower frequency components, grouping is not necessary. The results show again that the third-order interactions have functional relationships with respect to time during the wave growth process.

In figures 28, 29, and 30, we concentrate on the peak-energy frequency achieved at the latter stage of the episode by plotting the temporal growth of the frequency interacting with itself to the third order, the frequency interacting with itself and the next lower frequency, and the frequency interacting with the second-order interaction of the next higher frequency. These figures show quite clearly that the shifting of the peak-energy frequency toward the lower frequency is due to the stronger interactions of the peak-energy frequency with the lower frequency and that the interaction provides energy transfer from the peak-energy frequency to the lower frequency. This confirms that the higher-order nonlinear interactions are responsible for the shifting of spectral peaks during wave growth.

### 6.9 Further Remarks on Bispectra and Trispectra

What have we gained from bispectral and trispectral analysis? First, we have developed methods for computing and presenting bispectra and trispectra from data. This experience will be useful in the future. Second, and more important, we have presented evidence that during the later intensive part of wave growth, the interactions of the peak-energy frequency component with the next lower frequency component grow consistently stronger compared with the interactions with the next higher frequency component, and the next lower frequency subsequently becomes the peak-energy frequency. This result, which provides a clear explanation for the well-known fact of shifting spectral peaks toward lower frequencies, can be demonstrated only by bispectral and trispectral analysis.

Benjamin and Feir (1967) showed theoretically and experimentally that for deep-water waves with a fundamental frequency  $\omega$ , because of coupling through the nonlinear boundary conditions at the

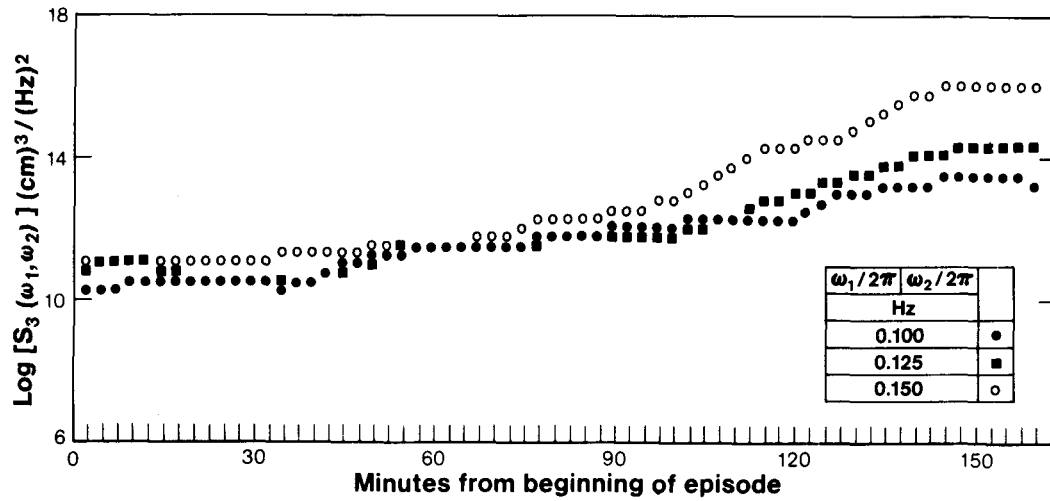


Figure 18a.—Growth of low-frequency bispectral components during the episode of 9 August 1972.

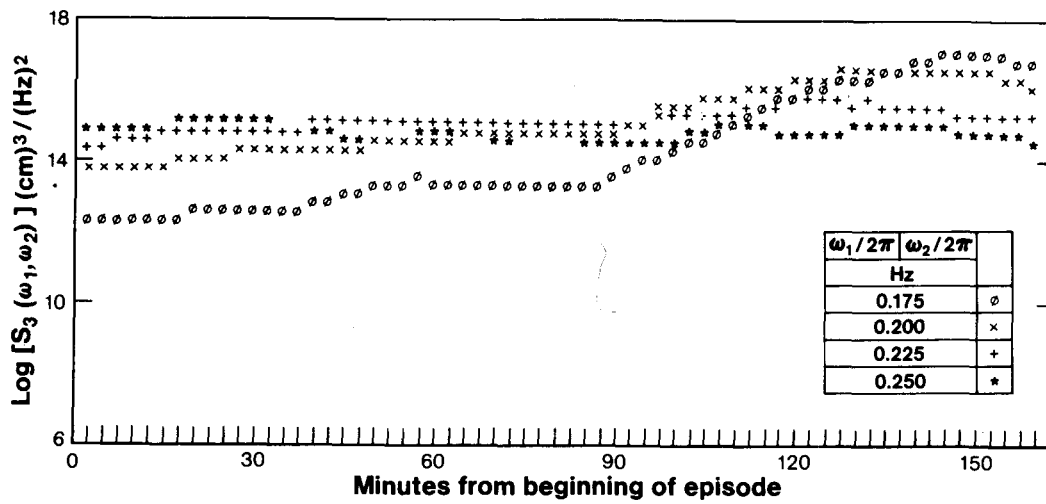


Figure 18b.—Growth of middle-frequency bispectral components during the episode of 9 August 1972.

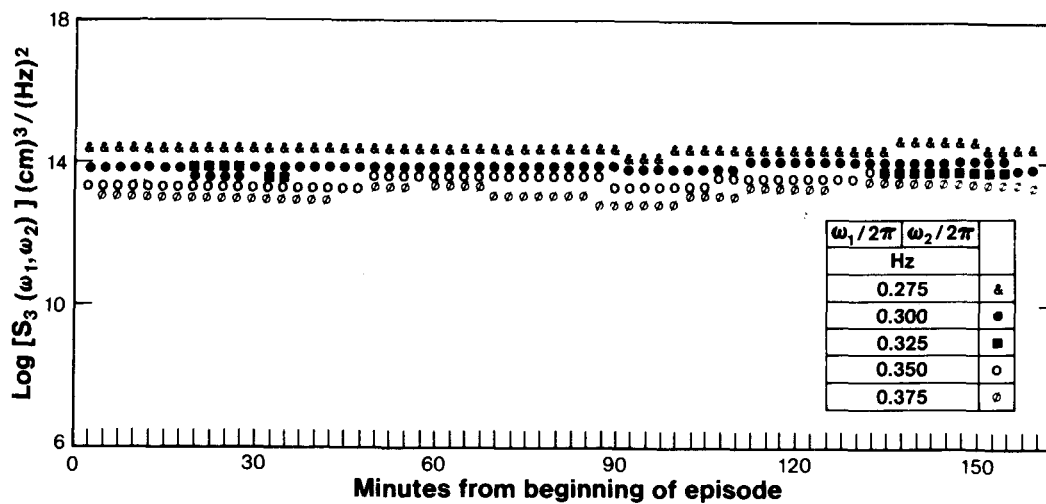


Figure 18c.—Growth of high-frequency bispectral components during the episode of 9 August 1972.

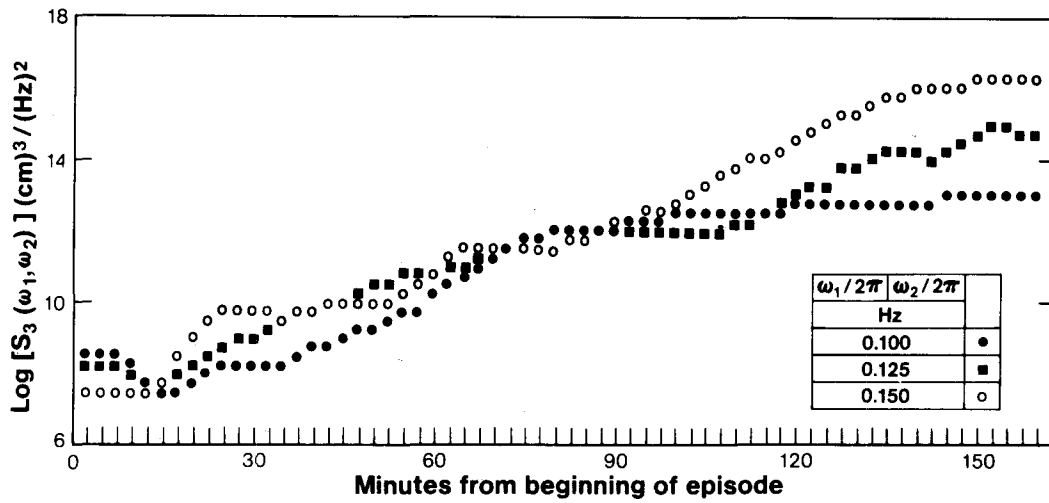


Figure 19a.—Growth of low-frequency bispectral components during the episode of 30 September 1972.

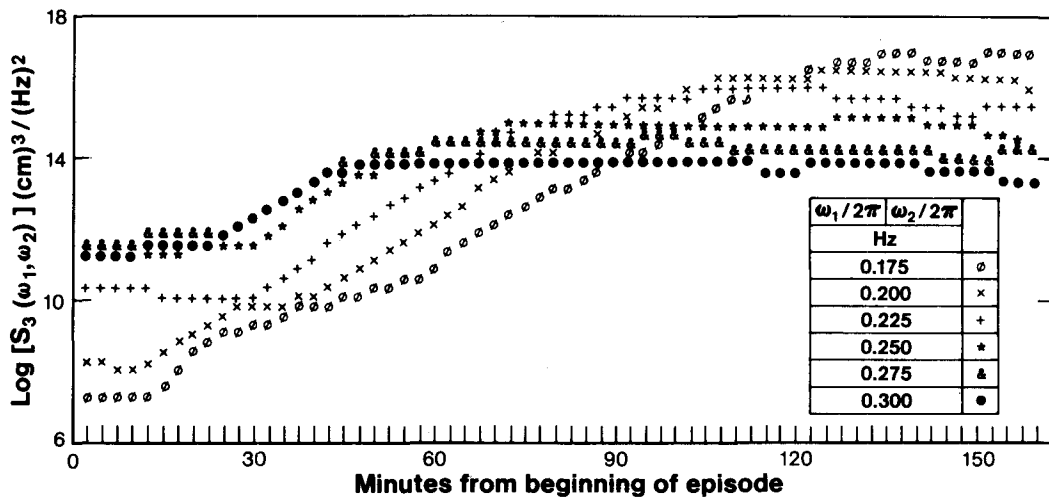


Figure 19b.—Growth of middle-frequency bispectral components during the episode of 30 September 1972.

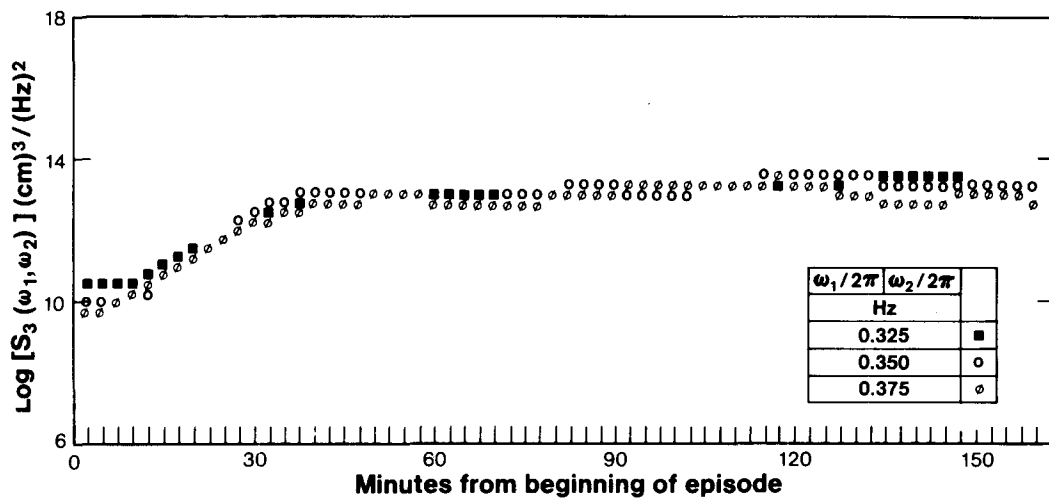


Figure 19c.—Growth of high-frequency bispectral components during the episode of 30 September 1972.

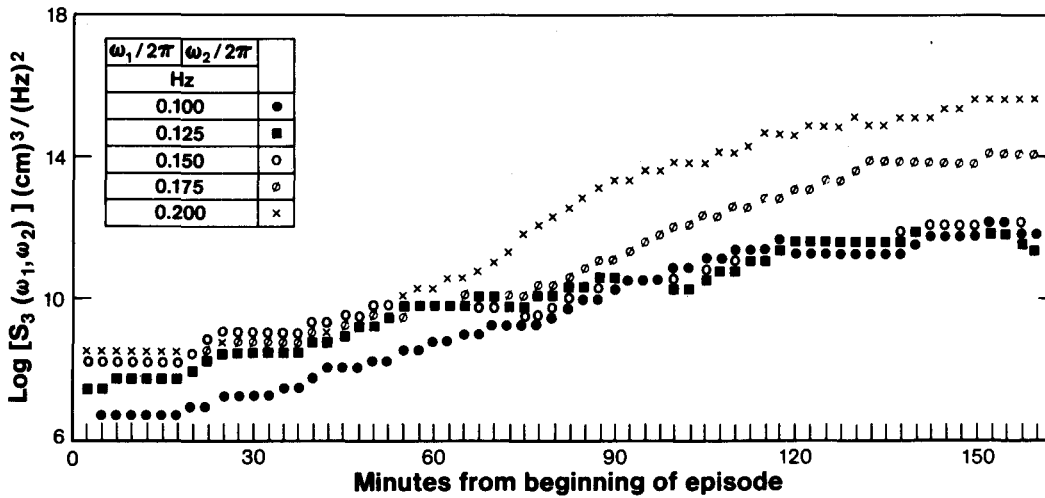


Figure 20a.—Growth of low-frequency bispectral components during the episode of 7 October 1972.

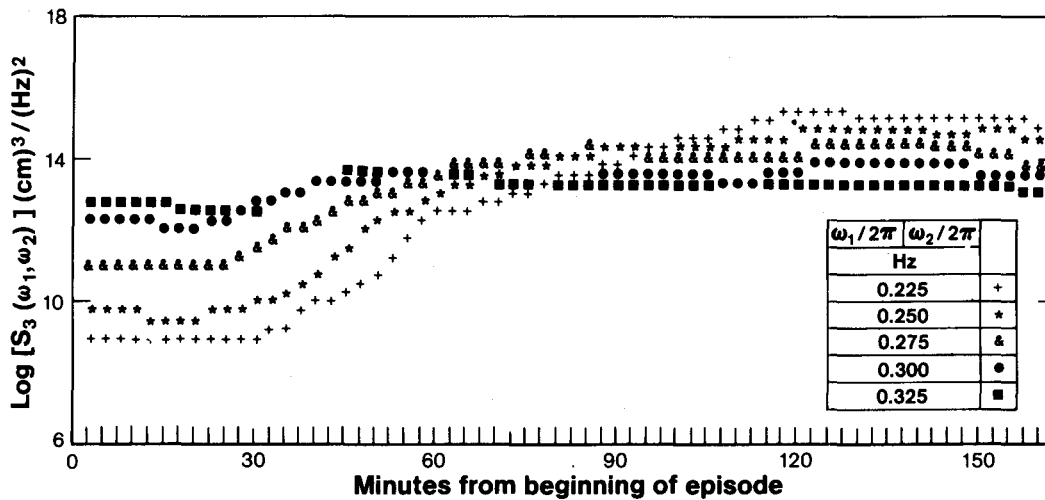


Figure 20b.—Growth of middle-frequency bispectral components during the episode of 7 October 1972.

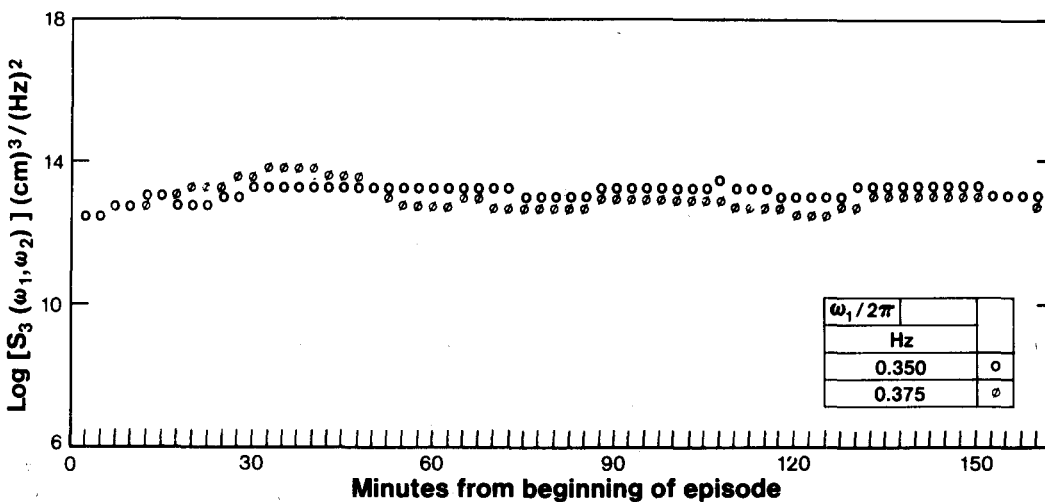


Figure 20c.—Growth of high-frequency bispectral components during the episode of 7 October 1972.

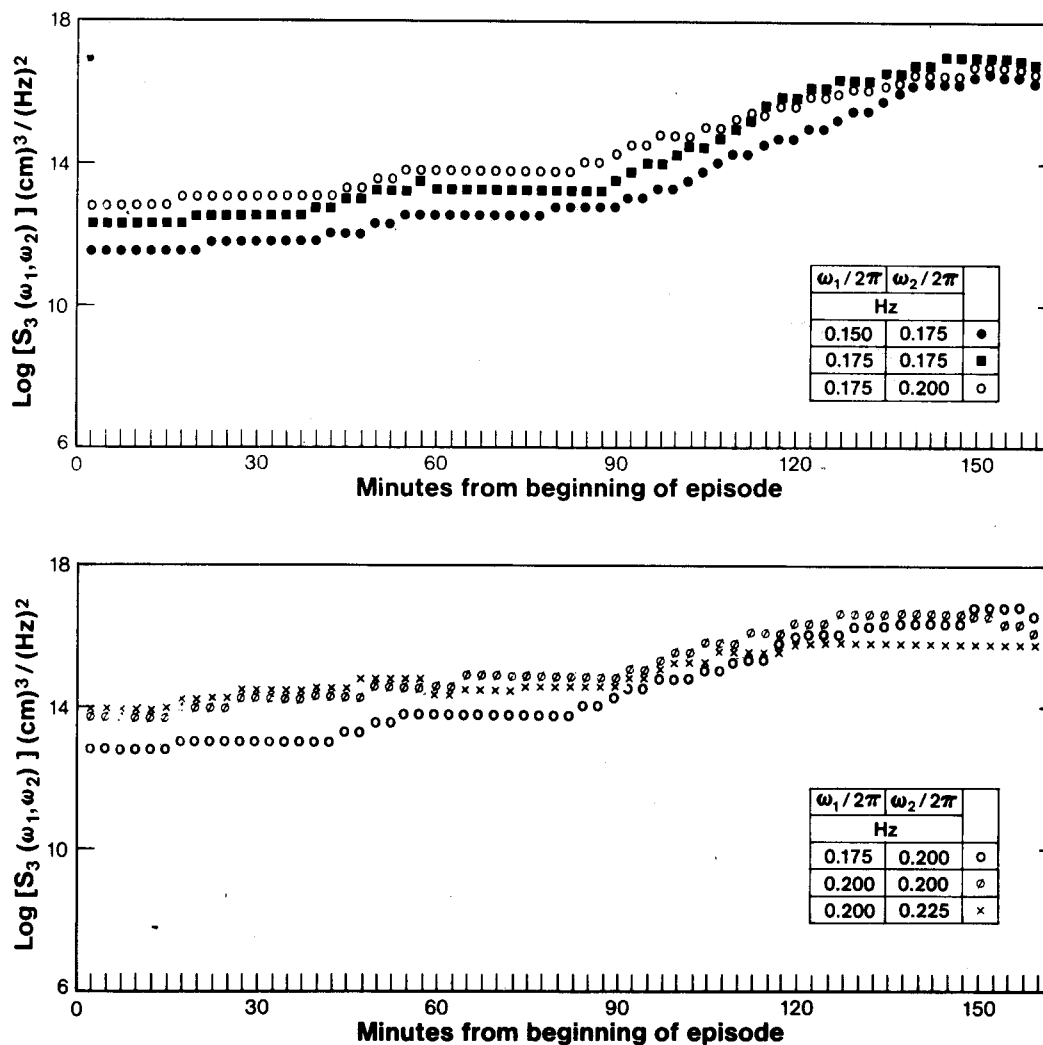


Figure 21.—Growth of bispectral components during the episode of 9 August 1972. Above: 0.175 Hz vs. 0.150, 0.175, and 0.200 Hz; Below: 0.200 Hz vs. 0.175, 0.200, and 0.225 Hz.

free surface, energy is transferred to the side-band frequencies  $\omega (1 \pm \zeta)$ . Our results appear to resemble, to some extent, this side-band energy transfer theory. We may conjecture that, analogously, the stronger interaction with the lower side-band frequency component than with the higher side-band frequency component is also due to the complicated couplings of the nonlinear boundary conditions at the free surface. Furthermore, Longuet-Higgins's (1976) recent theory, indicating that the transfer of energy tends to reduce any symmetry in the spectrum, can also be qualitatively attributed to these unequal side-band interactions.

## 7. SUMMARY AND CONCLUDING REMARKS

In this report we set out to empirically examine the temporal growth processes of wind-generated waves using data recorded in Lake Ontario. We have examined unispectra, bispectra, and trispectra computed consecutively for the three selected episodes. The scheme used for our study is based on the assumed property of local stationarity. This assumption allows us to apply successfully the analysis method developed for stationary processes to study nonstationary wave growth processes.

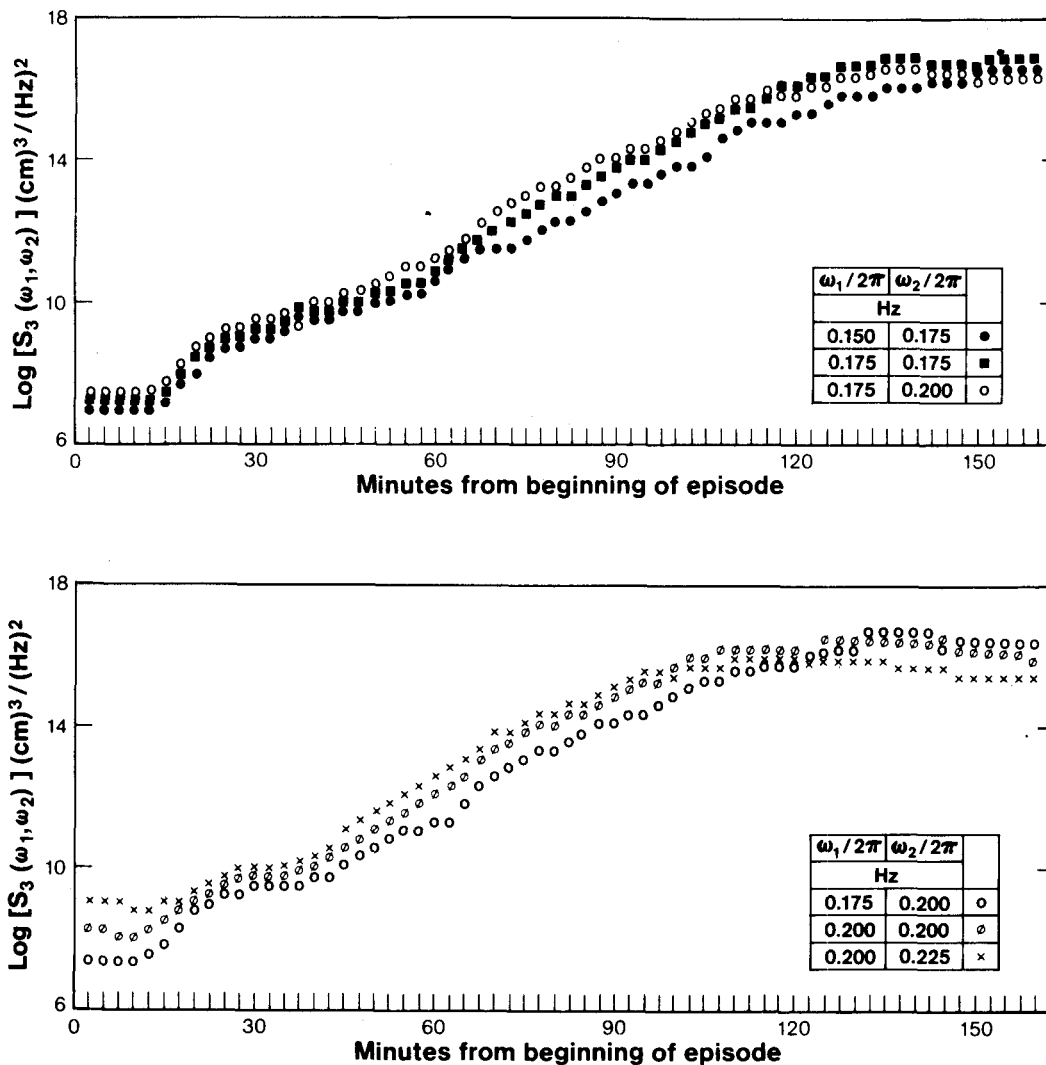


Figure 22.—Growth of bispectral components during the episode of 30 September 1972. Above: 0.175 Hz vs. 0.150, 0.175, and 0.200 Hz; Below: 0.200 Hz vs. 0.175, 0.200, and 0.225 Hz.

Results can be summarized as follows:

- (1) Wind waves grow fastest during increasing wind speeds.
- (2) Each unispectral component has a different temporal growth rate. The components can be grouped into three frequency groups: the low-frequency components, which consistently grow under increasing wind speeds; the high-frequency components, which are insensitive to wind speed and time; and the mid-frequency components, which contain those attaining spectral peaks during the episode and which contain mixed properties of both high- and low-frequency component groups.

(3) Bispectral and trispectral components generally demonstrate temporal growth behavior similar to that of unispectral components with smaller growth rates.

(4) From comparing empirical source functions with parameterized theoretical nonlinear source functions, we found that at the beginning and ending stages of wave growth the growth rate is low and the empirical source function is smaller; the larger nonlinear source function under the spectral peak must be balanced by significant dissipation processes. During intensive wave growth, where nonlinear and empirical source functions are both large, dissipation

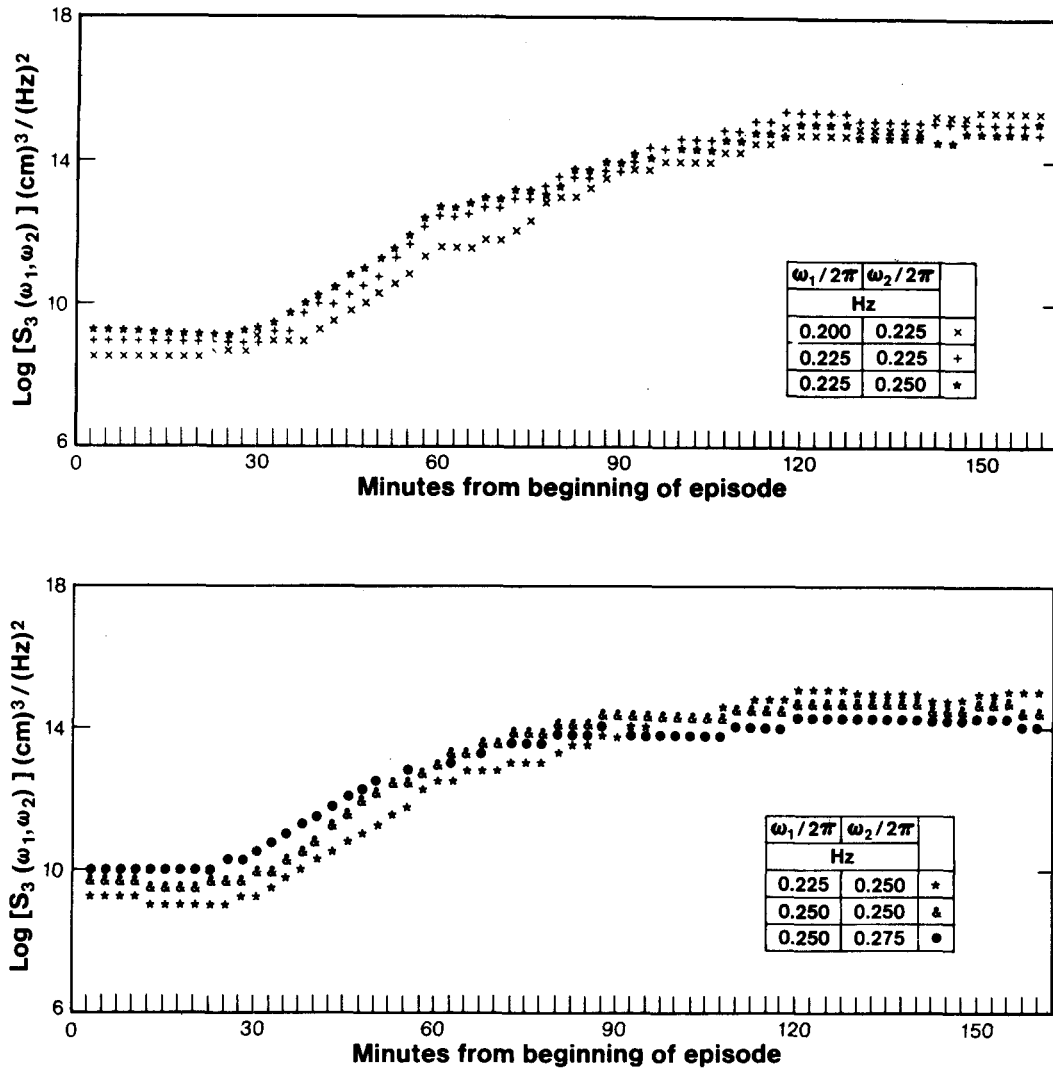


Figure 23.—Growth of bispectral components during the episode of 7 October 1972. Above: 0.225 Hz vs. 0.200, 0.225, and 0.250 Hz; Below: 0.250 Hz vs. 0.225, 0.250, and 0.275 Hz.

becomes less significant.

(5) During the latter part of wave growth, the interactions of the peak-energy frequency component with the next lower frequency component grow consistently stronger than the interactions with the next higher frequency component, and the next lower frequency subsequently becomes the peak-energy frequency. This result, as demonstrated clearly from an examination of the temporal growth of bispectral and trispectral components, provides an explanation for the well-known fact of unispectral peaks shifting toward lower frequencies during wave growth.

These results are consistent with our primary in-

terest of exploring the empirical aspects. Since the detailed process of wave growth is still far from being completely understood, we hope our results will provide some insight that can be useful for further understanding of it.

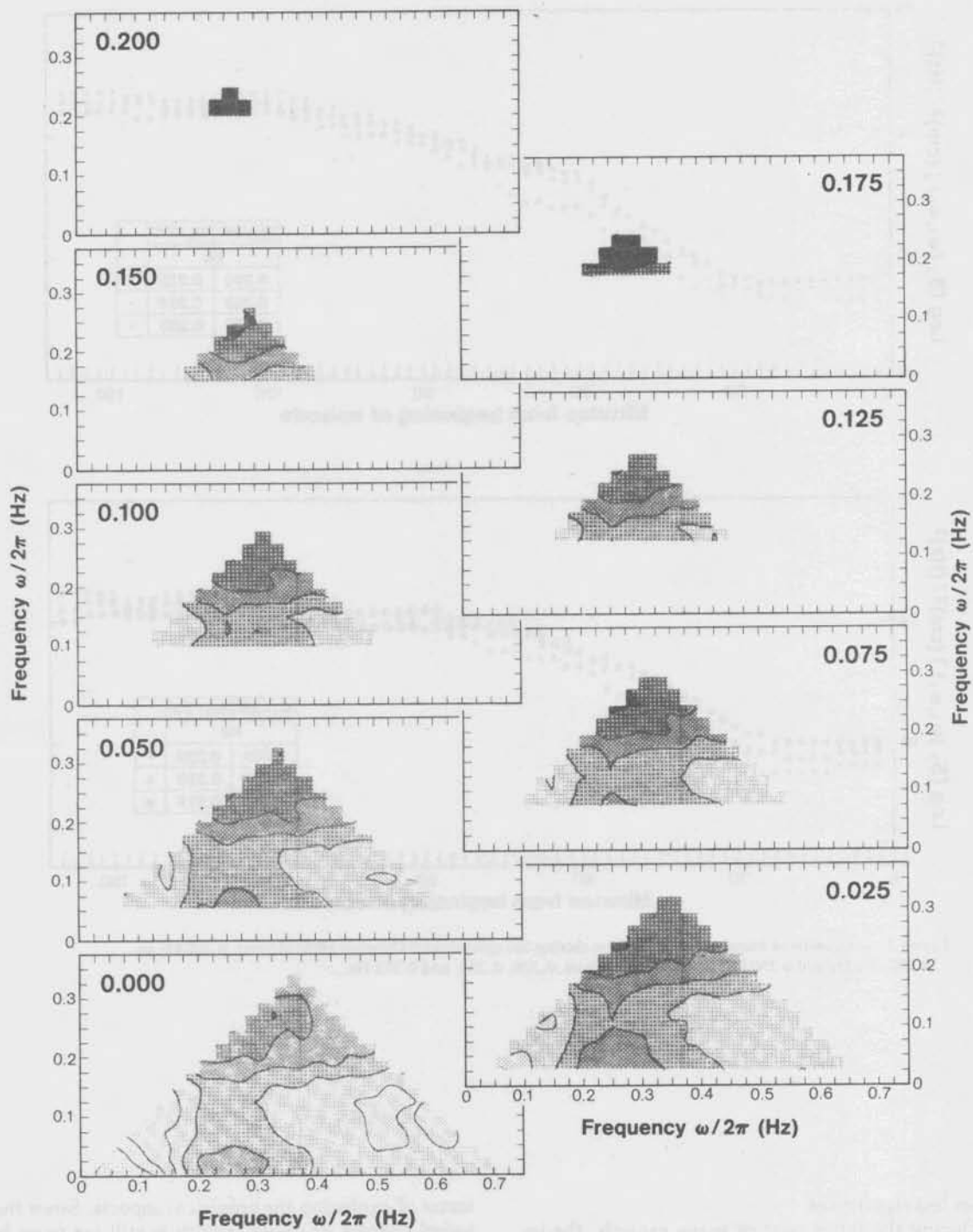


Figure 24a.—Trispectra during the episode of 9 August 1972, 2.5 minutes from beginning of episode.

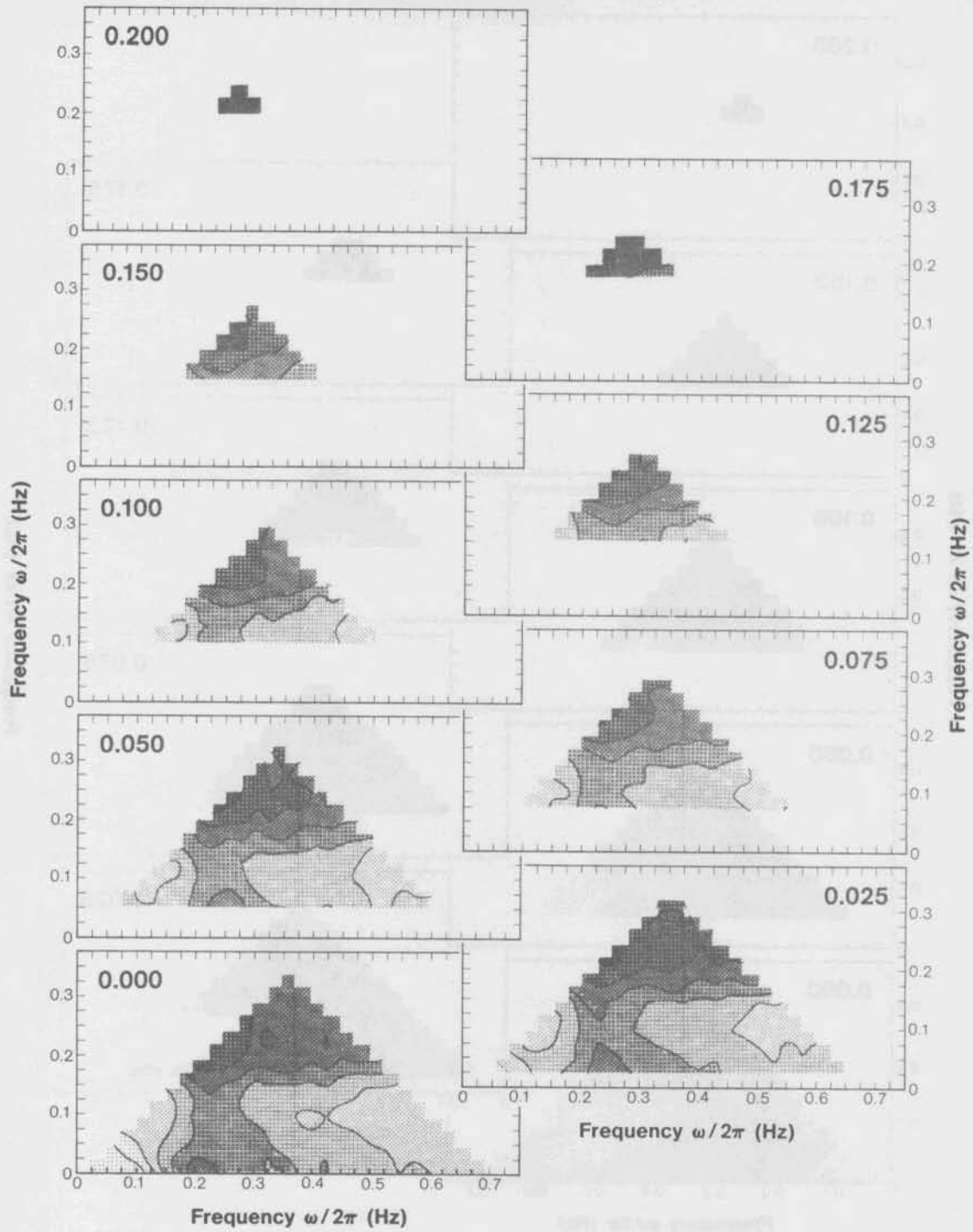


Figure 24b.—Trispectra during the episode of 9 August 1972, 32.5 minutes from beginning of episode.

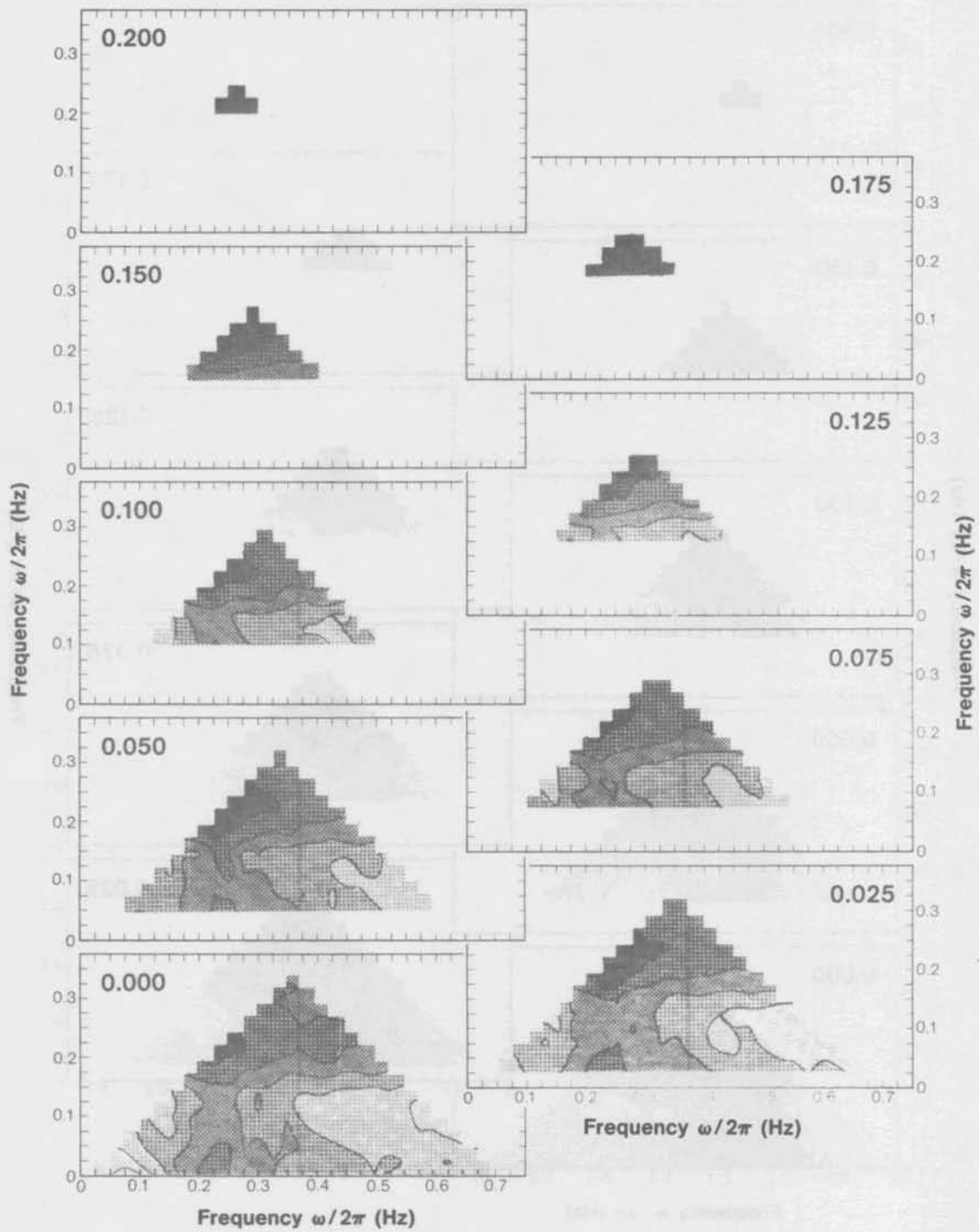


Figure 24c.—Trispectra during the episode of 9 August 1972, 62.5 minutes from beginning of episode.

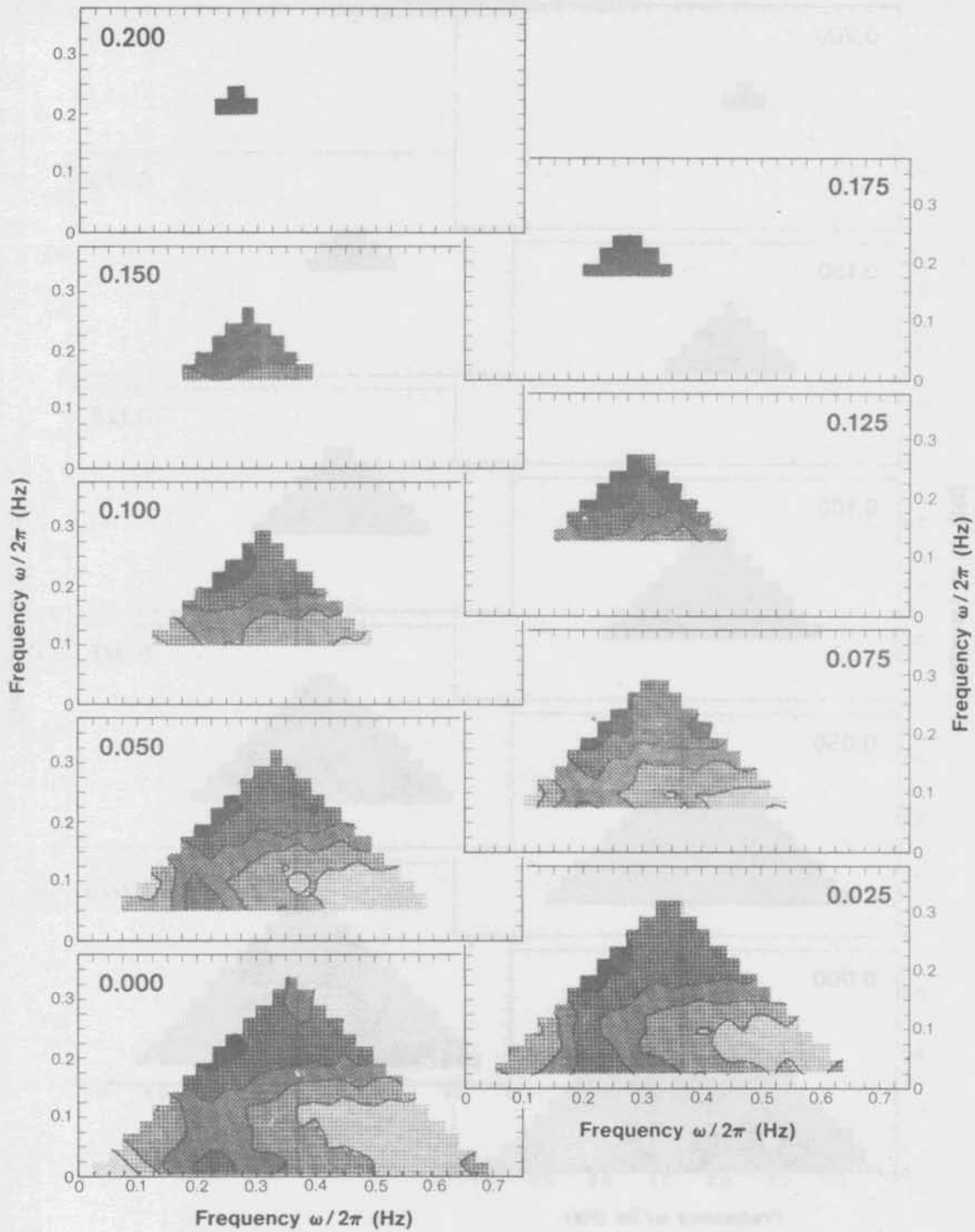


Figure 24d.—Trispectra during the episode of 9 August 1972, 92.5 minutes from beginning of episode.

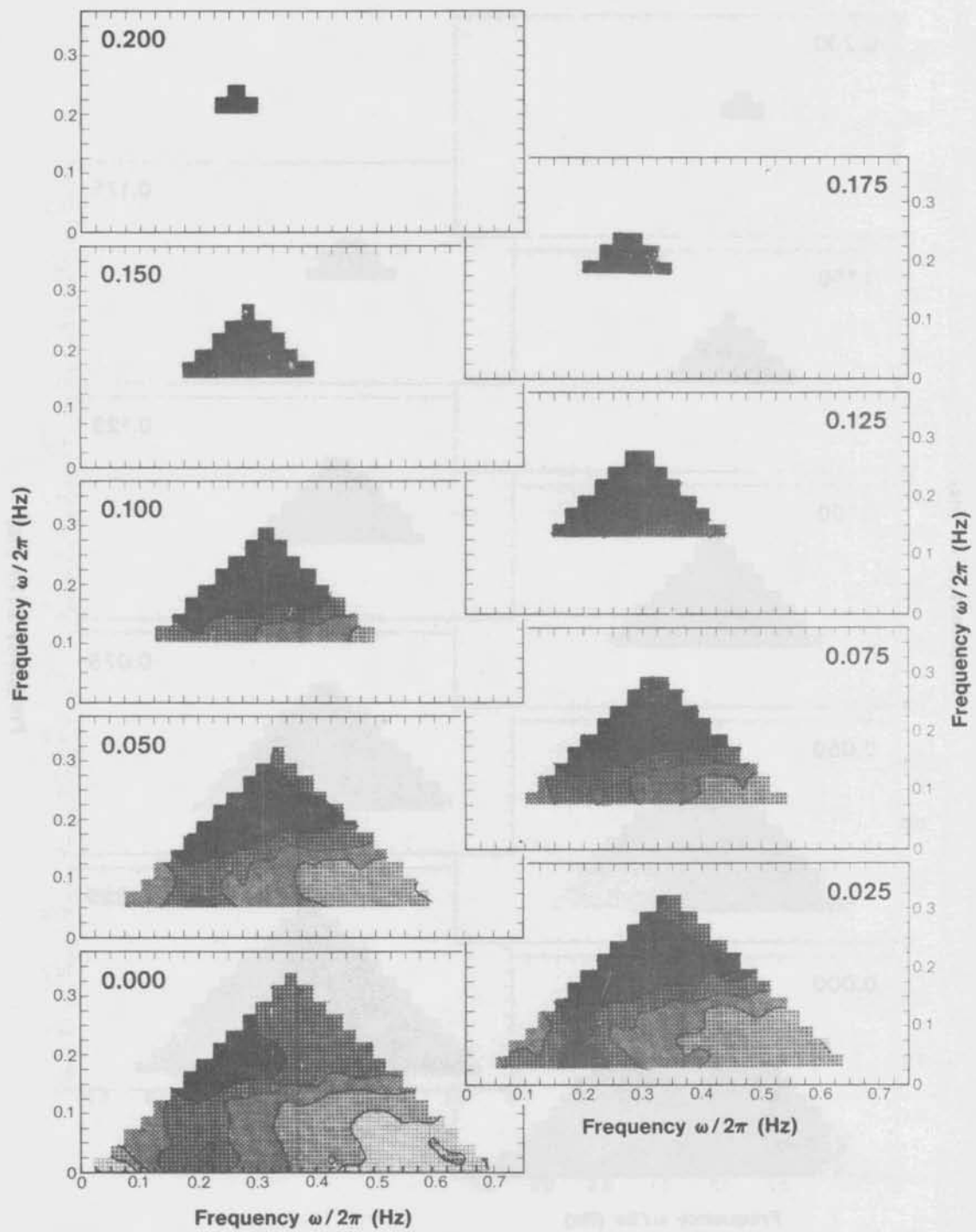


Figure 24e.—Trispectra during the episode of 9 August 1972, 122.5 minutes from beginning of episode.

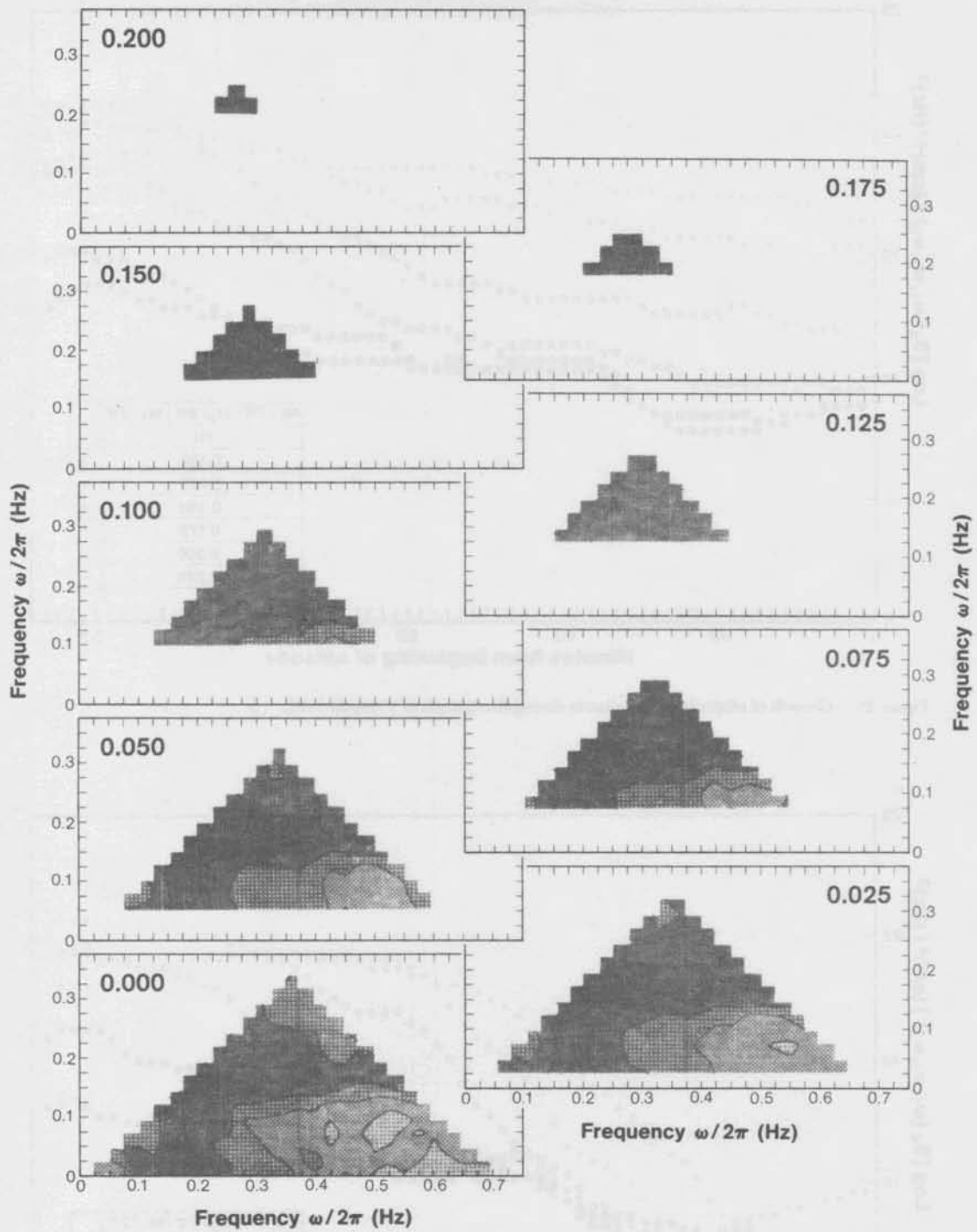


Figure 24f.—Trispectra during the episode of 9 August 1972, 152.5 minutes from beginning of episode.

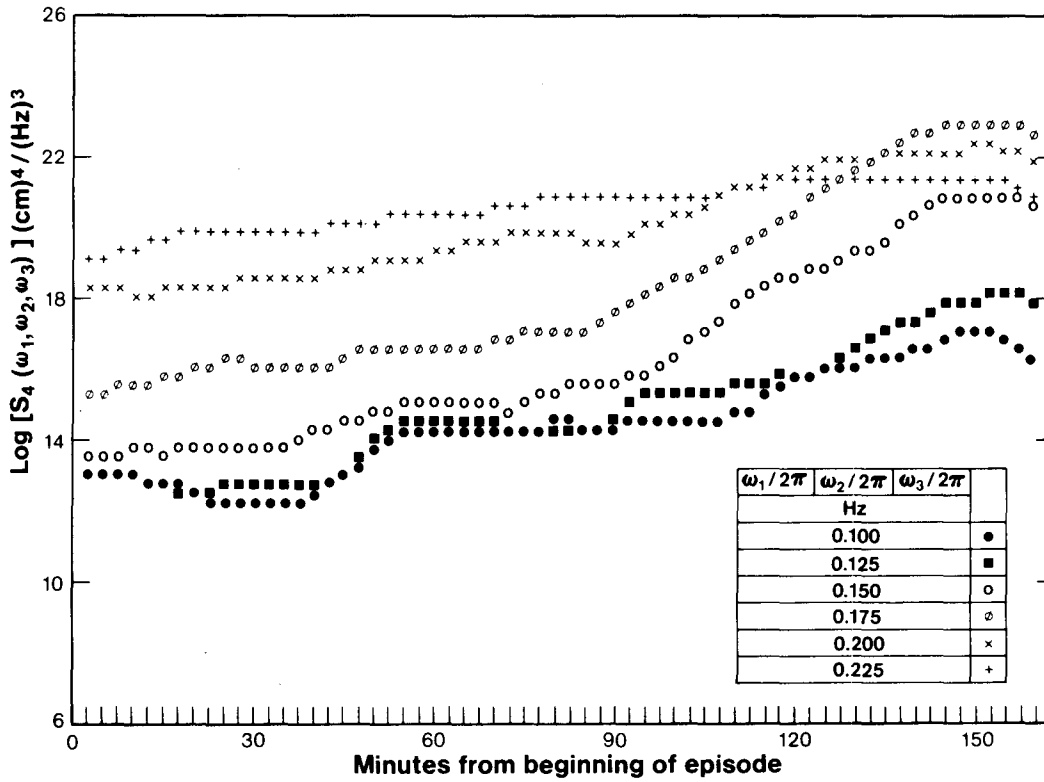


Figure 25.—Growth of trispectral components during the episode of 9 August 1972.

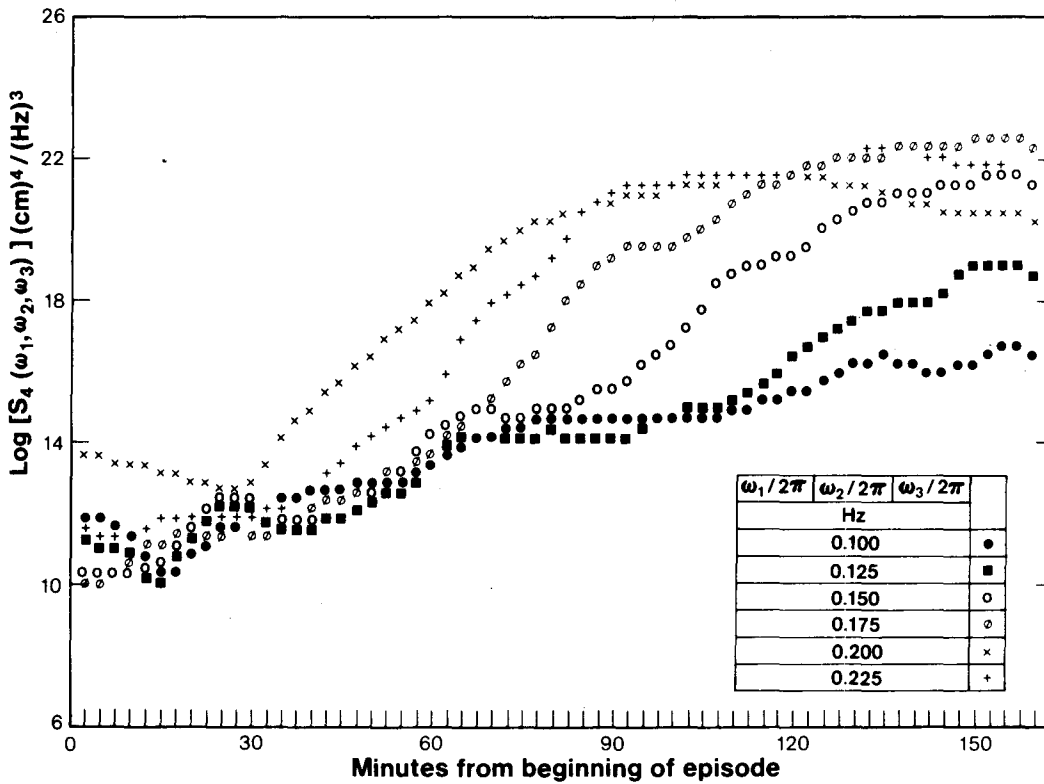


Figure 26.—Growth of trispectral components during the episode of 30 September 1972.

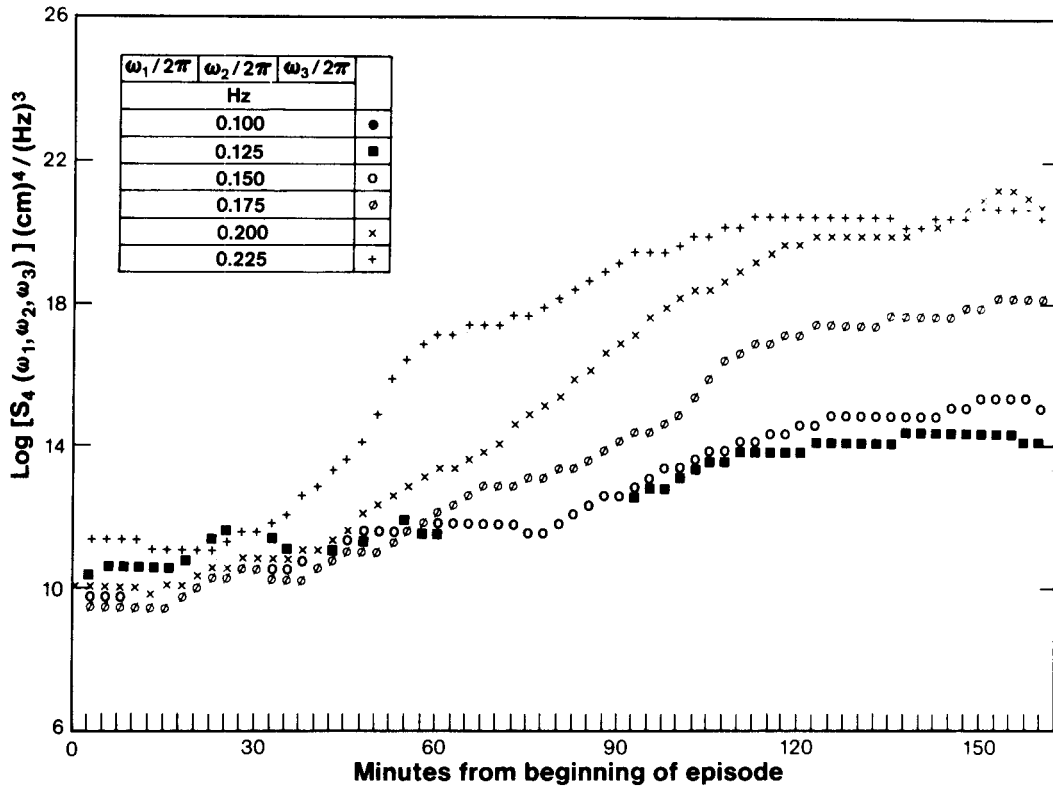


Figure 27.—Growth of trispectral components during the episode of 7 October 1972.

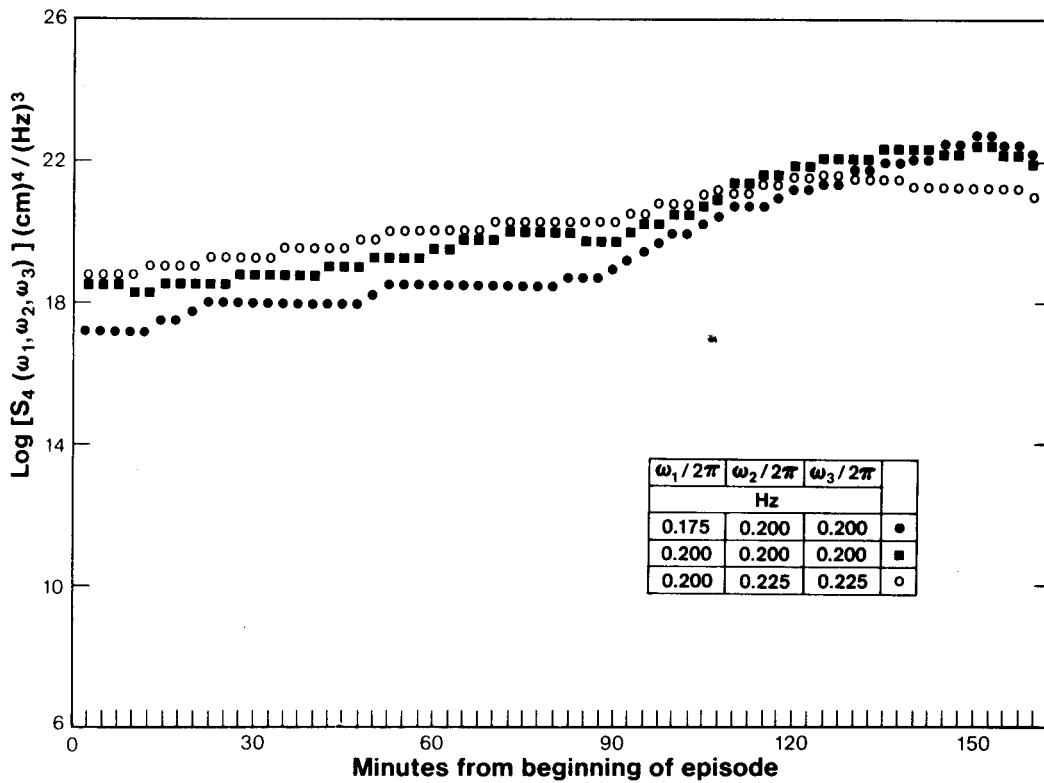


Figure 28a.—Growth of trispectral components during the episode of 9 August 1972: Third-order interactions among components 0.175, 0.200, and 0.255 Hz.

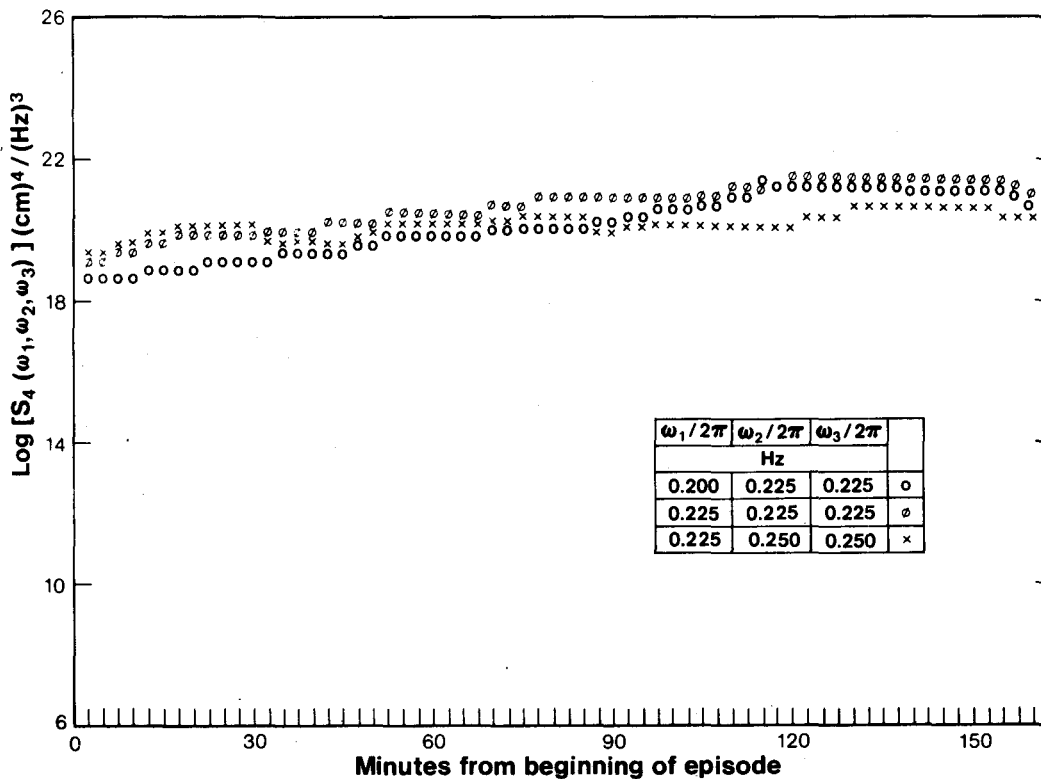


Figure 28b.—Growth of trispectral components during the episode of 9 August 1972: Third-order interactions among components 0.200, 0.225, and 0.250 Hz.

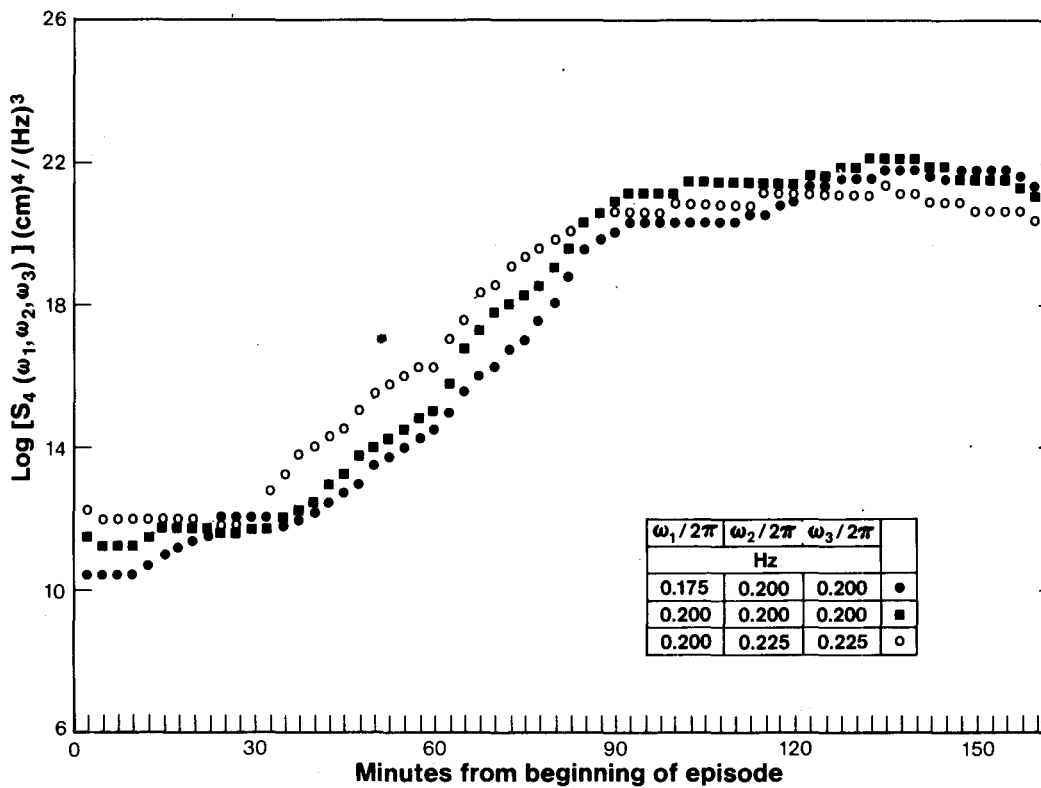


Figure 29a.—Growth of trispectral components during the episode of 30 September 1972: Third-order interactions among components 0.175, 0.200, and 0.225 Hz.

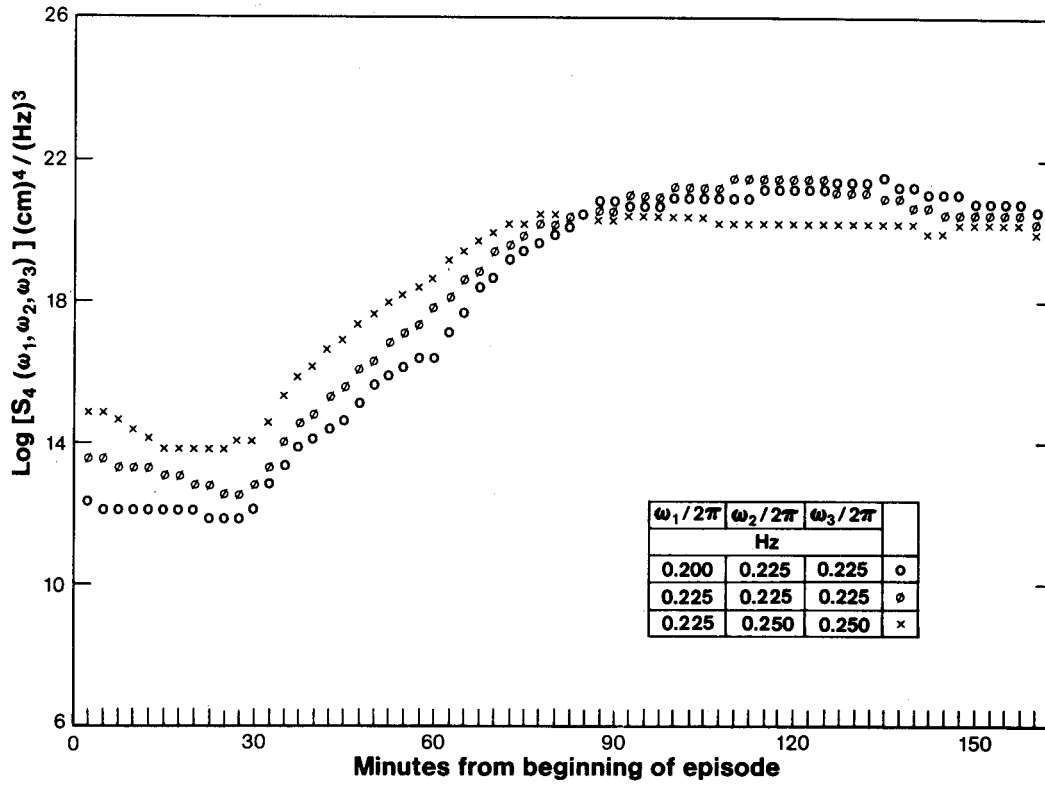


Figure 29b.—Growth of trispectral components during the episode of 30 September 1972: Third-order interactions among components 0.200, 0.225, and 0.250 Hz.

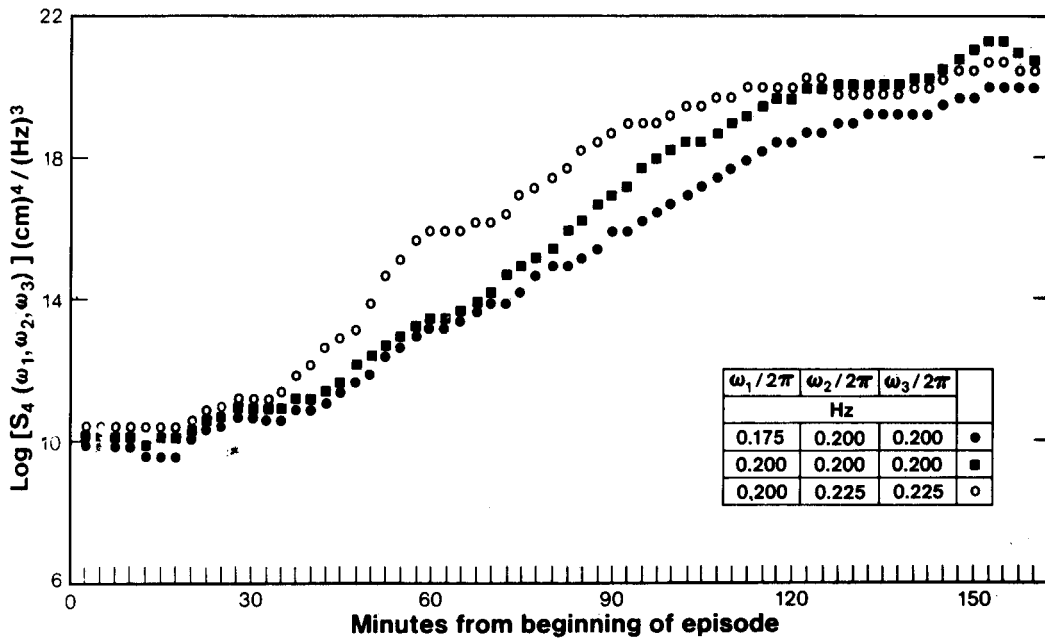


Figure 30a.—Growth of trispectral components during the episode of 7 October 1972: Third-order interactions among components 0.175, 0.200, and 0.225 Hz.

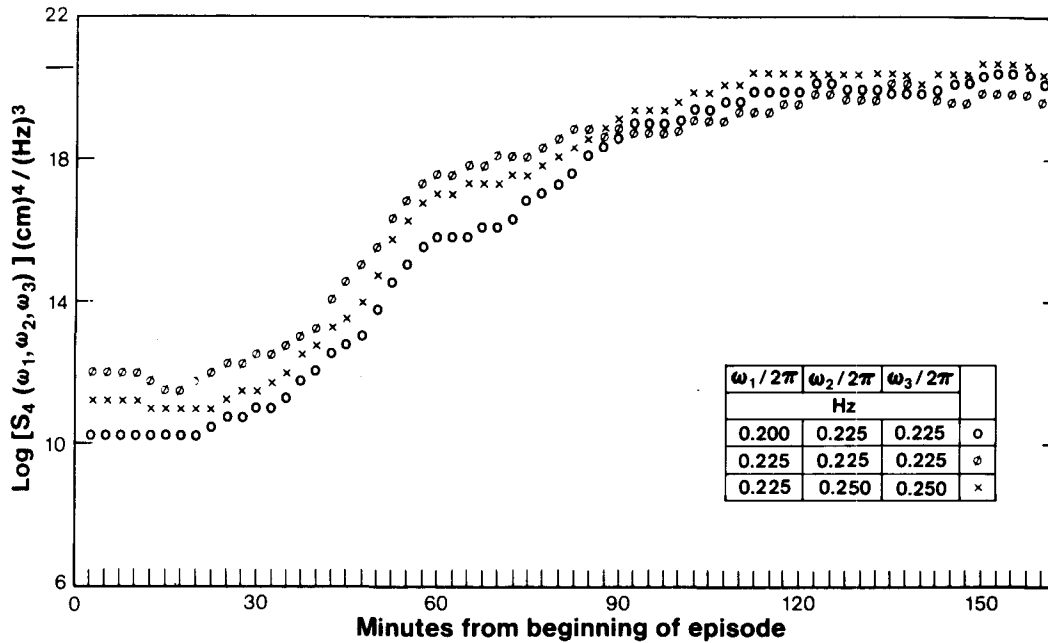


Figure 30b.—Growth of trispectral components during the episode of 7 October 1972: Third-order interactions among components 0.200, 0.225, and 0.250 Hz.

## 8. REFERENCES

- Barnett, T. P. (1966): On the generation, dissipation and prediction of ocean wind waves. Ph.D. thesis, Scripps Institution of Oceanography, San Diego, Calif., 190 pp.
- Barnett, T. P., and K. E. Kenyon (1975): Recent advances in the study of wind waves. *Rep. Prog. Phys.* 38:667-729.
- Batchelor, G. K. (1953): *The Theory of Homogeneous Turbulence*. Cambridge University Press, London, England, 197 pp.
- Bendat, J. S., and A. G. Piersol (1966): *Measurement and Analysis of Random Data*. Wiley, New York, 390 pp.
- Benjamin, T. B., and J. E. Feir (1967): The disintegration of wave trains on deep water. *J. Fluid Mech.* 27:417-430.
- Benney, D. J. (1962): Nonlinear gravity wave interactions. *J. Fluid Mech.* 14:577-584.
- Benney, D. J., and P. G. Saffman (1966): Nonlinear interactions of random waves in a dispersive medium. *Proc. Roy. Soc. Lond. (Ser. A)* 289:301-320.
- Bjerkaas, A. W. (1976): *Time series analysis applied to data from a single ocean wave gage*. Report of the Johns Hopkins Univ. Applied Physics Lab., Laurel, Maryland, 188 pp.
- Brillinger, D. R., and M. Rosenblatt (1967): Computation and interpretation of kth order spectra. In *Spectral Analysis of Time Series* (Ed.) B. Harris, Wiley, New York, 189-232.
- Cooley, J. W., and J. W. Tukey (1965): An algorithm for the machine calculation of complex Fourier series. *Math. Comput.* 19:297-301.
- Fox, M. J. H. (1976): On the nonlinear transfer of energy in the peak of a gravity-wave spectrum. II. *Proc. Roy. Soc. Lond. (Ser. A)* 348:467-483.
- Freeman, N. G., and T. S. Murty (1972): A study of a storm surge on Lake Huron. In *Proc. 15th Conf. Great Lakes Res.*, Int. Assoc. for Great Lakes Research, 565-581.
- Garrett, J. F. (1970): Field observations of frequency domain statistics and nonlinear effects in wind-generated ocean waves. Ph.D. thesis, The University of British Columbia, Vancouver, Canada, 177 pp.
- Gelci, R. H., H. Cazale, and J. Vassel (1956): Utilisation des diagrammes de propagation à la provision energetique de la houle. *Bull. Inform. Comité Central Oceanogr. d'Etude Côtes* 8:169-187.
- Hasselmann, K. (1960): Grundgleichungen der Seegangsvoraussage. *Schiffstechnik* 7:191-195.
- Hasselmann, K. (1962): On the nonlinear energy transfer in a gravity-wave spectrum. Part 1: General theory. *J. Fluid Mech.* 12:481-500.
- Hasselmann, K. (1963a): On the nonlinear energy transfer in a gravity-wave spectrum. Part 2: Conservation theorems, wave-particle correspondence, irreversibility. *J. Fluid Mech.* 15:273-281.
- Hasselmann, K. (1963b): On the nonlinear energy transfer in a gravity-wave spectrum. Part 3: Computation of the energy flux and swell-sea interaction for a Neumann spectrum. *J. Fluid Mech.* 15:385-398.
- Hasselmann, K., W. Munk, and G. McDonald (1963): Bispectra of ocean waves. In *Time Series Analysis*, (Ed.) M. Rosenblatt, Wiley, New York, 125-139.
- Hasselmann, K., T. P. Barnett, E. Bouws, H. Carlson, D. E. Cartwright, K. Enke, J. A. Ewing, H. Gienapp, D. E. Hasselmann, P. Kruseman, A. Merrburg, P. Miller, D. J. Olbers, K. Richter, W. Sell, and H. Walden (1973): Measurements of wind-wave growth and swell decay during the Joint North Sea Wave Project (JONSWAP). *Deut. Hydrogr. Z., Suppl. A*, 8:12.

- Haubrich, R. A. (1965): Earth noise, 5 to 500 millicycles per second. Part 1, Spectral stationarity, normality, and nonlinearity. *J. Geophys. Res.* 70:1415-1427.
- Hinch, M. J., and C. S. Clay (1968): The application of the discrete Fourier transform in the estimation of power spectra, coherence, and bispectra of geophysical data. *Rev. Geophys. Space Phys.* 6:347-363.
- Houmb, O. G. (1974): Spectra and bispectra of ocean waves. In *Proc. 14th Coastal Engineering Conf.* (Am. Soc. of Civil Engineers) 1:301-320.
- Jacobson, J. P., and J. M. Colonell (1972): Spectral development of wind-generated water waves in a laboratory facility. Report No. UM-72-8, School of Engineering, Univ. of Massachusetts, Amherst, 71 pp.
- Kolmogoroff, A. N. (1941): The local structure of turbulence in incompressible viscous fluid for very large Reynolds numbers. *C. R. Acad. Sci. U.S.S.R.* 30:299-303.
- Liu, P. C., and R. J. Robbins (1974): Wave data analysis at GLERL. In *Proc. Internat. Symp. on Ocean Wave Measurement and Analysis* (Am. Soc. of Civil Engineers) 1:64-73.
- Longuet-Higgins, M. S. (1976): On the nonlinear transfer of energy in the peak of a gravity wave spectrum. *Proc. Roy. Soc. Lond. (Ser. A)* 347:311-328.
- Miles, J. W. (1957): On the generation of surface waves by shear flows. *J. Fluid Mech.* 3:185-204.
- Mitsuyasu, H. (1968): A note on the nonlinear energy transfer in the spectrum of wind-generated waves. *Rep. of Res. Inst. for Appl. Mech.* 16:251-264.
- Neumann, G. (1953): On ocean wave spectra and a new method of forecasting wind-generated sea. Beach Erosion Board, U.S. Army Corps of Engineers, Tech. Memo. No. 43.
- Phillips, O. M. (1957): On the generation of waves by turbulent wind. *J. Fluid Mech.* 2:417-445.
- Phillips, O. M. (1960): On the dynamics of unsteady gravity waves of finite amplitude. Part I. *J. Fluid Mech.* 9:193-217.
- Phillips, O. M. (1961): On the dynamics of unsteady gravity waves of finite amplitude. Part II. *J. Fluid Mech.* 11:143-155.
- Phillips, O. M. (1966): *The Dynamics of the Upper Ocean*. Cambridge University Press, London, England, 261 pp.
- Priestly, M. B. (1965): Evolutionary spectra and nonstationary processes. *Roy. Statist. Soc. J. (Ser. B)* 27:204-237.
- Resio, D. T., and C. L. Vincent (1976): *Design wave information for the Great Lakes*. U.S. Army Engineer Waterways Experiment Station Technical Reports, Vicksburg, Miss.
- Sell, W., and K. Hasselmann (1972): Computations of nonlinear energy transfer for JONSWAP and empirical wind wave spectra. Report of Inst. Geophys., University of Hamburg, Hamburg, Germany, 248 pp.
- Silverman, R. A. (1957): Locally stationary random processes. *IRE Trans. Inf. Theory* 3:182-187.
- Watson, K. M., and B. J. West (1975): A transport-equation description of nonlinear ocean surface wave interactions. *J. Fluid Mech.* 70:815-826.
- Wu, H. Y., E. Y. Hsu, and R. L. Street (1979): Experimental study of nonlinear wave-wave interaction and white-cap dissipation of wind-generated waves. *Dyn. of Atmos. and Oceans* 3:55-78.



## Appendix A: Relationships Between Higher Order Covariances and Higher Order Spectra

In order to define a general higher order spectrum in terms of the Fourier components of the surface displacement, we follow Batchelor's (1953) basic approach by considering a stationary random function of both time and space defined by

$$\zeta(\mathbf{x}, X; t, T) = \begin{cases} \zeta(\mathbf{x}, t) & \text{for } -X \leq x_i \leq X \\ & \text{and } -T \leq t \leq T \\ 0 & \text{for } |x_i| > X \\ & \text{and } |t| > T \end{cases} \quad (\text{A.1})$$

which satisfies the condition for a Fourier integral to exist. The corresponding Fourier coefficient is

$$A(\mathbf{k}, X; \omega, T) = \frac{1}{(2\pi)^4} \int_{\mathbf{x}} \int_t \zeta(\mathbf{x}, X; t, T) e^{+i(\mathbf{k} \cdot \mathbf{x} - \omega t)} d\mathbf{x} dt. \quad (\text{A.2})$$

From Weiner's generalized harmonic analysis, it can be shown that as the parameters  $X$  and  $T$  extend to  $\infty$ , the limit exists as

$$[Y(\mathbf{k}, \omega)]_{\mathbf{k}, \omega}^{\mathbf{k}', \omega'} = \lim_{\substack{X \rightarrow \infty \\ T \rightarrow \infty}} \int_{k_1}^{k_1'} \int_{k_2}^{k_2'} \int_{k_3}^{k_3'} \int_{\omega}^{\omega'} A(\mathbf{k}, X; \omega, T) dk_1 dk_2 dk_3 d\omega \quad (\text{A.3})$$

$$= \frac{1}{(2\pi)^4} \int_{\mathbf{x}} \int_t \zeta(\mathbf{x}, t) \left( \prod_{j=1}^3 \frac{e^{+ik_j' x_j} - e^{+ik_j x_j}}{+ix_j} \right) \times \left( \frac{e^{-i\omega' t} - e^{-i\omega t}}{-it} \right) d\mathbf{x} dt.$$

We can write

$$dY(\mathbf{k}, \omega) = [Y(\mathbf{k}, \omega)]_{\mathbf{k}, \omega}^{\mathbf{k}+d\mathbf{k}, \omega+d\omega} = \frac{1}{2(\pi)^4} \int_{\mathbf{x}} \int_t \zeta(\mathbf{x}, t) e^{+i(\mathbf{k} \cdot \mathbf{x} - \omega t)} \times \left( \prod_{j=1}^3 \frac{e^{+idk_j x_j} - 1}{+ix_j} \right) \left( \frac{e^{-id\omega t} - 1}{-it} \right) d\mathbf{x} dt, \quad (\text{A.4})$$

which is the inverse relation of

$$\zeta(\mathbf{x}, t) = \int_{\mathbf{k}} \int_{\omega} dY(\mathbf{k}, \omega) e^{-i(\mathbf{k} \cdot \mathbf{x} - \omega t)}. \quad (\text{A.5})$$

Now we can obtain the ensemble average of an  $n$ th order product of  $dY(\mathbf{k}, \omega)$  as

$$\overline{dY(\mathbf{k}_1, \omega_1) dY(\mathbf{k}_2, \omega_2) \dots dY(\mathbf{k}_{n-1}, \omega_{n-1}) dY^*(\mathbf{k}_n, \omega_n)} = \frac{1}{(2\pi)^{4n}} \int \dots \int \overline{\zeta(\mathbf{x}_1, t_1) \zeta(\mathbf{x}_2, t_2) \dots \zeta(\mathbf{x}_n)} \quad (\text{A.6})$$

$$\times e^{+i \left[ \sum_{j=1}^{n-1} (\mathbf{k}_j \cdot \mathbf{x}_j - \omega_j t_j) - (\mathbf{k}_n \cdot \mathbf{x}_n - \omega_n t_n) \right]} \times \left( \prod_{m=1}^3 \frac{e^{+idk_{1m} x_{1m}} - 1}{+ix_{1m}} \right) \left( \frac{e^{-id\omega_1 t_1} - 1}{-it_1} \right) \dots \times \left( \prod_{m=1}^3 \frac{e^{+idk_{n-1,m} x_{n-1,m}} - 1}{+ix_{n-1,m}} \right) \left( \frac{e^{-id\omega_{n-1} t_{n-1}} - 1}{-it_{n-1}} \right) \times \left( \prod_{m=1}^3 \frac{e^{-idk_{nm} x_{nm}} - 1}{-ix_{nm}} \right) \left( \frac{e^{+id\omega_n t_n} - 1}{+it_n} \right) \times d\mathbf{x}_1 d\mathbf{x}_2 \dots d\mathbf{x}_n (dt)^n.$$

Now for stationarity with respect to both space and time, the right side can be written as

$$\frac{1}{(2\pi)^{4n}} \int \dots \int \overline{\zeta(\mathbf{x} + \mathbf{r}_1, t + \tau_1) \dots \zeta(\mathbf{x} + \mathbf{r}_{n-1}, t + \tau_{n-1}) \zeta(\mathbf{x}, t)} \times e^{+i \left[ \sum_{j=1}^{n-1} (\mathbf{k}_j \cdot (\mathbf{x} + \mathbf{r}_j) - \omega_j (t + \tau_j)) - (\mathbf{k}_n \cdot \mathbf{x} + \omega_n t) \right]} \times \left( \prod_{m=1}^3 \frac{e^{+idk_{1m} (x_m + r_{1m})} - 1}{+i(x_m + r_{1m})} \right) \left( \frac{e^{-id\omega_1 (t + \tau_1)} - 1}{-i(t + \tau_{n-1})} \right) \dots \times \left( \prod_{m=1}^3 \frac{e^{+idk_{n-1,m} (x_m + r_{n-1,m})} - 1}{+i(x_m + r_{n-1,m})} \right) \left( \frac{e^{-id\omega_{n-1} (t + \tau_{n-1})} - 1}{-i(t + \tau_{n-1})} \right) \times \left( \prod_{m=1}^3 \frac{e^{-idk_{nm} x_m} - 1}{-ix_m} \right) \left( \frac{e^{+id\omega_n t} - 1}{+it} \right) \times d\mathbf{x} d\mathbf{r}_1 \dots d\mathbf{r}_{n-1} dt d\tau_1 \dots d\tau_{n-1} = \frac{1}{(2\pi)^{4(n-1)}} \int \dots \int R_n(\mathbf{r}_1, \dots, \mathbf{r}_{n-1}, \tau_1, \dots, \tau_{n-1}) \times e^{+i \left[ \sum_{j=1}^{n-1} (\mathbf{k}_j \cdot \mathbf{r}_j - \omega_j \tau_j) \right]} \times e^{-i[(\mathbf{k}_n - \mathbf{k}_1 - \dots - \mathbf{k}_{n-1}) \cdot \mathbf{x} - (\omega_n - \omega_1 - \dots - \omega_{n-1})t]} \times \left( \prod_{m=1}^3 \frac{e^{+idk_{1m} r_{1m}} - 1}{+ir_{1m}} \right) \left( \frac{e^{-id\omega_1 \tau_1} - 1}{-i\tau_1} \right) \dots \times \left( \prod_{m=1}^3 \frac{e^{+idk_{n-1,m} r_{n-1,m}} - 1}{+ir_{n-1,m}} \right) \left( \frac{e^{-id\omega_{n-1} \tau_{n-1}} - 1}{-i\tau_{n-1}} \right) \times d\mathbf{r}_1 \dots d\mathbf{r}_{n-1} d\tau_1 \dots d\tau_{n-1}. \quad (\text{A.7})$$

Since the stationary process is independent of both  $\mathbf{x}$  and  $t$ , the above relation is identically zero unless

$$\mathbf{k}_n - \mathbf{k}_1 - \mathbf{k}_2 - \dots - \mathbf{k}_{n-1} = 0$$

and

$$\omega_n - \omega_1 - \omega_2 - \dots - \omega_{n-1} = 0.$$

Furthermore we let  $d\mathbf{k}$ 's and  $d\omega$ 's approach zero to obtain

$$\begin{aligned} & \frac{dY(\mathbf{k}_1, \omega_1) dY(\mathbf{k}_2, \omega_2) \dots dY(\mathbf{k}_{n-1}, \omega_{n-1}) dY^*(\mathbf{k}_n, \omega_n)}{d\mathbf{k}_1 d\mathbf{k}_2 \dots d\mathbf{k}_{n-1} d\omega_1 d\omega_2 \dots d\omega_{n-1}} \\ &= \frac{1}{(2\pi)^{4(n-1)}} \int \dots \int R_n(\mathbf{r}_1, \mathbf{r}_2, \dots, \mathbf{r}_{n-1}, \tau_1, \tau_2, \dots, \tau_{n-1}) \\ & \times e^{+i \left[ \sum_{j=1}^{n-1} (\mathbf{k}_j \cdot \mathbf{r}_j - \omega_j \tau_j) \right]} \\ & \times d\mathbf{r}_1 \dots d\mathbf{r}_{n-1} d\tau_1 \dots d\tau_{n-1} \\ & \equiv S_n(\mathbf{k}_1, \dots, \mathbf{k}_{n-1}, \omega_1, \dots, \omega_{n-1}), \end{aligned} \quad (\text{A.8})$$

$$\text{if } \mathbf{k}_n = \mathbf{k}_1 + \mathbf{k}_2 + \dots + \mathbf{k}_{n-1}$$

$$\text{and } \omega_n = \omega_1 + \omega_2 + \dots + \omega_{n-1}$$

and

$$\begin{aligned} & \frac{dY(\mathbf{k}_1, \omega_1) dY(\mathbf{k}_2, \omega_2) \dots dY(\mathbf{k}_{n-1}, \omega_{n-1}) dY^*(\mathbf{k}_n, \omega_n)}{d\mathbf{k}_1 d\mathbf{k}_2 \dots d\mathbf{k}_{n-1} d\omega_1 d\omega_2 \dots d\omega_{n-1}} \\ &= 0 \end{aligned} \quad (\text{A.9})$$

$$\text{if } \mathbf{k}_n \neq \mathbf{k}_1 + \dots + \mathbf{k}_{n-1}$$

$$\text{and } \omega_n \neq \omega_1 + \dots + \omega_{n-1}.$$

The last expression in (A.8) gives the general definition of the  $n$ th order energy spectrum, where

$$\begin{aligned} & R_n(\mathbf{r}_1, \dots, \mathbf{r}_{n-1}; \tau_1, \dots, \tau_{n-1}) \\ & \equiv \int \dots \int S_n(\mathbf{k}_1, \dots, \mathbf{k}_{n-1}; \omega_1, \dots, \omega_{n-1}) \\ & \times e^{-i \left[ \sum_{j=1}^{n-1} (\mathbf{k}_j \cdot \mathbf{r}_j - \omega_j \tau_j) \right]} \\ & \times d\mathbf{k}_1 \dots d\mathbf{k}_{n-1} d\omega_1 \dots d\omega_{n-1}. \end{aligned} \quad (\text{A.10})$$

For observations at single points, we may integrate and normalize the above equations over all directions and wave numbers to obtain

$$S_n(\omega_1, \dots, \omega_{n-1}) = \frac{1}{2\pi^{(n-1)}} \int \dots \int R_n(\tau_1, \dots, \tau_{n-1})$$

$$\times e^{-i \sum_{j=1}^{n-1} \omega_j \tau_j} d\tau_1 \dots d\tau_{n-1}, \quad (\text{A.11})$$

and

$$\begin{aligned} R_n(\tau_1, \dots, \tau_{n-1}) &= \int \dots \int S_n(\omega_1, \dots, \omega_{n-1}) \\ & \times e^{i \sum_{j=1}^{n-1} \omega_j \tau_j} d\omega_1 \dots d\omega_{n-1}. \end{aligned} \quad (\text{A.12})$$

For  $n = 2$ , we have the following familiar pair of classic spectral analyses:

$$S_2(\omega) = \frac{1}{2\pi} \int R_2(\tau) e^{-i\omega\tau} d\tau, \quad (\text{A.13})$$

and

$$R_2(\tau) = \int S_2(\omega) e^{i\omega\tau} d\omega. \quad (\text{A.14})$$

Detailed discussions corresponding to the formal definitions (A.11) and (A.12), as well as conditions for existence and convergence of estimates, are beyond the scope of our present study and can be found in Brillinger and Rosenblatt (1967).

In practical applications, we may define

$$\begin{aligned} \zeta_T(t) &= \zeta(t), \quad 0 < t \leq T; \\ &= 0, \quad t > T. \end{aligned} \quad (\text{A.15})$$

Let the Fourier transform of  $\zeta_T(t)$  be  $X(\omega)$ ; then we have

$$X(\omega) = \int_0^T \zeta_T(t) e^{-i\omega t} dt, \quad (\text{A.16})$$

and

$$\zeta_T(t) = \int_{-\infty}^{\infty} X(\omega) e^{i\omega t} d\omega. \quad (\text{A.17})$$

Now for the  $n$ th order covariance we have

$$\begin{aligned} R_n(\tau_1, \dots, \tau_{n-1}) &= \overline{\zeta(t) \zeta(t + \tau_1) \dots \zeta(t + \tau_{n-1})} \\ &= \lim_{T \rightarrow \infty} \frac{1}{T} \int_0^T \zeta_T(t) \zeta_T(t + \tau_1) \dots \zeta_T(t + \tau_{n-1}) dt \\ &= \lim_{T \rightarrow \infty} \frac{1}{T} \int_0^T \zeta_T(t) \int_{\omega_1} \dots \int_{\omega_{n-1}} X(\omega_1) \dots X(\omega_{n-1}) \\ & \times e^{i[(\omega_1 + \dots + \omega_{n-1})t + \omega_1 \tau_1 + \dots + \omega_{n-1} \tau_{n-1}]} \\ & \times d\omega_1 \dots d\omega_{n-1} dt \\ &= \lim_{T \rightarrow \infty} \frac{1}{T} \int_{\omega_1} \dots \int_{\omega_{n-1}} X(\omega_1) \dots X(\omega_{n-1}) \\ & \times e^{i(\omega_1 \tau_1 + \dots + \omega_{n-1} \tau_{n-1})} \\ & \times \int_0^T \zeta_T(t) e^{i(\omega_1 + \dots + \omega_{n-1})t} dt d\omega_1 \dots d\omega_{n-1} \end{aligned}$$

$$\begin{aligned}
&= \lim_{T \rightarrow \infty} \frac{1}{T} \int_{\omega_1} \dots \int_{\omega_{n-1}} X(\omega_1) \dots X(\omega_{n-1}) \\
&\times X^*(\omega_1 + \dots + \omega_{n-1}) \\
&\times e^{i(\omega_1 \tau_1 + \dots + \omega_{n-1} \tau_{n-1})} d\omega_1 \dots d\omega_{n-1}. \quad (\text{A.18})
\end{aligned}$$

Comparing (A.18) with integrated (A.12), we have formally

$$\begin{aligned}
&S_n(\omega_1, \dots, \omega_{n-1}) \\
&= \lim_{T \rightarrow \infty} \frac{1}{T} [X(\omega_1) \dots X(\omega_{n-1}) X^*(\omega_1 + \dots + \omega_{n-1})]. \quad (\text{A.19})
\end{aligned}$$

Thus, in practical applications we can use the product of Fourier transforms of  $\xi_T(t)$ , with the aid of the fast Fourier transform algorithm, to facilitate the calculations of higher order spectra.



## Appendix B: Testing for Stationarity

In this report we have assumed local stationarity to study the temporal growth of spectral components that are in general nonstationary. To test the assumption of local stationarity, we adopted a testing method similar to that used by Bjerkaas (1976). The scheme divides each data set into  $P$  equal-length sub-segments; calculates the  $\zeta$ ,  $\zeta^2$ ,  $\zeta^3$ , and  $\zeta^4$  for each sub-segment; and then applies two nonparametric tests, the run test, and the reverse arrangement test (Bendat and Piersol, 1966) to the data set to examine its stationarity.

In the run test, the test parameter for each interval is compared to the median value of the test parameter for all intervals. If the test parameter is greater than or equal to the median value, +1 is assigned to the interval; otherwise, -1 is assigned. A sequence of consecutive +1's or -1's is called a run, and the number of runs  $N_r$  in the  $P$  intervals is determined.  $N_r$  gives an indication as to whether or not results are independent random observations of the same random variable. The reverse arrangement test is most useful in detecting monotonic trends in the time series. Consider the test parameter  $A_i$ , with  $i = 1, 2, \dots, P$ . If  $A_i > A_j$  for  $i < j$ , the pair of parameters is called a reverse arrangement.

The total number of reverse arrangements,  $N_a$ , is defined as follows:

Let

$$h_{ij} = \begin{cases} 1 & \text{if } A_i > A_j \\ 0 & \text{if } A_i \leq A_j. \end{cases}$$

Then

$$N_{ai} = \sum_{j=i+1}^P h_{ij}$$

and

$$N_a = \sum_{i=1}^{P-1} N_{ai}.$$

Based on  $P$  and the level of significance, the acceptance ranges for  $N_r$  and  $N_a$  can be calculated (Bendat and Piersol, 1966) and used as a basis to accept or reject the stationarity assumption.

Accordingly, in our analysis eight separate tests were performed for each data set. The results, presented in terms of the percentage of data failing the tests for the three episodes studied, are shown in table B.1. At a level of significance  $\alpha = 0.10$ , the overall failure rate was 29 percent; the rate reduced to 19 percent for  $\alpha = 0.02$ . Every data set passed at least two of the eight tests performed. A total of 27 percent passed all eight tests. The parameter  $\zeta^3$  posed the best results;  $\zeta^4$ , on the other hand, posed the worst results. Although, ideally, absolute stationarity requires that the data pass all the tests, we find that for a basically nonstationary process these results generally tend to enhance the acceptability of our assumption of local stationarity. Thus, without pursuing more complicated physical and statistical nonstationary analysis, we can employ available stationary analysis methods to study an otherwise nonstationary process.

Table B.1. Stationarity test results

		Percentage of Data Failed							
		August 9		September 30		October 7		All Data	
		$\alpha=0.10$	$\alpha=0.02$	$\alpha=0.10$	$\alpha=0.02$	$\alpha=0.10$	$\alpha=0.02$	$\alpha=0.10$	$\alpha=0.02$
Level of Significance									
Run Test	$\zeta$	45	17	45	14	16	6	35	13
	$\zeta^2$	16	8	36	25	25	16	26	16
	$\zeta^3$	3	0	6	0	3	0	4	0
	$\zeta^4$	98	92	73	63	52	41	74	65
Reverse Arrangement Test	$\zeta$	0	0	2	0	2	0	1	0
	$\zeta^2$	28	17	53	30	50	33	44	27
	$\zeta^3$	8	2	5	0	0	0	4	0
	$\zeta^4$	34	20	53	38	48	33	45	30
All Parameters	29	19	34	21	24	16	29	19	



## Appendix C: Application of Barnett's Parameterization of a Nonlinear Source Function

Theoretical results have shown that the nonlinear energy transfer of gravity waves can be expressed by the Boltzmann integral as

$$\begin{aligned} \frac{\partial N_4}{\partial t} = & \int \dots \int T(\mathbf{k}_1, \mathbf{k}_2, \mathbf{k}_3, \mathbf{k}_4) [(N_3 + N_4)N_1N_2 \\ & - (N_1 + N_2)N_3N_4] \delta(\omega_1 + \omega_2 - \omega_3 - \omega_4) \\ & \times \delta(\mathbf{k}_1 + \mathbf{k}_2 - \mathbf{k}_3 - \mathbf{k}_4) d\mathbf{k}_1 d\mathbf{k}_2 d\mathbf{k}_3 \end{aligned} \quad (\text{C.1})$$

where  $N_i = N(\mathbf{k}_i) = S(\mathbf{k}_i)/\omega_i$  with  $\omega_i = (gk_i)^{1/2}$  and  $S(\mathbf{k}_i)$  is the two-dimensional wave spectrum with respect to wave numbers  $|\mathbf{k}_i| = k_i$ . The delta functions express conditions for resonance between waves. The coupling coefficient  $T(\mathbf{k}_1, \mathbf{k}_2, \mathbf{k}_3, \mathbf{k}_4)$  is a very complicated function and its precise form does not provide any physical interpretation. While the Boltzmann integral has been applied to other fields of study, Hasselmann (1962, 1963a,b) first derived equation (C.1) for gravity waves. Other derivations have been given by Benney and Saffman (1966) and Watson and West (1975). Recently Longuet-Higgins (1976) presented a simplified model and showed that  $T(\mathbf{k}_1, \mathbf{k}_2, \mathbf{k}_3, \mathbf{k}_4)$  is equal to  $4\pi$  when the four wave numbers  $k_1, k_2, k_3$ , and  $k_4$  are nearly equal. This result implies that the exchange of energy within the peak of the spectrum is of dominant importance. No practical application of this simplified model has been developed, however.

Attempts to evaluate the integral (C.1) have been made by Hasselmann (1963b) and more recently by Sell and Hasselmann (1972). The latter computations, typically 30 minutes per spectrum on a CDC6600 computer, lead to interpretations of the JONSWAP measurements that strongly suggest that the nonlinear transfers of energy play an essential role in the development of the wave spectrum, particularly in the growth of the wave energy at low frequencies.

Because of the complexity of the direct calculations of (C.1), Barnett (1966), using a Neumann spectrum, obtained a parameterization of (C.1) as part of a wave prediction scheme based on the earlier Hasselmann (1963a,b) results. Mitsuyasu (1968) applied this parameterization to his studies on nonlinear energy transfer in wave spectrum and obtained fair agreement between calculated and observed nonlinear source functions. Resio and Vincent (1976) satisfactorily applied Barnett's prediction scheme for hindcasting waves in the Great Lakes.

Barnett's parameterization was based on Hasselmann's (1962) theoretical results, which demonstrated that the wave-wave interaction of a spectral component consists of an active part that transfers its energy to other components and a passive part that receives energy from other components. Thus,

$$\frac{\partial S(f, \theta)}{\partial t} = G - DS(f, \theta) \quad (\text{C.2})$$

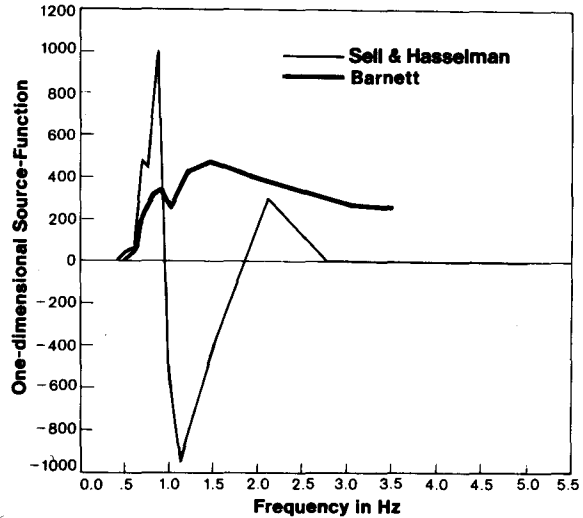
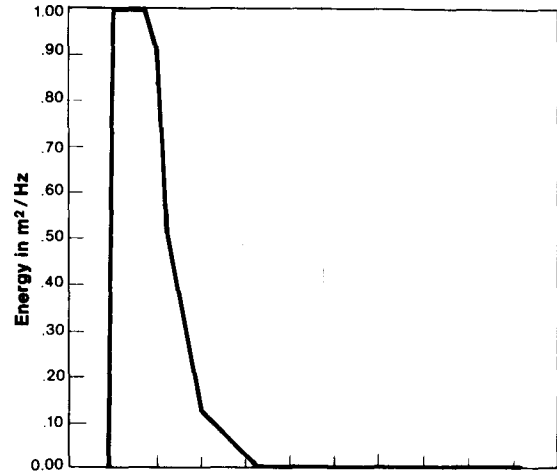


Figure C.1.—A white spectrum and its computed source functions.

with

$$\begin{aligned} G = & \frac{4.4 \times 10^8 E^3 f_0^8}{g^4} \cos^4(\theta - \theta_0) \left(1 - 0.42 \frac{f_0}{f}\right)^3 \\ & \times \exp \left[ -4 \left(1 - \frac{f_0}{f}\right)^2 + 0.1 \left(\frac{f_0}{f}\right)^5 \right], \end{aligned} \quad (\text{C.3})$$

for  $f > 0.42 f_0$ , and  $|\theta - \theta_0| < \frac{\pi}{2}$ ;

$G = 0$ , otherwise;

and

$$D = \frac{7.5 \times 10^7 E^2 f_0^7}{g^4 f} [1 + 16|\cos(\theta - \theta_0)|] (f - 0.53 f_0)^3, \quad (\text{C.4})$$

for  $f > 0.53 f_0$ ;

$D = 0$ , otherwise,

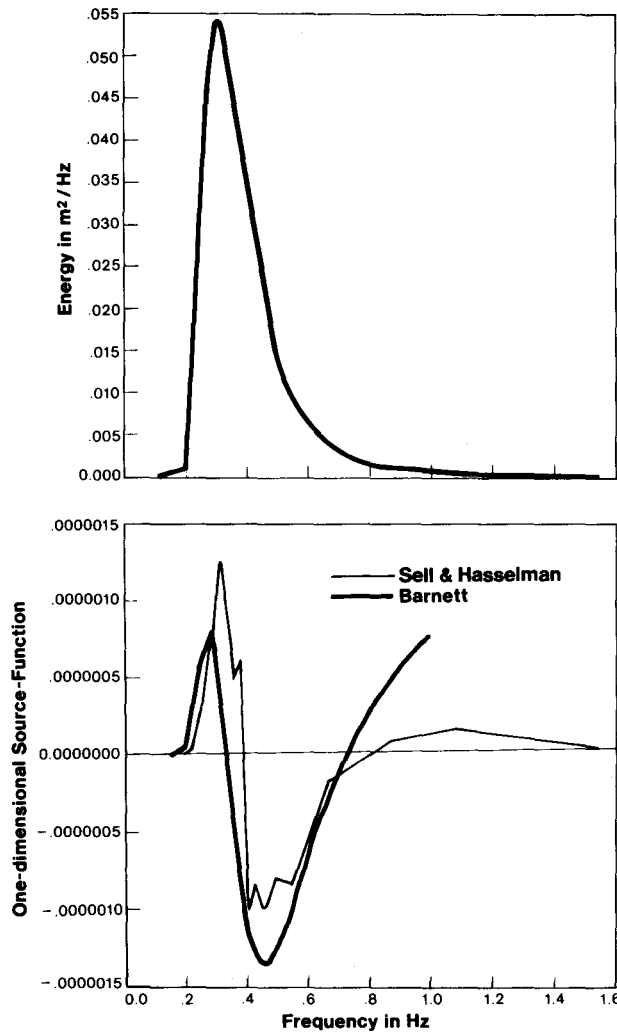


Figure C.2.—Pierson-Moskowitz spectrum and its computed source functions.

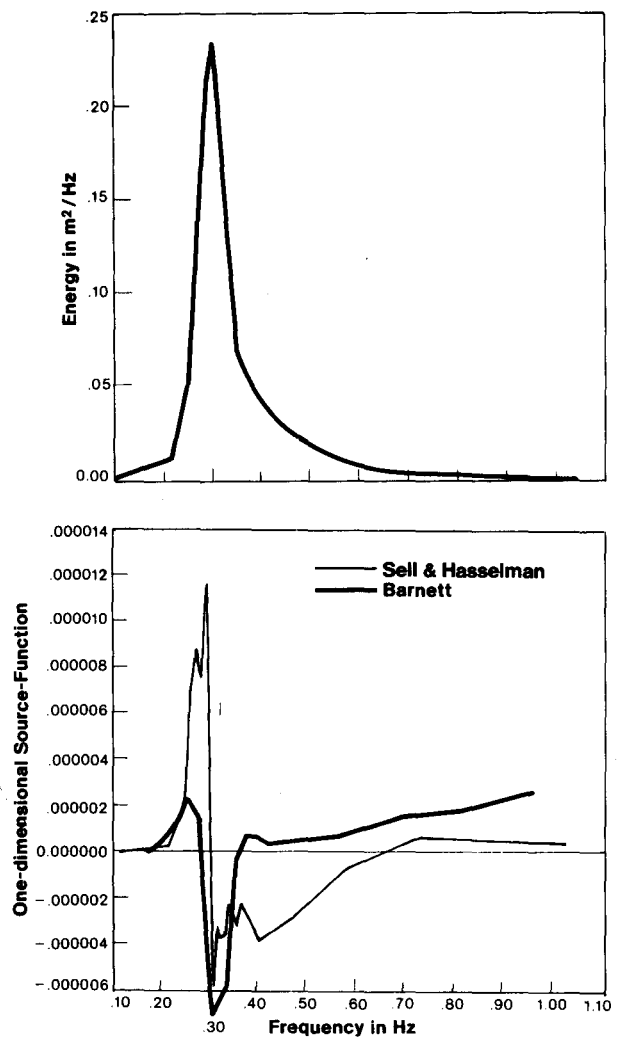


Figure C.3.—JONSWAP spectrum and its computed source functions.

where  $E$ ,  $f_0$ , and  $\theta_0$  are total energy, mean frequency, and mean direction, respectively, defined by

$$E = \iint S(f, \theta) df d\theta, \quad (C.5)$$

$$f_0 = \frac{1}{E} \iint f S(f, \theta) df d\theta, \quad (C.6)$$

and

$$\theta_0 = \frac{1}{E} \iint \theta S(f, \theta) df d\theta. \quad (C.7)$$

In the above equations,  $\theta$  is the wave direction and  $f = \omega/2\pi$  is the linear wave frequency.

We applied the above parameterization by further assuming a directional spreading factor of  $(8/3\pi) \cos^4\theta$  to compare some of the results given in Sell and Hasselmann (1972) that led to the major conclusions based on JONSWAP measurements. The results for a fairly white spectrum, a Pierson-Moskowitz spectrum, and a mean JONSWAP spectrum are

presented in figures C.1, C.2, and C.3, respectively. The JONSWAP study (Hasselmann et al., 1973) concluded that, as the sharpness increases from figure C.1 to figure C.3, the evolution of a sharp peak is primarily controlled by the nonlinear energy transfer evidenced by the shifting of the positive lobe in Sell and Hasselmann's calculations toward lower frequencies. While not necessarily profound, the same conclusion can also be drawn from the shifting of the positive lobe as a result of Barnett's parameterization. Therefore, with an overwhelming savings in effort and computer time, Barnett's parameterization can be used approximately for the examination of theoretical nonlinear energy transfers, particularly with respect to the location of the positive lobes of the parameterized nonlinear source function.

## Appendix D: Trispectra During the Episodes 30 September 1972 and 7 October 1972

We present here the calculated trispectra for the episodes of 30 September and 7 October as figures D.1 and D.2. Each figure contains six sets of trispec-

tral sheets located 30 minutes apart, corresponding in time to the bispectra shown in figures 16 and 17.

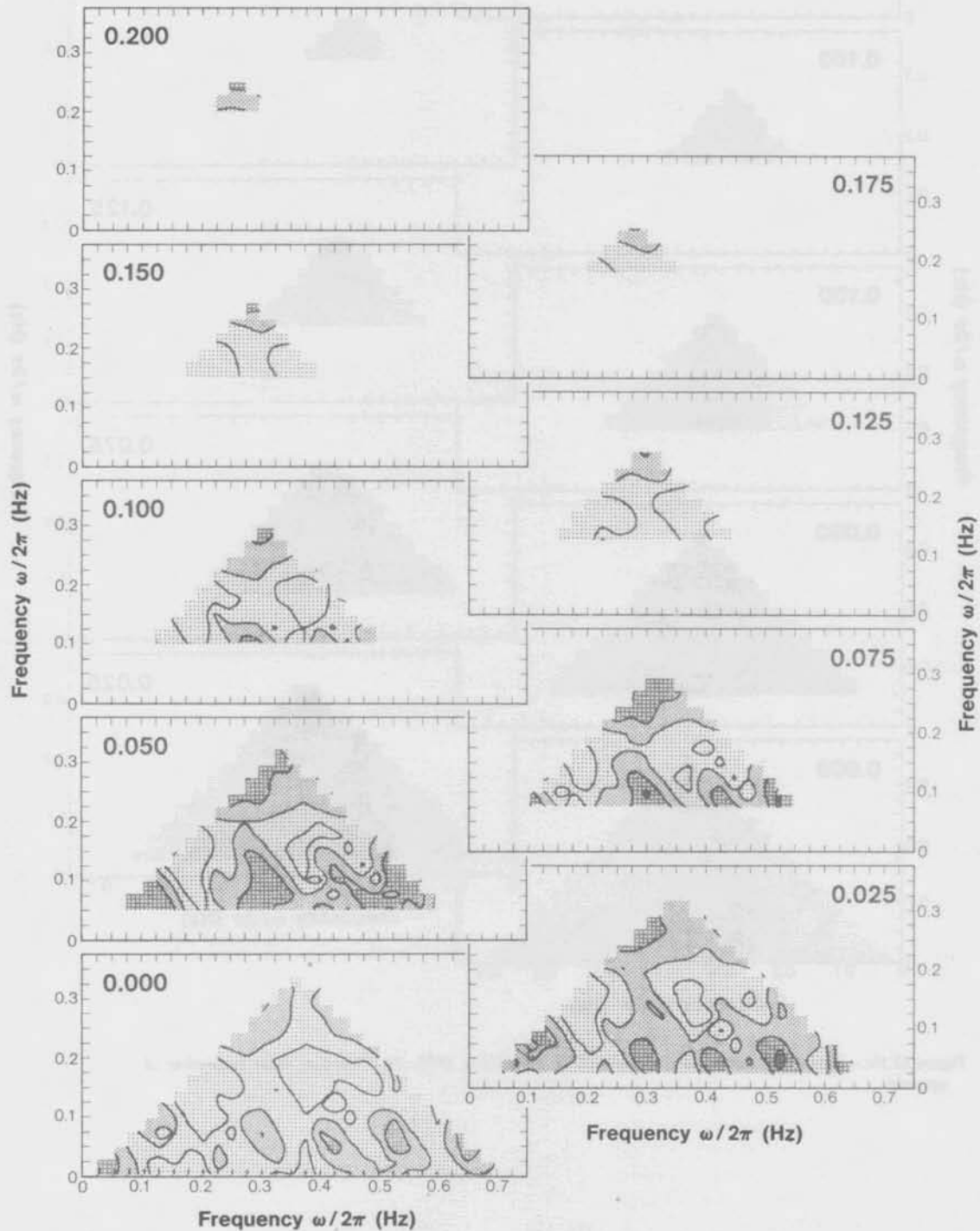


Figure D.1a.—Trispectra during the episode of 30 September 1972, 2.5 minutes from beginning of episode.

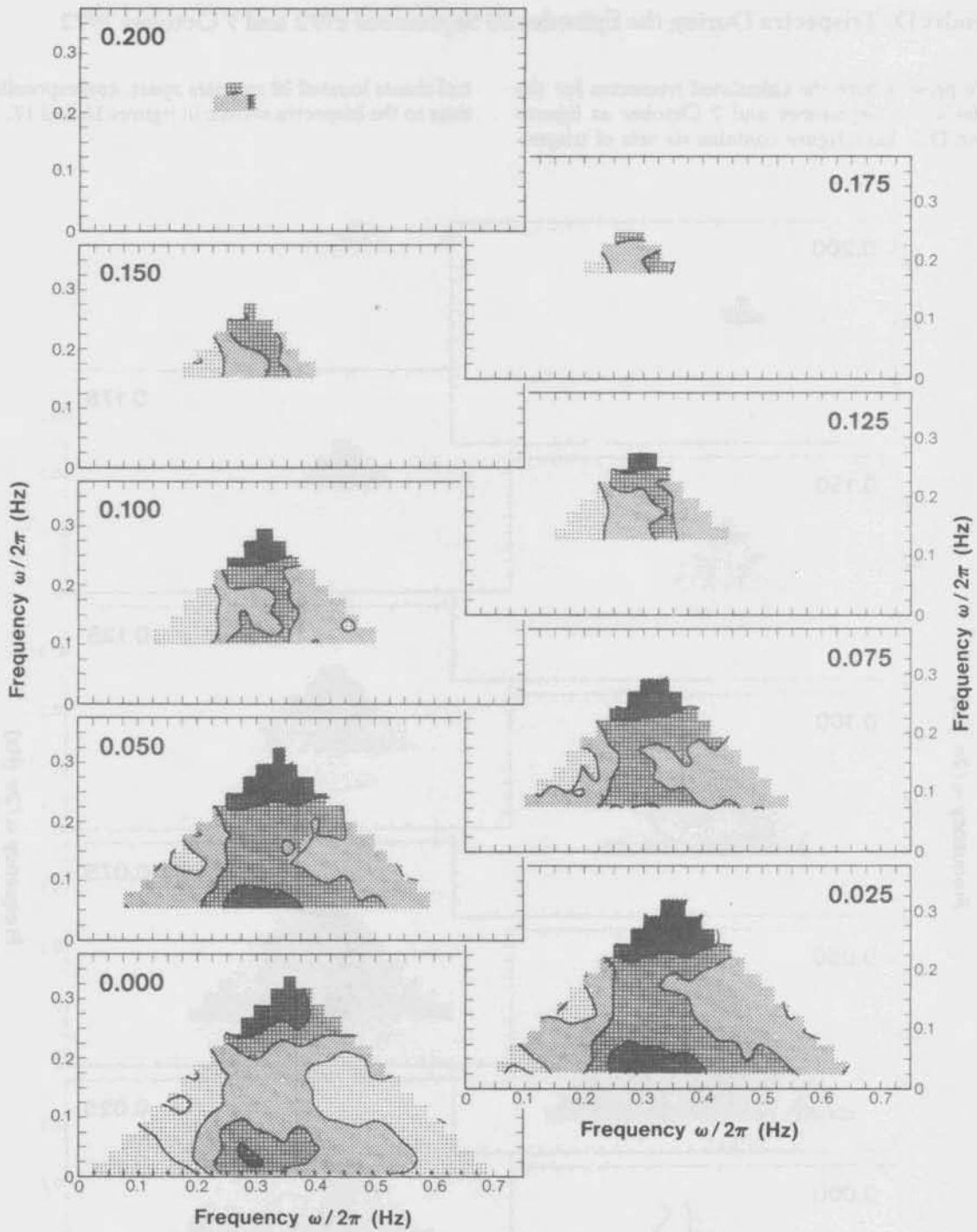


Figure D.1b.—Trispectra during the episode of 30 September 1972, 32.5 minutes from beginning of episode.

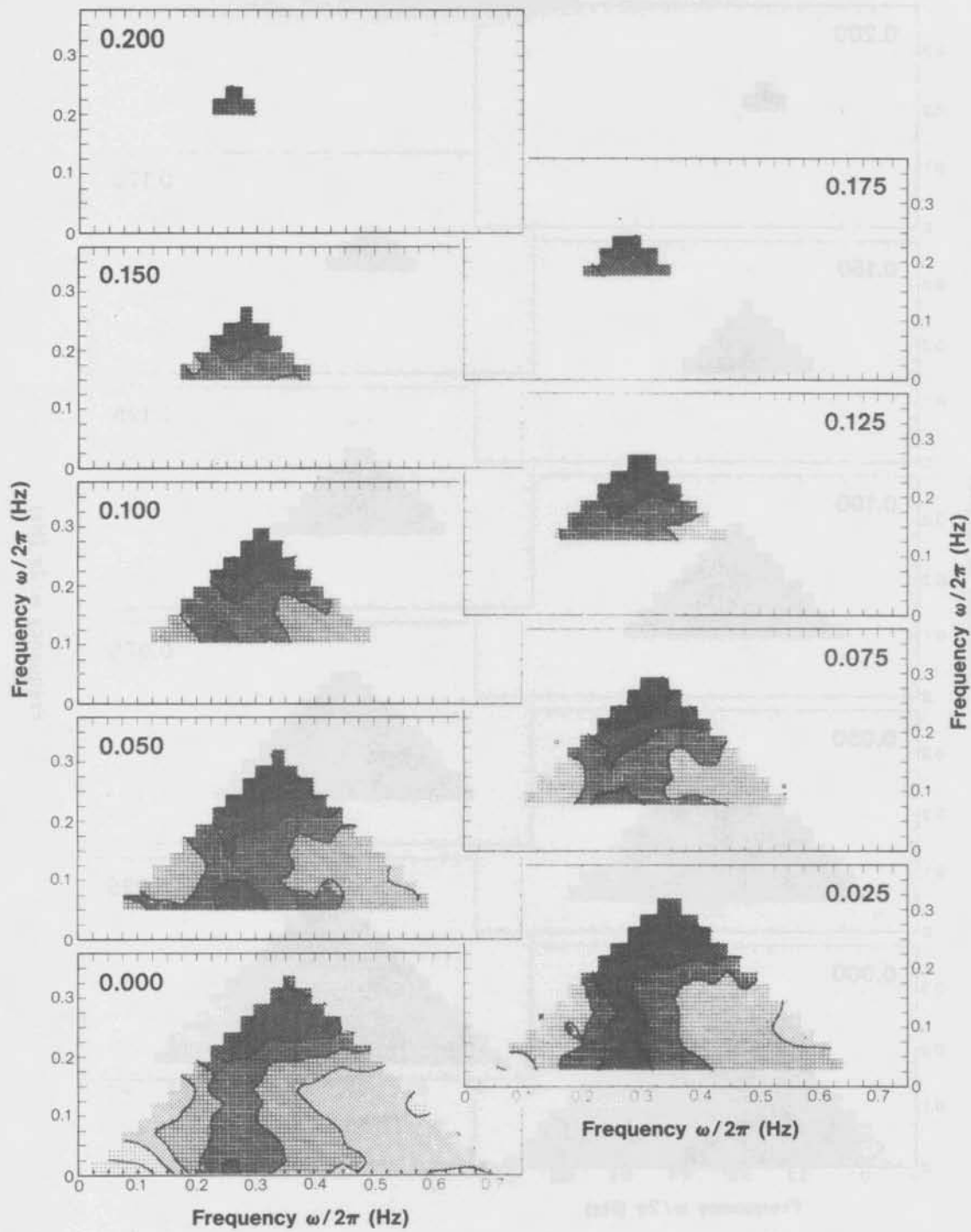


Figure D.1c.—Trispectra during the episode of 30 September 1972, 62.5 minutes from beginning of episode.

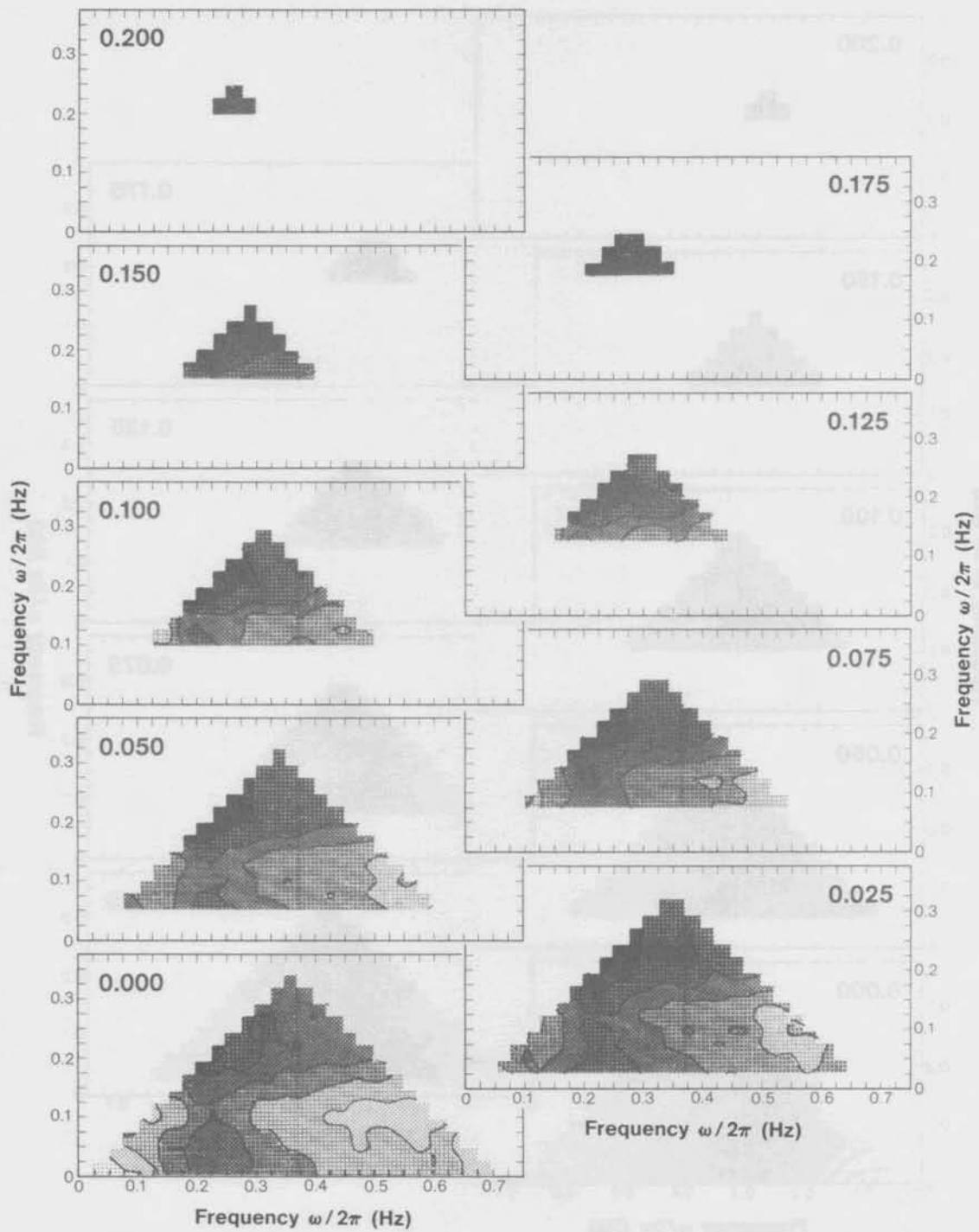


Figure D.1d.—Trispectra during the episode of 30 September 1972, 92.5 minutes from beginning of episode.

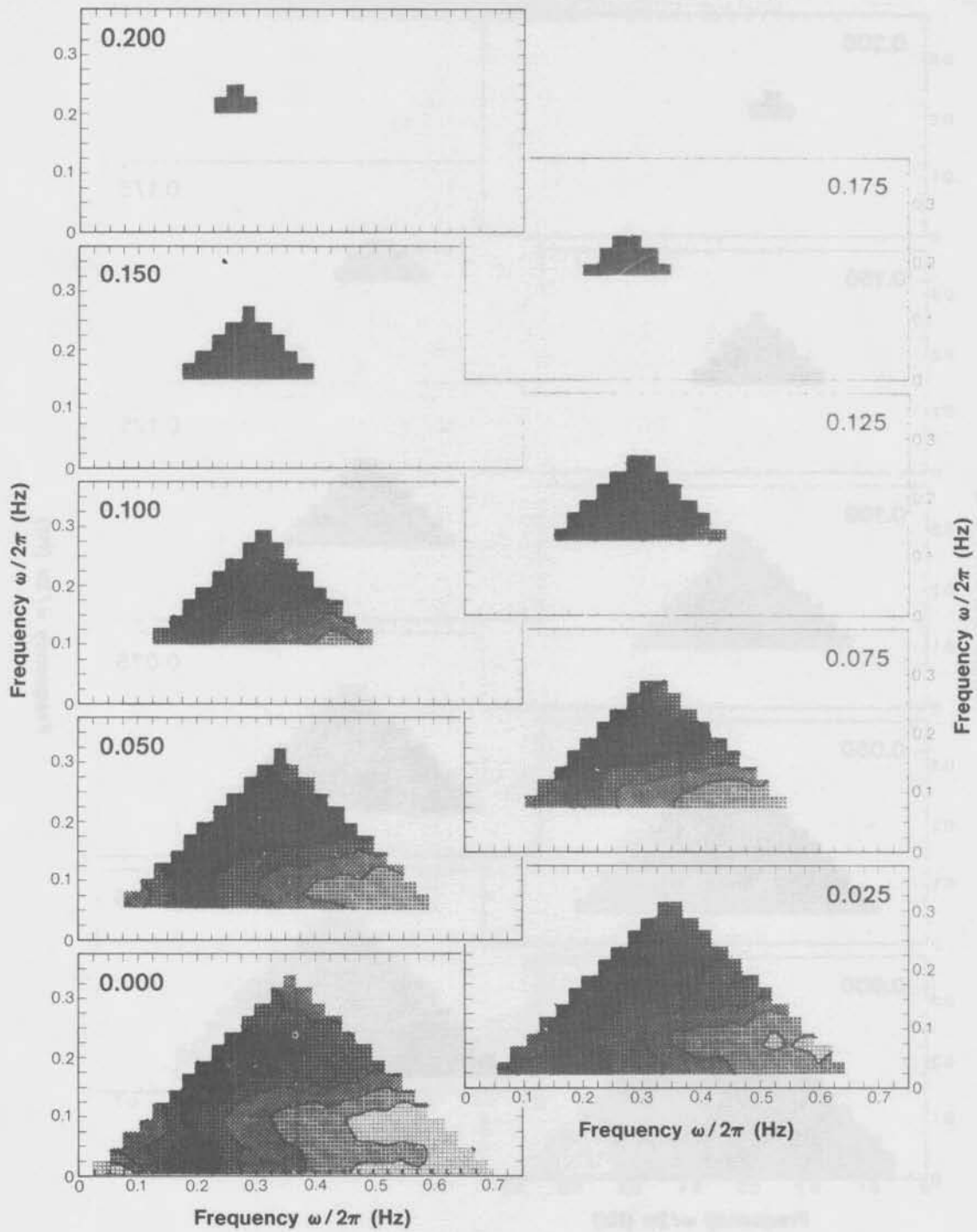


Figure D.1e.—Trispectra during the episode of 30 September 1972, 122.5 minutes from beginning of episode.

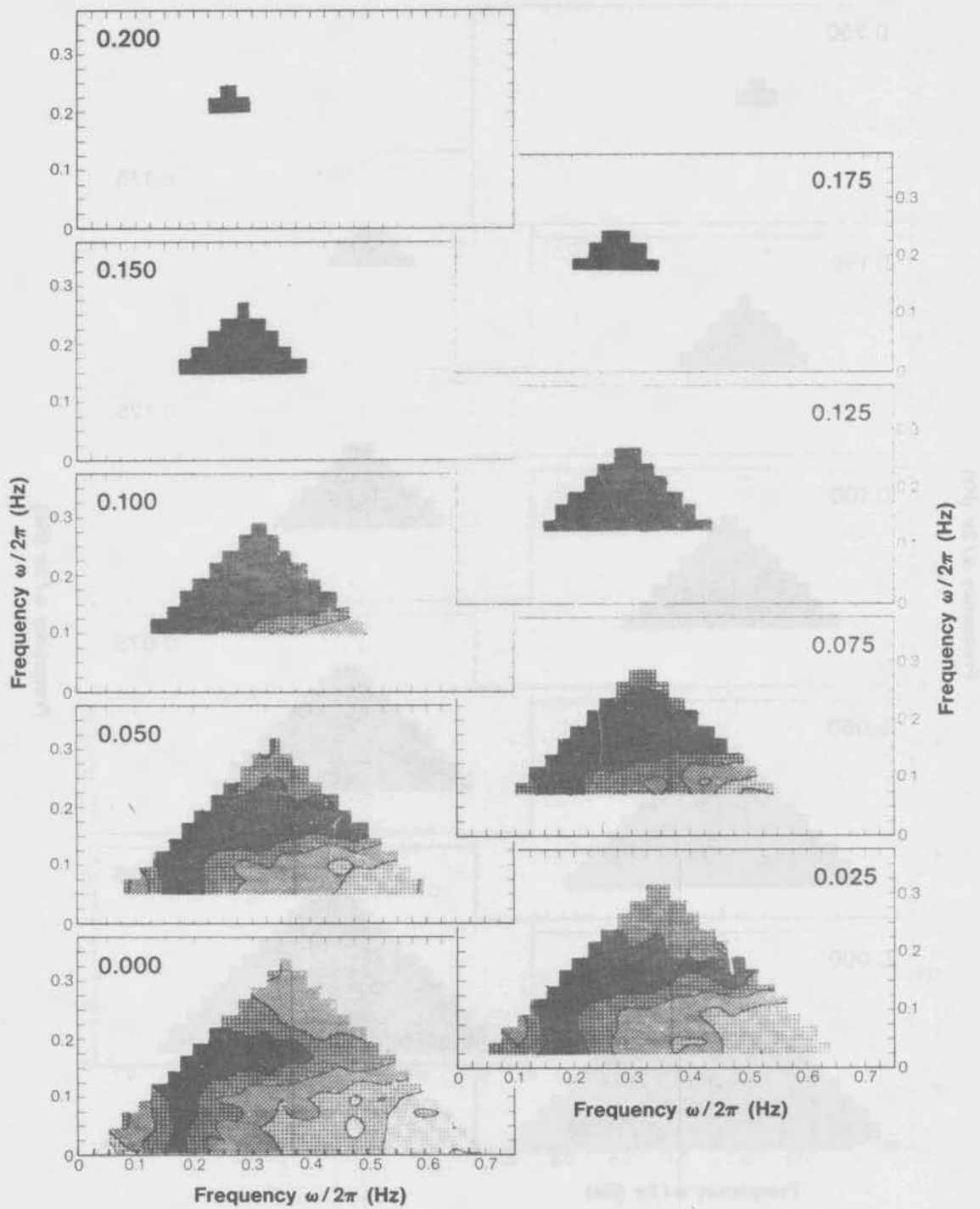


Figure D.1f.—Trispectra during the episode of 30 September 1972, 152.5 minutes from beginning of episode.

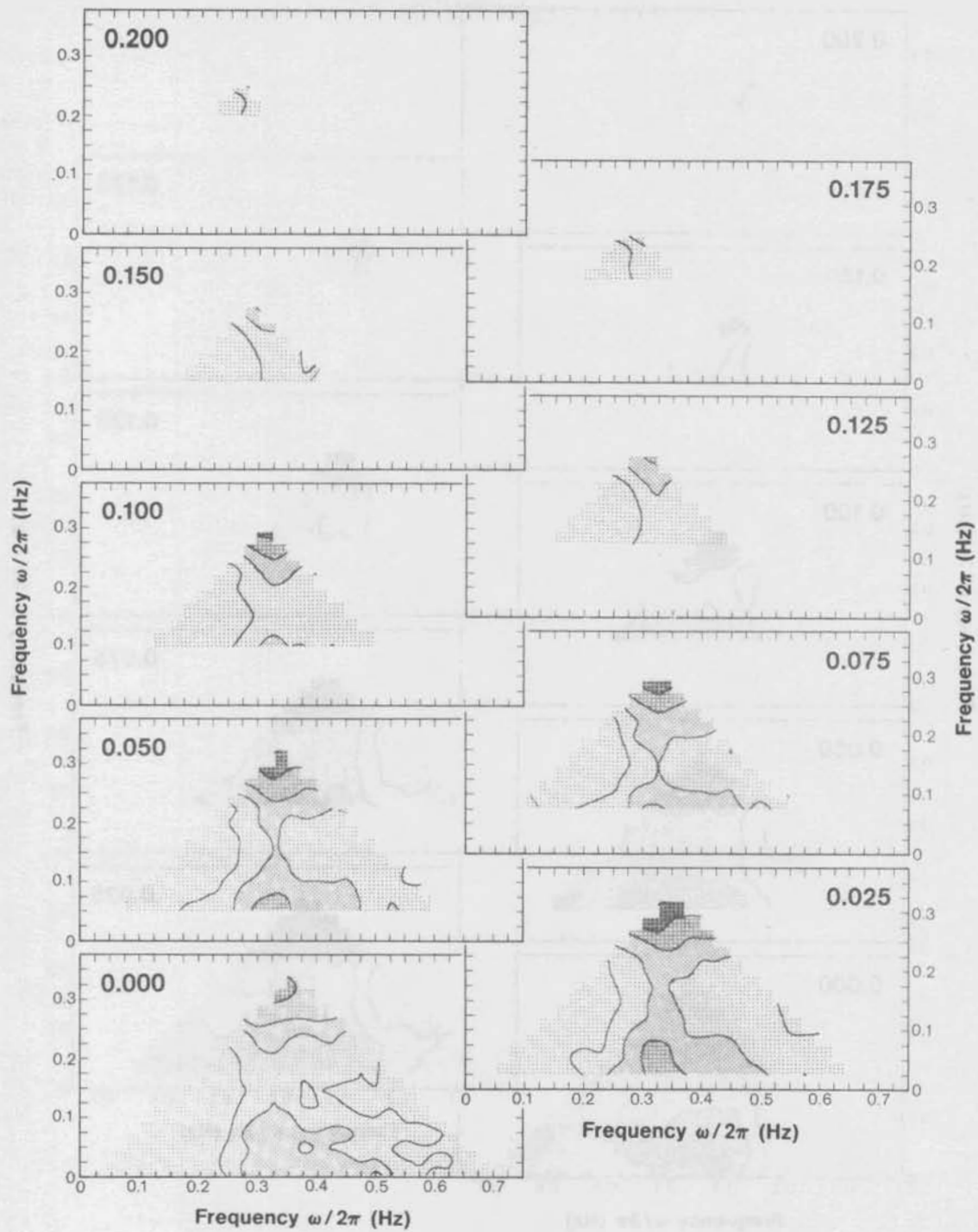


Figure D.2a. — Trispectra during the episode of 7 October 1972, 2.5 minutes from beginning of episode.

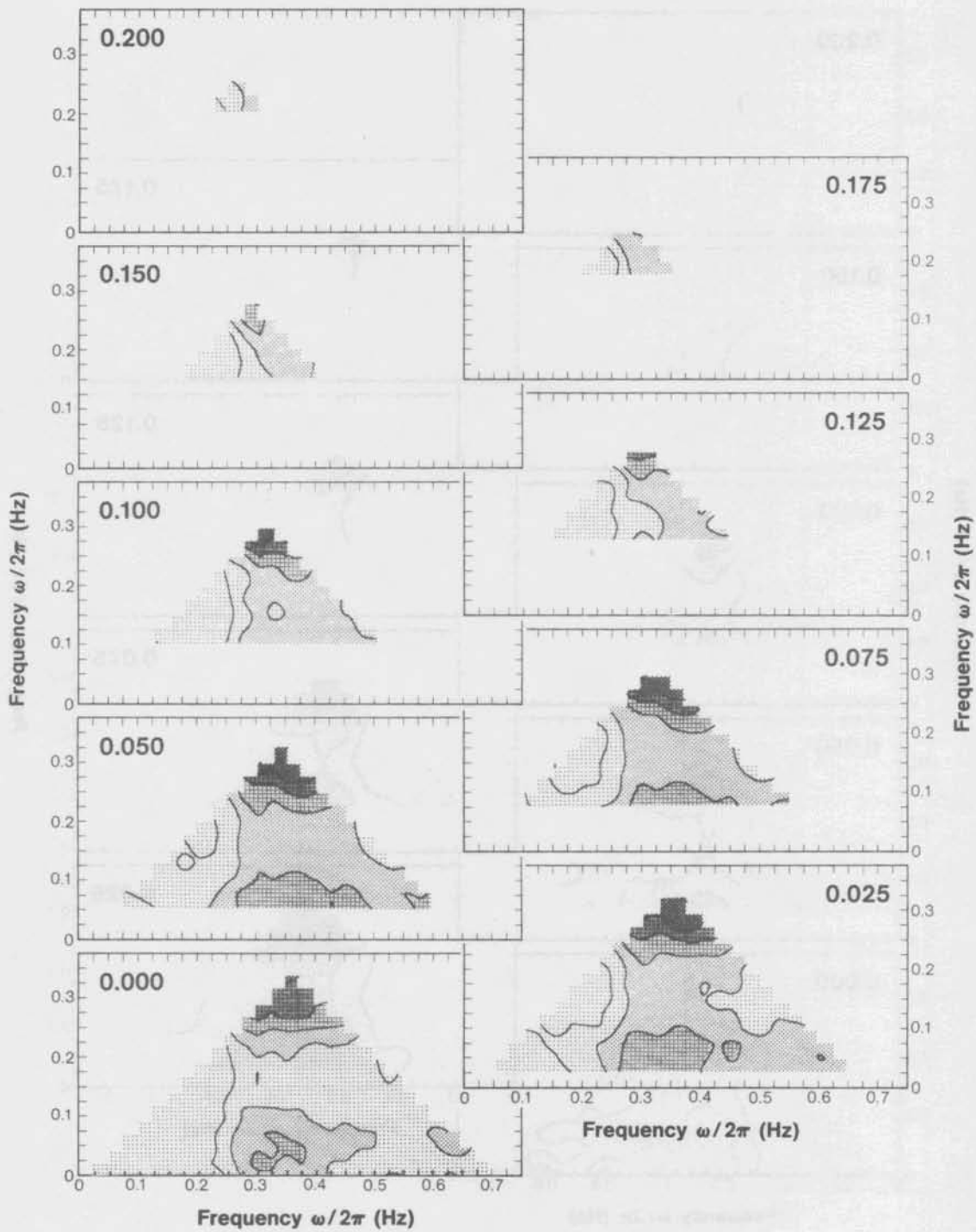


Figure D.2b.—Trispectra during the episode of 7 October 1972, 32.5 minutes from beginning of episode.

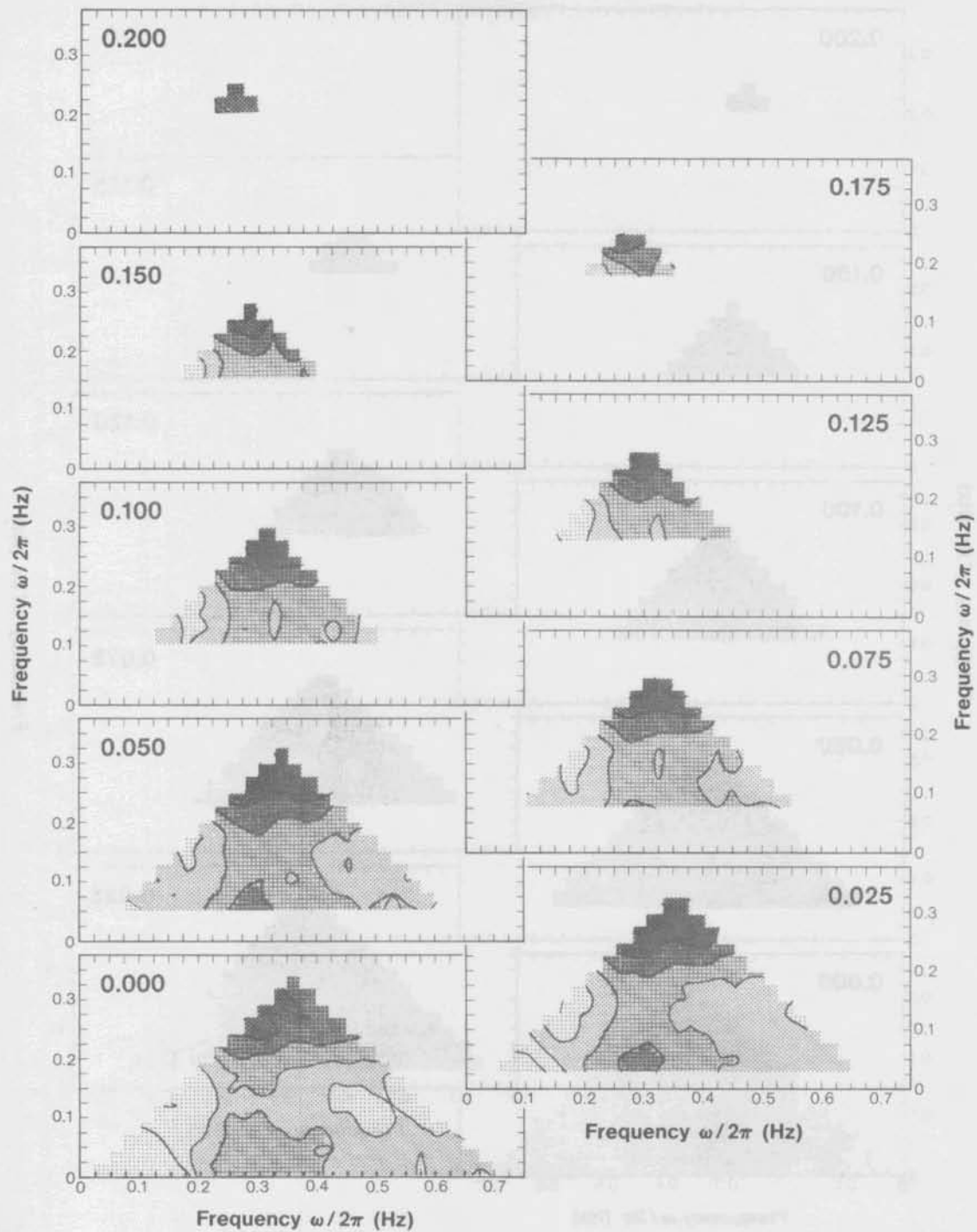


Figure D.2c.—Trispectra during the episode of 7 October 1972, 62.5 minutes from beginning of episode.

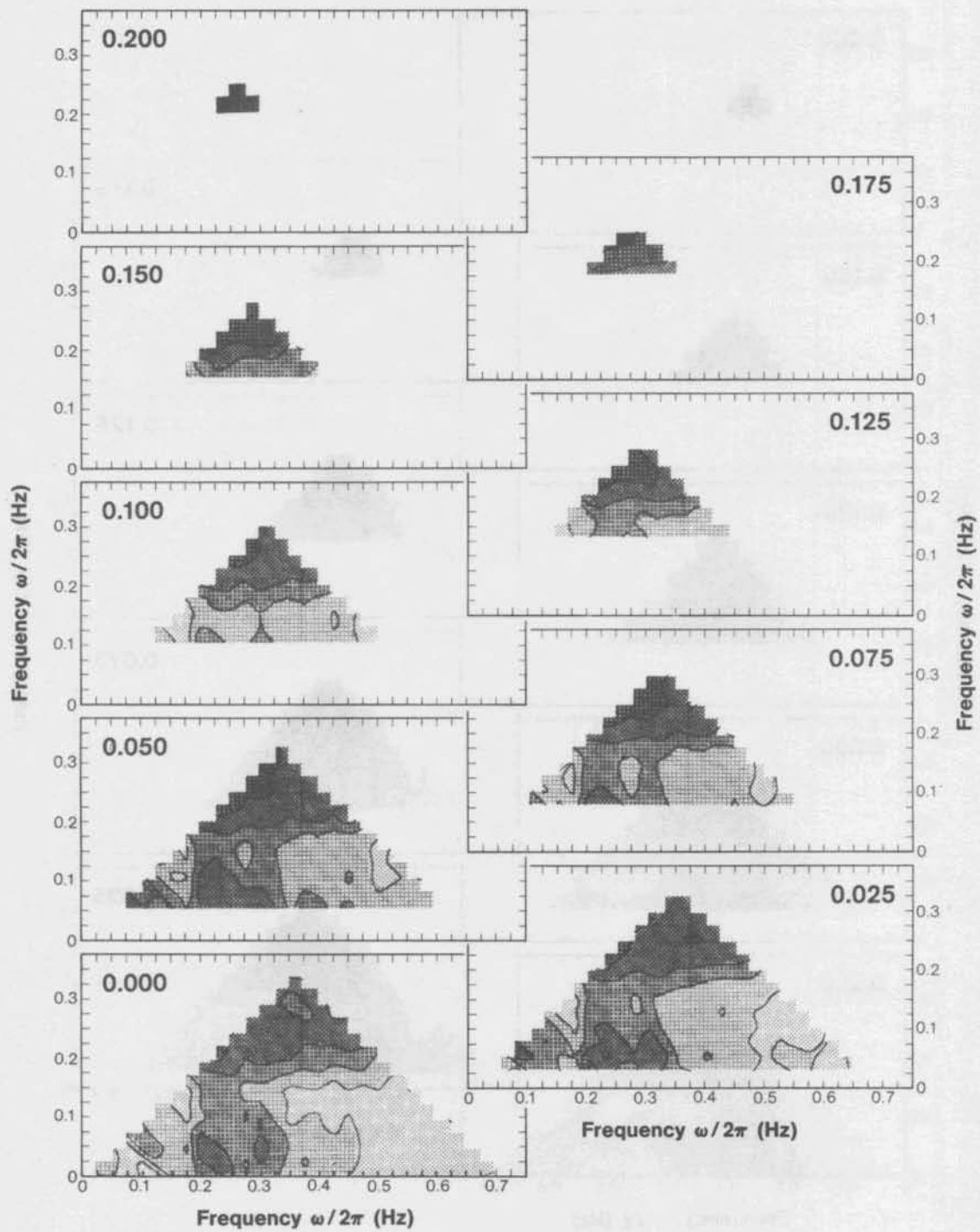


Figure D.2d.—Trispectra during the episode of 7 October 1972, 92.5 minutes from beginning of episode.

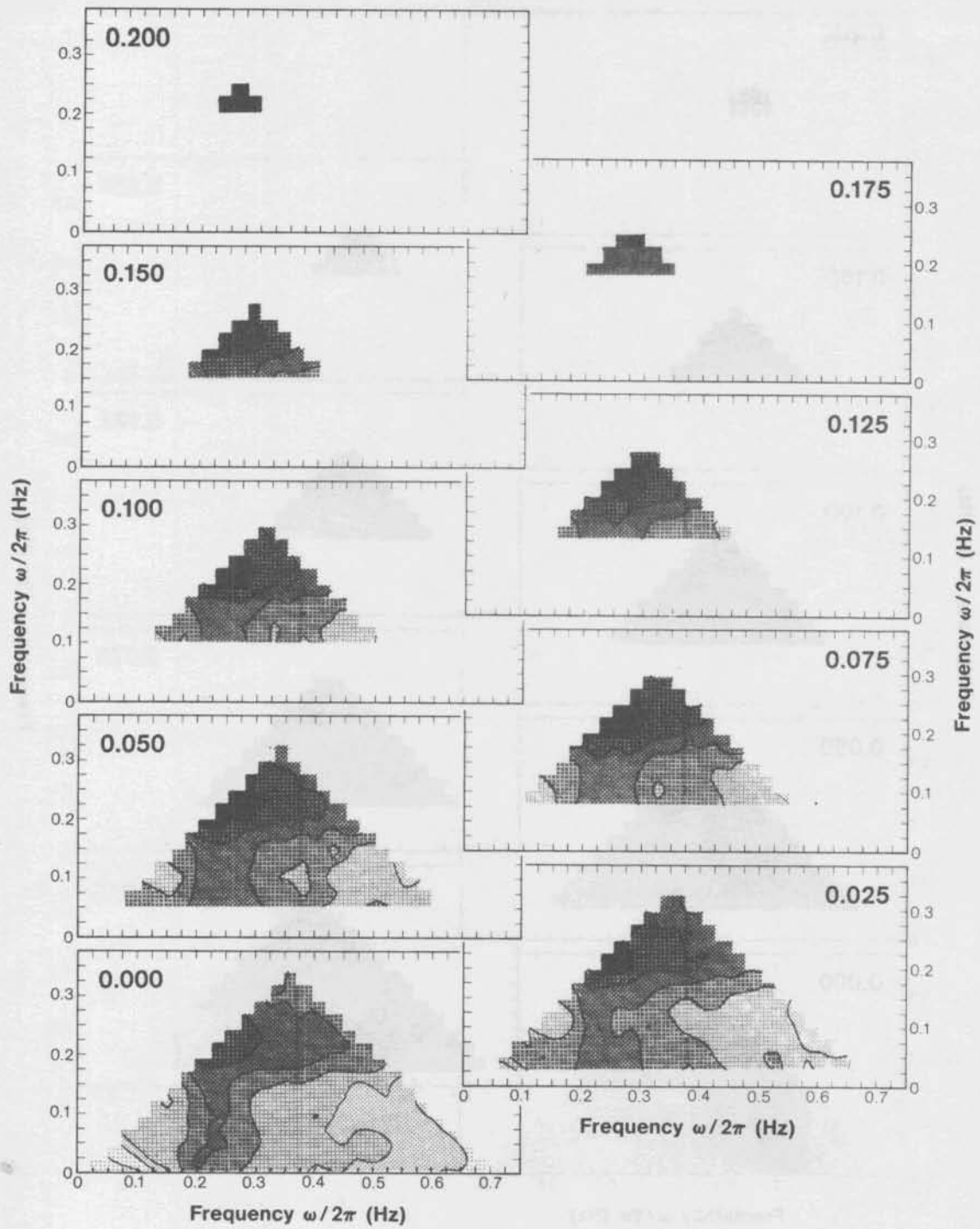


Figure D.2e.—Trispectra during the episode of 7 October 1972, 122.5 minutes from beginning of episode.

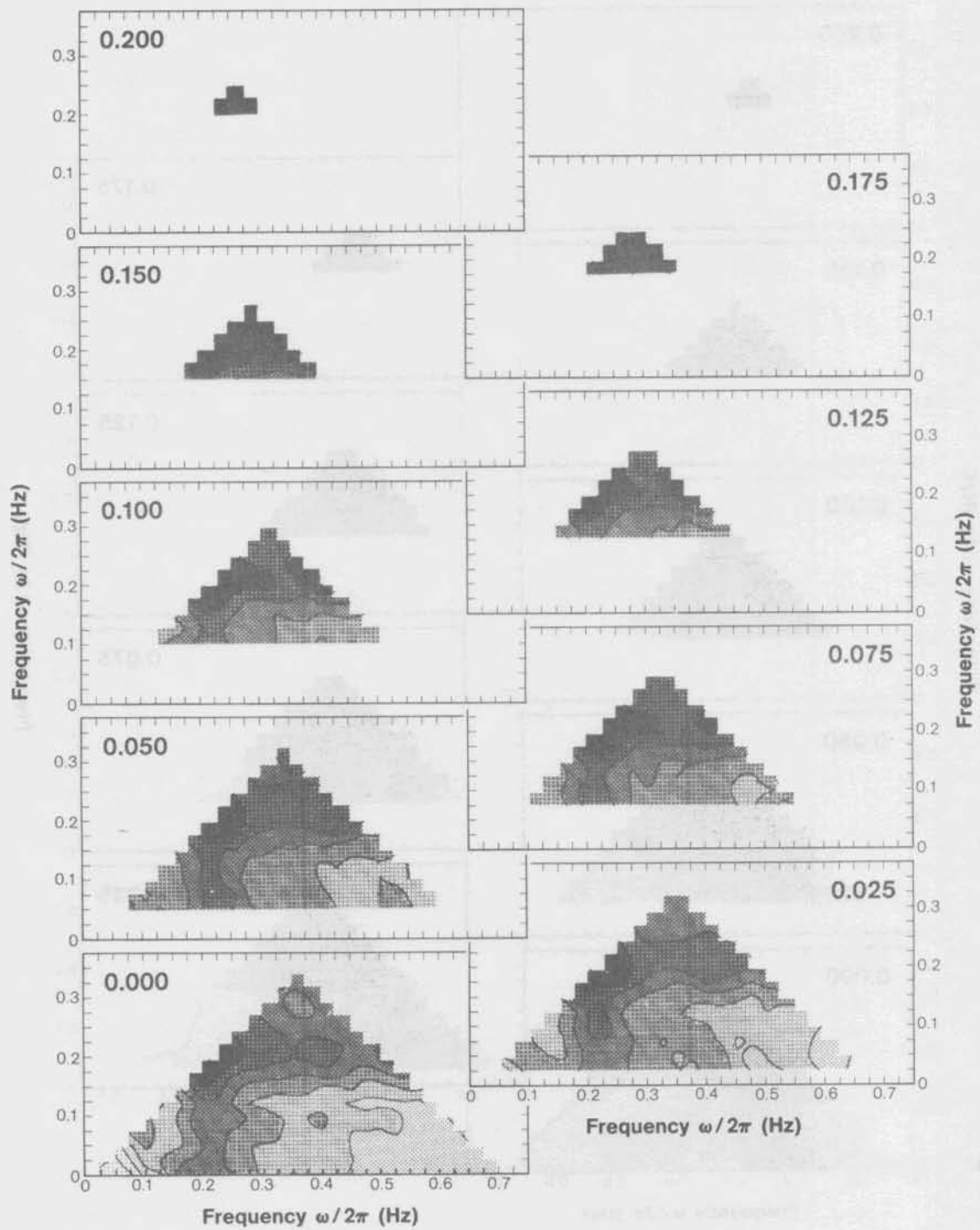


Figure D.2f. — Trispectra during the episode of 7 October 1972, 152.5 minutes from beginning of episode.